HER2 Prognostic Significance and Therapeutic Implications in Gastric Cardia Adenocarcinoma: Insights from Multi-Omics Profiling

Li-Dong Wang[1, *], Pengwei Xing[2], Xue-Ke Zhao[1], Xin Song[1], Meng-Xia Wei[1], Ling-Ling Lei[1], Rui-Hua Xu[1], Ran Wang[1], Lei Ma[3], Duo You[1, 4], Pei-Nan Chen[5], Minglu Xie[2], Miao Zhao[2], He Zhang[6], Hui-Fang Lv[4], Ai-Li Li[7], Xian-Zeng Wang[8], Fu-You Zhou[9], She-Gan Gao[10, *], Xingqi Chen[2, *]

[1]State Key Laboratory of Esophageal Cancer Prevention & Treatment and Henan Key Laboratory for Esophageal Cancer Research of the First Affiliated Hospital, Zhengzhou University, Zhengzhou 450052, China.

[2]Department of Immunology, Genetics and Pathology, Uppsala University and Science for Life Laboratory, Uppsala, Sweden

[3]Henan key Laboratory of Tumor Molecular Biology Medicine of First People's Hospital of Nanyang, Nanyang, 473004, China.

[4]Department of Medical Oncology, the Affiliated Cancer Hospital of Zhengzhou University, Zhengzhou, Henan Province, 450008, China

[5]Deaprtment of Thoracic Surgery, the Affiliated Cancer Hospital of Zhengzhou University, Zhengzhou, Henan Province, 450008, China

[6]Deaprtment of Pathology, the Affiliated Cancer Hospital of Zhengzhou University, Zhengzhou, Henan Province, 450008, China

[7]Department of Pathology, Linzhou Tumor Hospital, Linzhou, Henan Province, 456500, China

[8]Department of Thoracic Surgery, Linzhou People's Hospital, Linzhou, Henan Province, 456500, China

[9]Department of Thoracic Surgery, Anyang Tumor Hospital; Henan Key Medical Laboratory of Precise Prevention and Treatment of Esophageal Cancer; Henan Province Engineering Research Center of Cellular Immunotherapy for Esophageal Cancer, Anyang, Henan Province, 455000, China

[10]Henan Key Laboratory of Microbiome and Esophageal Cancer Prevention and Treatment; Henan Key Laboratory of Cancer Epigenetics; Cancer Hospital, The First Affiliated Hospital, College of Clinical Medicine of Henan University of Science and Technology, Luoyang, 471003, China

*Correspondence: ldwang2007@126.com, gsg112258@163.com, or xingqi.chen@igp.uu.se

Abstract:

Therapeutic targets for Gastric Cardia Adenocarcinoma (GCA), particularly for HER2-negative patients, are lacking. Here, we conducted multi-omics profiling on 128 GCA patients using mass spectrometry, whole-exome sequencing, RNA-Seq, and metabolomics. We found HER2 to be a favorable prognostic marker for GCA. Employing molecular counting, we categorized patients into HER2-high, -low, and -negative groups. We uncovered an enrichment of DNA repair features in the HER2-high group, while HER2-low and -negative groups exhibited strong inflammation. We found that tumor mutation burden may not be the distinguishing factor among these three groups. We revealed that the HER2-negative and -low groups have a tumor-suppressive immune microenvironment, and HER2 expression is associated with fatty acid metabolic profiles and inflammation in the blood of patients. Our study revealed anti-inflammatory and immune checkpoint inhibition, targeting PD-L2 and the CD47/SIRPA pair, as therapeutic strategies for HER2-negative GCA patients. These findings highlight promising avenues for personalized treatment for GCA.

Keywords: Gastric cardia adenocarcinoma, HER2-negative, Prognosis, Tumor microenvironment, anti-inflammation, Immune inhibitory checkpoints

Introduction

The cardia is located between the esophagus and the stomach. Gastric cardia adenocarcinoma (GCA) occurs in the Taihang Mountains of north central China at high rates[1-3]. Gastric cancer in this area occurs primarily in the uppermost portion of the stomach and is referred to as GCA, while those in the remainder of the stomach are called gastric noncardia adenocarcinoma (GNCA)[4]. Adenocarcinomas from junction of esophagogastric junction are usually classified as Siewert type II of esophagogastric junction adenocarcinoma in western countries[5-9], where Barrett's esophagus is considered an important precancerous lesion of adenocarcinoma at the esophagogastric junction [10]. However, GCA from a Chinese population in this area has distinct features compared to Western countries[3,10,11], and a very low frequency of Barrett's esophagus is observed[10]. Even GCA presents distinct features compared GNCA[12-16], therapeutic strategies often mirror those for GNCA. Consequently, therapeutic targets specifically for GCA are lacking. Human Epidermal Growth Factor Receptor 2 (HER2), the protein product of the Erb-B2 Receptor Tyrosine Kinase 2 (*ERBB2*) gene, plays a crucial role in regulating cell growth and division[17]. In certain cancers, such as breast cancer[18,19] and gastroesophageal cancer[20], HER2 can become overexpressed or amplified, leading to uncontrolled cell growth. Targeted therapies, such as trastuzumab (Herceptin) and others, have been developed to specifically inhibit HER2 signaling and are effective in treating HER2-positive breast[21] and gastroesophageal[22] cancers. Currently, HER2 targeted therapy has become a vital treatment option for certain types of gastroesophageal cancers, including esophageal Adenocarcinoma (EAC), GCA, GNCA, and stomach adenocarcinoma (STAD), particularly in advanced or metastatic cases[20,23,24]. Anti-HER2 targeted therapies have improved survival outcomes in advanced gastroesophageal cancer patients with HER2 overexpression[23-25]. However, the relatively low prevalence (less than 30%) of HER2-positive cases poses challenges[26-28], particularly for HER2-negative patients. The first-line treatment for advanced HER2-negative gastric cancer and esophagogastric junction adenocarcinoma mainly involves immunotherapy combined with chemotherapy, without specific targets[9]. In solid malignancies, the overexpression or amplification of HER2 is associated with an adverse prognosis[29], paradoxically, independent studies including our recent study, have shown that *ERBB2* gene focal amplification or HER2 overexpression might confer a favorable prognostic impact in patients with esophagogastric junction adenocarcinoma, EAC[30] and GCA[13] . Hence, the role of HER2 as either a therapeutic target or a prognostic marker in GCA remains uncertain. Consequently, conducting a comprehensive multi-omics molecular profiling of GCA patients, stratified by the degree of HER2 expression, is imperative for elucidating this paradox and

94 gaining a more profound understanding that can inform targeted therapy strategies for these
95 malignancies, particularly the HER2-negative patients.
96
97 In this investigation, we assembled a cohort comprising 128 patients diagnosed with GCA. We
98 conducted an extensive array of analyses on our GCA cohort, including RNA-Seq for
99 transcriptome profiling, whole exome sequencing (WES) for examining genetic alterations,
100 mass spectrometry for the identification and quantification of proteins, and metabolic profiling
101 to gain insights into metabolic alterations. With a highly sensitive molecular counting approach,
102 we stratified GCA patients into HER2-high, -low, and -negative groups. This method enabled
103 us to undertake a comprehensive and detailed characterization of molecular features for each
104 patient group, including the exploration of gene expression patterns, profiling of proteins, and
105 examination of genetic alterations. We identified HER2 as a favorite prognostic marker for
106 esophagogastric junction adenocarcinoma, GCA and EAC. Furthermore, our investigations
107 unveiled a substantial enrichment of DNA repair pathways in the HER2 high-expression group,
108 while the HER2 low-expression and negative group prominently exhibited features indicative
109 of inflammation. We found that tumor mutation burden (TMB) may not be the primary
110 distinguishing factor among these three groups, but the HER2 high group showed substantially
111 higher genome instability compared with the HER2 negative group. Notably, we identified
112 disparate tumor microenvironments and variations in immune inhibitory checkpoints across
113 the distinct HER2 expression groups. Furthermore, our results also suggested that the HER2
114 negative and low groups have a tumor suppressive immune microenvironment compared with
115 the HER2 high group. Our study pinpointed anti-inflammatory and immune checkpoint
116 inhibition, targeting PD-L2 and the CD47/SIRPA pair, as therapeutic strategies for HER2-
117 negative GCA patients.
118
119 **Results**
120 **ERBB2 expression as a favorable prognostic marker in esophagogastric junction**
121 **adenocarcinoma**
122 Previously, we and others found that *ERBB2* gene focal amplification or HER2 overexpression
123 might confer a favorable prognostic impact on patients with esophagogastric junction
124 adenocarcinoma, esophageal adenocarcinoma (EAC) and gastric cardia adenocarcinoma
125 (GCA)[13,30]. This conclusion is derived from immunohistochemistry (IHC) staining of HER2
126 or gene amplification detection using whole-genome sequencing. These measurements involve
127 positive and negative HER2 staining or amplification assessments of patients. The HER2

128 scoring system typically employs immunohistochemistry (IHC) and/or fluorescence in situ
129 hybridization (FISH) techniques to evaluate the quantity and distribution of HER2 protein and
130 gene amplification in cancer tissue samples[31]. A score from 0 to 3+ based on membranous
131 staining of HER2 protein is assigned by a pathologist following guidelines, and the DNA FISH
132 method is combined with 2+ samples. Only HER2 2+, *ERBB2* FISH-positive samples, and 3+
133 patients are defined as HER2 positive samples. In the whole-genome sequencing method,
134 HER2 amplification is examined within amplification regions[31]. Both of these strategies are
135 not for quantitative stratification, and bias could be introduced. In addition, it is well known
136 there is a big heterogeneous expression of HER2 protein in different regions of the tumor from
137 the same patient[26]. RNA-Seq is a molecular counting method used to calculate the number of
138 transcripts. Thus, to avoid a biased strategy when evaluating whether *ERBB2* could be a
139 prognostic marker, we collected data from 54 GCA patients and performed RNA-seq and mass
140 spectrometry from both tumors and normal tissue adjacent to the tumor (NAT) (**Materials and**
141 **methods**). We observed a positive correlation in *ERBB2* RNA expression levels and HER2
142 protein levels (**Figure 1A**, Pearson correlation = 0.7559), and we stratified GCA patients into
143 high and low *ERBB2* groups based on the median expression level of *ERBB2* RNA molecules
144 (**Figure 1B**). In parallel, we downloaded RNA-Seq data for EAC, esophageal squamous-cell
145 carcinomas (ESCC), and Stomach adenocarcinoma (STAD) from TCGA[32] to stratify patients
146 into HER2 high and HER2 low group using the median value of normalized *ERBB2* RNA
147 expression level as the reference point (**Figure 1B**). Then we calculated the survival times of
148 patients in each cancer type (**Figure 1C**). It clearly showed a significant difference in survival
149 probabilities between *ERBB2* high and low groups from GCA patients ($p = 0.015$, using Rényi
150 family test with Fleming-Harrington weights ($p = 0$, $q = 1$)) (**Figure 1C**), where the survival
151 probability of the *ERBB2* high group was lower than that of the *ERBB2* low group when their
152 survival time was under 0.9 years. However, the trend reversed when their survival time
153 exceeded 0.9 years. This trend we observed with the RNA molecule counting strategy is very
154 similar to what we observed with IHC staining of HER2 in our previous cohort[15]. From the
155 TCGA cohort, we did not observe a significant survival difference between the *ERBB2* high
156 and low groups in ESCC ($p = 0.59$, **Figure 1C**) and in STAD ($p = 0.57$, **Figure 1C**). We also
157 examined the survival difference in subtypes of STAD and found no difference in diffuse
158 carcinoma and intestinal types (**Figure 1C**). However, there is a tendency for the *ERBB2* high
159 group to have better survival in STAD tubular adenocarcinoma ($p = 0.19$) and STAD NOS (not
160 otherwise specified) adenocarcinoma ($p = 0.4$), even though it is not statistically significant
161 (**Figure 1C**). Nevertheless, there is a significant difference in patient prognosis between the

162 *ERBB2* high and low groups in EAC patients (p = 0.0096, **Figure 1C**), where the *ERBB2* high
163 group has a better prognosis.
164
165 Since there is a clear positive correlation between RNA and protein from ERBB2 (**Figure 1A**),
166 we enlarged our cohort to include 128 GCA patients to perform protein quantification with
167 mass spectrometry (MS) of tumors and NAT (**Methods**, **Supplementary Figure 1**,
168 **Supplementary Table 1**). With molecular quantification of MS, we observed that 31 patients
169 are HER2 negative in both tumor and NAT parts, and 97 patients (75.78%) are HER2 positive
170 (**Figure 1D**). Due to the variation of genetic backgrounds among different patients, we assumed
171 that the observed HER2 noise differs among patients. Thus, we calculated the ratio of HER2
172 level between the tumor and its corresponding NAT to quantify the HER2 protein level from
173 different patients. We first divided HER2-positive patients into HER2 high and HER2 low
174 groups based on the median of the HER2 ratio between the tumor and NAT. Then we stratified
175 patients into three groups: HER2 high (n = 48), HER2 low (n = 49), and HER2 negative (n =
176 31) groups, based on the ratio of HER2 levels between the tumor and corresponding NAT
177 (**Figure 1D**). Simultaneously, the HER2 scoring system of immunohistochemistry (IHC) was
178 also applied to the tumor part of these GCA patients (**Figure 1E**). 6.3% of patients in our GCA
179 cohort are HER2 3+, which is in the similar range as previous reports[26-28]. The HER2 high
180 group has the highest proportion of HER2 3+ patients (14% in HER2 high group, 2% in HER2
181 low group, and 0% in HER2 negative group), and IHC HER2 scoring is significantly correlated
182 with MS HER2 grouping method (p = 0.034), which indicates our MS groups may reflect the
183 nature of HER2 expression (**Figure 1F**). Strikingly, the HER2 high group has the best survival
184 rates compared to the other two groups (p = 0.015, **Figure 1G**). The HER2 low group has a
185 slightly better prognosis compared to that of the HER2 negative group; however, it is not
186 significant. We also assessed the therapeutic strategies among our GCA cohort after surgery.
187 It clearly shows that HER2 grouping is irrelevant to treatment methods (p = 0.320) ((**Figure**
188 **1H**), and different therapeutic strategies did not contribute to different prognosis in our GCA
189 cohort (p = 0.58) ((**Figure 1I**). We also performed detailed correlation analysis between HER2
190 groups and clinicopathological features (**Supplementary Figure 2A**, **Supplementary Table**
191 **1**). We found that HER2 grouping is relevant to age (p = 0.005046), family history (p =
192 0.04937), alcohol consumption (p = 0.0313), tumor differentiation (p = 0.029), and Lauren
193 classification (p = 0.02193), but independent of other clinicopathological features, e.g., sex,
194 incidence area, smoking, metastasis, stage, etc. (**Supplementary Figure 2B-D**).
195

196 In summary, by integrating our findings with RNA-Seq data from TCGA, we have confirmed
197 that *ERBB2* RNA expression and the quantification of HER2 protein level with MS could serve
198 as robust prognostic markers for esophagogastric junction adenocarcinoma, GCA and EAC.
199 Grouping GCA patients based on the ratio of HER2 protein between the tumor and NAT
200 provides a novel strategy to stratify GCA patients, and the detailed molecular profiling of
201 different HER2 groups could identify new therapeutic avenues, particularly for the HER2
202 negative group. To better understand molecular features in each HER2 group from GCA
203 patients, we also conducted an extensive array of analyses on our GCA cohort (128 patients),
204 with whole exome sequencing (WES) for the examination of genetic alterations, RNA-Seq for
205 transcriptome profiling, and metabolic profiling of peripheral blood to gain insights into
206 metabolic alterations (**Figure 2A**).
207
208 **Unique protein expression features of different HER2 groups of GCA patients**
209 First, we examined protein expression in our cohort and identified 8,864 proteins in both tumor
210 and NAT, where a similar number of proteins were identified in both tumor tissues (median
211 number = 5,088) and NAT (median number = 5,089). Among all identified proteins, 4,929
212 proteins could be quantified (50% NA cut-off in both tumors and NAT) (**Supplementary**
213 **Table 2**). We extracted signature proteins for each HER2 group using two independent
214 strategies in parallel: comparing protein expression from tumors only in different HER2 groups
215 and comparing protein expression by evaluating protein levels from the tumor vs. NAT in each
216 HER2 group.
217
218 In the strategy of tumor comparison only (**Methods**), we identified 23 specific proteins for the
219 HER2 high group, 6 proteins for the HER2 low group, and 92 proteins for the HER2 negative
220 group (Fold Change > 1.5, $p < 0.05$) (**Supplementary Figure 3A**, **Figure 2B**, **Supplementary**
221 **Table 3**). Not surprisingly, the HER2 protein was found in the protein list of the HER2 high
222 group (**Figure 2B**, **Supplementary Table 3**). Only 6 proteins, from coding genes of
223 SLC25A19, TTC17, P2RX4, STAT5A, C5orf51, and H3.3A, were specifically enriched in the
224 HER2 low group. Among these 6 proteins, genes of P2RX4 and STAT5A were reported to be
225 involved in tumor inflammation[33,34]. The HER2 negative group exhibited the highest number
226 of differentially expressed proteins, which includes an oncogene of EGFR, and couples of
227 extracellular proteins, COL3A1, VCAM1, SFRP4, and GJA1. To better understand the
228 biological functions of HER2 group-specific proteins, we performed gene set enrichment
229 analysis (GSEA) of hallmark gene sets on each HER2 group comparing with the rest, and

230 different hallmark gene sets were found in each HER2 group (False discovery rate (FDR) <
231 0.05) (**Figure 2C**, **Supplementary Figure 3B**, **Supplementary Table 4**). In the HER2 high
232 group, hallmark gene sets of Myc target v1, Myc targets v2, mTORC1 signaling, Unfolded
233 protein response, E2F targets, Glycolysis, and Peroxisome were enriched. Enrichments of E2F
234 targets, Myc targets, and mTORC1 signaling probably reflect the stronger proliferation feature
235 of high expression of HER2 protein. Similar to the HER2 high group, the hallmark gene set of
236 E2F targets was also observed in the HER2 low group; it may also reflect the proliferation
237 features in the HER2 low group. Very strikingly, five of the six hallmark gene sets enriched in
238 the HER2 low group have strong inflammation features, including Interferon alpha response,
239 Interferon gamma response, TNFA signaling via NFκB, Inflammatory response, and Allograft
240 rejection. Such observations may indicate stronger inflammation in the HER2 low group.
241 In addition, HER2-negative groups are enriched with four hallmark gene sets: Myogenesis,
242 KRAS signaling DN, Hypoxia, and Epithelial-mesenchymal transition (EMT). The hallmark
243 enrichments of Myogenesis and EMT in the HER2 negative group agree with the HER2
244 negative specific proteins list with extracellular proteins, which may also explain the
245 correlation of HER2 grouping with tumor differentiation and Lauren classification
246 (**Supplementary Figure 2B-D**).
247
248 Since the genetic background for each patient is diverse, extracting protein signatures only
249 from the tumor part has the potential to filter away tumor features from patients and may also
250 potentially remove key features due to a statistical cutoff. Thus, we also performed GSEA
251 hallmark gene sets by using tumors from each HER2 group vs. their corresponding NAT
252 (**Figure 2D**, **Supplementary Table 5**). In the hallmark gene sets enrichment from GSEA, cell
253 proliferation-relevant hallmarks, including Myc targets v1, G2/M checkpoint, and E2F targets,
254 are all enriched in the three HER2 groups. Meanwhile, we observed that the hallmark of Myc
255 targets v1 is more strongly enriched in HER2 high and low groups compared to the HER2
256 negative group, and the hallmark of Myc targets v2 is enriched in HER2 high and HER2 low
257 groups but not in the HER2 negative group. This probably reflects the role of the HER2 protein
258 in the regulation of the cell cycle. Even though the hallmark of EMT is enriched in all three
259 HER2 groups, it is much more significantly enriched in the HER2 negative group, which agrees
260 with the GSEA enrichment from tumor only. Enrichments of inflammation relevant hallmarks
261 of GSEA terms, including Interferon gamma response, Interferon alpha response, Allograft
262 rejection, Complement, and Inflammatory response, are observed in all three groups; however,
263 it clearly shows that the hallmark of interferon-alpha response is much more enriched in the

264 HER2 low group. This is also consistent with the observation that the HER2 low group exhibits
265 inflammation features by GSEA enrichment analysis using the tumor only. Very specifically,
266 hallmarks of DNA repair and Angiogenesis are only enriched in the HER2 high group; the
267 hallmark of PI3K/Akt/mTOR signaling is only observed in the HER2 low group; and the
268 hallmark of Apical junction only shows in the HER2 negative group. Since the tumor
269 differential stage of GCA patients is significantly associated with HER2 groups from clinical
270 pathological association analysis, and the enrichment of the Apical junction hallmark and
271 stronger enrichment of EMT in the HER2 negative group from tumor vs. NAT, our GSEA
272 analysis strongly indicates HER2 expression is associated with cancer differentiation.
273
274 Next, we performed differential protein expression analysis between tumor vs. NAT for each
275 HER2 group (Fold Change > 1.5, $p < 0.05$) (**Figure 2E-G**, **Supplementary Figure 3C**,
276 **Supplementary Table 6**). We identified 167 up-regulated proteins and 299 down-regulated
277 proteins in tumors of the HER2 high group, 99 up-regulated proteins and 251 down-regulated
278 proteins in the tumors of the HER2 low group, and 154 up-regulated proteins and 305 down-
279 regulated proteins in the tumors of the HER2 negative group. The significant difference of
280 HER2 protein level is only observed in the HER2 high group but not in the low and negative
281 groups (**Supplementary Table 6**), which further indicates our grouping strategy works well.
282 Gene ontology (GO) terms enrichment analysis from three HER2 groups using significant up-
283 regulated proteins from the tumor part as the input (**Figure 2H**, **Supplementary Table 7**). The
284 top 10 enriched GO terms in the HER2 high group are about extracellular matrix organization
285 (4 GO terms), DNA replication (2 GO terms), defense response to bacterium (2 GO terms),
286 protein hydroxylation, and biological process involved in symbiotic interactions (**Figure 2H**).
287 Minichromosome maintenance (MCM) proteins, MCM2, MCM3, and MCM7, are involved in
288 replication control[35] and in the differential protein list of the HER2 high group, which further
289 demonstrates the stronger proliferation features in the HER2 high groups. Very interestingly,
290 the top 10 GO terms in the HER2 low group are all from immune-response-relevant terms, e.g.,
291 antigen processing and presentation of peptide antigen, major histocompatibility complex
292 (MHC) protein complex, and defense response. Seven of the top 10 enriched GO terms in the
293 HER2 negative groups overlap with the top 10 enriched GO term from the HER2 low group.
294 However, three GO terms from the Top 10 enriched GO term in the HER2 low group about
295 response to virus, defense response to virus, defense response to symbiont, and Response to
296 virus are both significantly enriched in HER2 high and low groups but not in the HER2 negative
297 group. Interestingly, three GO terms of extracellular matrix, including Extracellular matrix

organization, Extracellular structure organization, External encapsulating structure organization, are both enriched in HER2 high and negative groups but containing different gene sets (**Figure 2H**), where TGFB1 is specifically up-regulated in the HER2 negative group. It is well known that TGFB1 plays an important role in epithelial to mesenchymal transition (EMT)[36]; thus, the up-regulated of TGFB1 in the HER2 negative group further suggests the distinct cancer differentiation stage in the HER2 negative group compared with the others.

We also focused on the tumor up-regulated protein analysis and extracted the common and unique proteins in the three HER2 groups (**Supplementary Figure 4**, **Figure 2E-G**). With cross-comparison, there are 60 HER2 high group-specific proteins, where HER2 protein is one of them. MCM2, MCM3, and MCM7, which are included in DNA replication and repair[37,38], are specifically enriched in the HER2 high group; such observations further demonstrate the function of HER2 in the regulation of the cell cycle. In the HER2 low group, there are only 15 specific up-regulated proteins, where inflammatory-relevant proteins[39], including TAP1, TAP2, IFT1, and IFIT3, are specifically enriched in those proteins, which agrees with the findings in GSEA and GO term enrichment analysis and further indicates the strong inflammation features in the HER2 low group. In the HER2 negative group, 47 specific proteins are identified, where extracellular matrix organization proteins, such as FBLN5, TGFB1, FSCN1, VWA1, COL4A1, MMP2, RB1, and EFEMP2, are included. The MHC is also known as the human leukocyte antigen (HLA) system, and it plays a pivotal role in the immune system's ability to recognize and respond to tumors and antigen processing and presentation proteins[40]. It is worth noting that HLA-DRA and HLA-A are only enriched in HER2 negative groups. Sixty-two common proteins with higher expression in tumors compared to NAT were also identified with such a comparison. In summary, the comprehensive analysis of protein expression from MS in different HER2 GCA patients revealed very distinct protein expression features based on HER2 expression level. HER2 high groups have stronger proliferation and DNA repair features, while HER2 negative and low groups exhibit stronger inflammation features. EMT features observed in HER2 negative groups also indicate that HER2 may play important roles in tumor differentiation. Our detailed characterization of protein expression for each HER2 group may provide unique guidance for therapeutical design.

Variations in genome instability across HER2 subgroups in GCA with consistent tumor mutational burden

331 Next, we examined genome mutation and amplification with WES of tumors (n = 113),
332 peripheral blood (n = 112), and NAT (n = 1) among the three HER2 groups (**Figure 3**,
333 **Supplementary Figure 5A**, **Supplementary Table 8**). Somatic short variants, including
334 single nucleotide variants (SNV) and insertions and deletions (InDels), frequencies analysis of
335 the three distinct HER2 groups showed: the HER2 high group, with a median count of short
336 variants 96; the HER2 low group, with a median count of short variants 87; and the HER2
337 negative group, with a median count of short variants 80 (**Supplementary Figure 5B**). It's
338 worth noting that although a slight reduction in frequencies of SNV and InDels were observed
339 in the HER2 negative group compared to the other two groups, statistical analysis did not reveal
340 any significant differences (**Supplementary Figure 5B**). Additionally, our investigation
341 revealed a high degree of similarity in mutation types across all three groups (**Supplementary**
342 **Figure 5C**). Furthermore, our assessment of tumor mutation burden (TMB) in these groups
343 showed no significant distinctions in either non-synonymous or SNV frequency
344 (**Supplementary Figure 5D**). Moreover, we delved deeper into the mutation landscape by
345 ranking the top 15 mutated cancer genes in the whole cohort and within different HER2 groups
346 (**Figure 3A**, **Supplementary Table 9**). These cancer genes included *TP53* (77.9%), *MUC16*
347 (27.4%), *CSMD3* (23.0%), *FAT3* (23.0%), *LRP1B* (19.5%), *FAT4* (19.5%), *MUC4* (19.5%),
348 *PREX2* (15.0%), *SPTA1* (14.1%), *ARID1A* (13.2%), *BIRC6* (12.3%), *DCC* (11.5%), *GNAS*
349 (10.6%), *CTNNA2* (10.6%), *COL5A1* (9.7%), *APOB* (9.7%), *DMD* (8.8%), *NBEA* (8.8%),
350 *ZFHX3* (8.8%), and *PTPRT* (8.0%). Notably, *TP53,* a tumor suppressor gene, emerged as the
351 top-ranked mutated one, with a prevalence of 77.9% across all patients, 88.1% in the high
352 group, 71.1% in the low group, and 73.1% in the negative group. *MUC16* was present in 27.4%
353 of all patients, 21.4% in the high group, and higher in both the low (31.1%) and negative (30.8%)
354 groups. *FAT3* exhibited a higher prevalence in the high group (22.6%) and the low group
355 (22.4%), but was found in only 15.4% of the negative group. Additionally, we ranked the most
356 mutated genes based on gene pathways, revealing that genes involved in the Cell cycle, T cell
357 differentiation and proliferation, Ras signaling, Notch signaling, MAPK, and Histone
358 modification are prominently featured at the top of the ranking list (**Supplementary Figure**
359 **5E**). In summary, our findings suggest that the mutations observed in different HER2 groups
360 do not exhibit significant variation, underscoring that TMB may not be the primary
361 distinguishing factor among these three groups.
362
363 Subsequently, we conducted an assessment of chromosomal instability (CIN) in three distinct
364 groups using genome integrity index (GII). The results unequivocally demonstrate

365 substantially higher genome instability in the HER2 high group when compared to the HER2
366 negative group (**Figure 3B**, p = 0.015). Even with a higher number of copy number alterations
367 (CNA) from the HER2 high group, the analysis of CNA reveals a statistically non-significant
368 difference among the three groups (**Figure 3C**, p = 0.064). To have a better understanding of
369 genome amplification among the three HER2 groups, we also calculated the amplification
370 frequency of the genome based on bins of the genome with a 1Mbp window size (**Method**,
371 **Figure 3D**, **Supplementary Figure 6**, **Supplementary Table 10**). With such an approach, 158
372 regions (1Mbp) have a significantly different amplification among these three HER2 groups.
373 In brief, 142 regions amplify more than the other two groups in the HER2 high group, and 16
374 regions amplify more than the HER2 high and low groups in the HER2 negative group
375 (**Supplementary Table 10**). However, there are no regions amplifying more from the HER2
376 low group compared to the other two. Furthermore, we also observed substantial copy number
377 amplifications in specific subregions of Chromosome 15 and Chromosome 20 in both the
378 HER2 high and low groups, which were not as prevalent in the HER2 negative group (**Figure**
379 **2D**, **Supplementary Figure 6**). Clearly, subregions of Chromosome 13, 15, and Chromosome
380 17 in HER2 high amplify more than the other two groups (**Figure 3D**, **3E**). Surprisingly,
381 subregions of Chromosome 19 have high amplification in both HER2 high and negative groups
382 but not in the low group (**Figure 3D**). We also checked the occupancy of oncogenes and tumor
383 suppressor genes (TSG) in the different amplification regions (**Figure 3D**, **3E**). Many
384 oncogenes presenting subregions, e.g., *CCNE1*, *MLLT1*, *CCND3*, *FGFR3*, et al., are highly
385 amplified in HER2 high but not the other two groups (**Figure 3D**). Very surprisingly, the
386 subregion of chromosome 13, containing a TSG, *BRCA2*, amplified higher in the HER2 high
387 group than that of HER2 low and negative groups (**Figure 3E**, p = 0.0455). We also observed
388 there is a markedly higher frequency of amplifications observed in the *ERBB2* gene loci within
389 the HER2 high group (31%, p = 1.4397e-06), whereas such amplifications are not prominent
390 in the low or negative groups (0%) (**Figure 3D**, **3E**). This observation aligns with our prior
391 research, which established a link between *ERBB2* focal amplification and improved prognosis
392 in GCA patients[13]. It is worth noting, another TSG, *BRCA1*, also located on Chromosome 17
393 and ~2Mbp away from the *ERBB2* gene, is also with a higher number of amplifications in the
394 HER2 high group comparing with others, even statistically such difference is not significant
395 (7.14% for high group, 2.27% for low group, and 0% for the negative group, p = 0.249) (**Figure**
396 **3D**, **3E**). *BRCA1* and *BRCA2* are both TSGs, and their functions are well-studied in breast
397 cancer[41], playing an important role in DNA repair in tumors[42]. The high-frequency
398 amplification of these two TSGs in the HER2 high group may interpret the enrichment of

399 GSEA and GO terms related to DNA repair in the HER2 high group. High levels of HER2
400 expression are well-known as a worse prognostic marker for breast cancer[43], which is very
401 different from GCA patients. The high amplification of *BRCA1* and *BRCA2* in the HER2 high
402 group may also explain the potential reason for the favorable prognosis in the HER2 high group
403 of GCA patients. In summary, our findings lead us to conclude that HER2 subgroups in GCA
404 with consistent tumor mutational burden, but the HER2 high group exhibits a notably higher
405 frequency of genome amplifications in comparison to the other two groups.
406
407 **Strong inflammation features are observed in HER2-negative groups**
408 Next, we examined the gene expression features in each HER2 group with RNA-seq
409 (**Supplementary Figure 7A**), namely the High group (n = 19), Low group (n = 18), and
410 Negative group (n = 17). Clearly, the RNA expression profiles from tumors are distinct from
411 NATs (**Supplementary Figure 7B**). We undertook a comprehensive investigation of gene
412 signatures of each HER2 group, employing two distinct analytical strategies: tumor-only
413 comparison and tumors comparison with their corresponding NAT within the same group
414 (**Figure 4**).
415
416 In the tumor-only comparison, we first conducted GSEA of cancer hallmarks for the signature
417 genes specific to each group. This analysis revealed that the HER2 high group exhibited
418 significant enrichment in six cancer hallmark terms (**Figure 4A**, **Supplementary Table 11**),
419 including E2F target, MYC targets v1 and v2, G2/M checkpoint, DNA repair, and Oxidative
420 phosphorylation. The stronger proliferation feature in the HER2 high group agreed with
421 features captured from GSEA enrichment from the protein assay. It is worth noting that DNA
422 repair features are extracted from gene expression but not the protein assay; one possibility is
423 the number of proteins captured in MS is much less than in RNA-seq. Meantime, the strong
424 DNA repair feature in the HER2 high group further indicates that the HER2 high group has a
425 better capacity to repair DNA damage. In the HER2 low group, with a notable 20 cancer
426 hallmarks being enriched, where terms, E2F target, MYC targets v1 and v2, G2/M checkpoint,
427 and DNA repair, were observed in both the HER2 high and low groups. In addition, TNFA
428 signaling via NFκB and Interferon gamma response, signifying stronger inflammation, were
429 also enriched in the HER2 low group. In contrast, the HER2 negative group only displayed
430 enrichment in Inflammatory response and Allograft rejection. Enrichment of inflammation
431 feature in both the HER2 low and negative groups suggests there is stronger inflammation in
432 the HER2 low and negative GCA tumor. Then, we conducted a differential gene expression

433 analysis across the three different HER2 groups, identifying a total of 572 significantly
434 differentially expressed genes (Fold Change > 1.5, FDR < 0.05) (**Figure 4B**, **Supplementary**
435 **Figure 7C**, **Supplementary Table 12**). These genes were assigned to the HER2 high (n = 35),
436 HER2 low (n = 34), HER2 negative (n = 89), common HER2 high and low group (n = 322),
437 common HER2 low and negative group (n = 25), and common HER2 high and negative group
438 (n = 67) (**Figure 4B**). The presence of the *ERBB2* gene within the signature gene list of the
439 HER2 high group further corroborates the accuracy of our grouping strategy. Interestingly, we
440 found oncogenes, *MYC*, *FOSL1*, *EREG*, *EGF*, *IER5*, and *BCL6,* are enriched in the HER2 low
441 group only. But, *CCNE1*, a cell cycle-controlling gene, is enriched in both HER2 high and low
442 groups but not in the HER2 negative group, which probably reflects the stronger proliferation
443 features of HER2 high and low groups. *H2AFX* gene plays an important role in DNA repair[44]
444 and is also enriched in only HER2 high and low groups, which also agrees with the enrichment
445 of DNA repair hallmark in the HER2 high group from protein analysis (**Figure 2D**). Infection
446 and immune response genes[45], e.g., Tumor necrosis factor (TNF) superfamily genes (*TNFSF4*
447 and *TNFSF18*), and Tripartite motif family genes (*TRIM50*), are only enriched in HER2
448 negative groups. In addition, the inflammatory cytokine interleukin 6 (*IL-6*) [46] was observed
449 with a much higher expression level in the HER2 negative group compared with the HER2
450 high and low groups, even statically not significant (log2 (Fold Change) = 1.52, p = 0.056)
451 (**Supplementary Table 12**). Such observation further suggests the stronger inflammation in
452 the HER2 negative group.
453
454 We subsequently performed GSEA analysis in each HER2 group with tumor vs. their
455 corresponding NAT (**Figure 4C**, **Supplementary Table 13**). Notably, we identified common
456 strong enrichment in cancer hallmarks among these three groups, such as Interferon gamma
457 response, Myc targets v1, G2/M checkpoint, interferon alpha response, E2F targets, and
458 allograft rejection. The hallmark of EMT was also observed in all three groups, but there is
459 much stronger enrichment in the HER2 low and negative groups, similar to the observation in
460 protein analysis among different groups. Furthermore, terms related to complement,
461 coagulation, and Kras signaling were enriched in all three HER2 groups. However, specific
462 enrichment patterns distinguished these groups, with TNFA signaling via NFκB, Apical
463 junction, IL-6/JAK2/STAT3 signaling, Apoptosis, IL2 STAT5 signaling, UV response UP, and
464 TGF-beta signaling being unique to HER2 low and negative groups. Myogenesis, Hypoxia,
465 and UV response DN were only enriched in the HER2 negative group. Meanwhile, terms
466 related to mitotic spindle, mTORC1 signaling, glycolysis, and unfolded protein response were

467 exclusively enriched in the HER2 high and low groups. The hallmark of DNA repair is much
468 more strongly enriched in the HER2 high and low groups. In summation, our analysis
469 underscores the presence of a robust DNA repair signature in the HER2 high group, potentially
470 indicative of a positive prognostic indicator for HER2 high patients. Furthermore, the stronger
471 enrichment of the inflammatory response in the HER2 low and HER2 negative groups suggests
472 the presence of prominent inflammatory features within these groups.
473
474 Additionally, we conducted a differential gene expression analysis by comparing tumor tissues
475 with their corresponding NATs (Fold Change > 2, FDR < 0.05). This analysis identified 3409
476 differentially expressed genes in the HER2 high group, 3603 differentially expressed genes in
477 the HER2 low group, and 3057 differentially expressed genes in the HER2 negative group
478 (**Supplementary Figure 8A**, **Figure 4D**, **Supplementary Table 14**). We focused on up-
479 regulated genes in tumors comparing with NAT and found that 605 genes are commonly up-
480 regulated in all three groups, 599 genes are HER2 high group-specific up-regulated, 409 genes
481 are HER2 low group-specific up-regulated, and 649 genes are HER2 negative group-specific
482 up-regulated (**Supplementary Figure 8B**, **Supplementary Table 15**). The common
483 upregulated genes among different groups are: 434 genes between HER2 high and low group;
484 386 genes between HER2 low and negative group; 112 genes between HER2 high and negative
485 group. As expected, *ERBB2* is significantly expressed in the HER2 high group of tumors
486 comparing with their NAT but not in low and negative groups. Intriguingly, among these genes,
487 the MHC class II gene *HLA-DRB1* is exclusively active in the HER2 negative and low groups
488 (**Figure 4D**). Given the significance of the MHC in immune responses against tumors, our
489 observations prompted a comprehensive examination of all MHC molecules (**Figure 4E**),
490 including both class I and class II genes, across the three distinct HER2 groups. Our analysis
491 revealed that *HLA-A* and *HLA-B* were highly expressed in tumors of all three HER2 groups,
492 while *HLA-G* exhibited high expression in the tumors of both the HER2 high and low groups.
493 Interestingly, *HLA-C* displayed high expression exclusively in the HER2 negative groups.
494 Strikingly, with the remaining MHC class II genes, *HLA-DMB*, *HLA-DRA*, *HLA-DQB1*, and
495 *HLA-DQA1*, being active solely in the HER2 low and negative groups.
496
497 In our subsequent analysis, we delved into GO term analysis using the list of up-regulated
498 genes in tumors obtained from the comparison of tumors with NATs (**Supplementary Table**
499 **16**). To confirm the strong proliferation and DNA repair features of HER2 high expression,
500 and the inflammation feature of the HER2 negative group from GSEA analysis, we first

501 extracted and compared the GO terms from the cell cycle (**Supplementary Figure 9A**), DNA
502 repair (**Supplementary Figure 9B**), and inflammatory (**Supplementary Figure 9C**)
503 signatures in three groups. It clearly showed cell cycle and DNA break repair-relevant GO
504 terms strongly enriched in the HER2 high group and low group (**Supplementary Figure 9**),
505 but inflammatory terms strongly enriched in the HER2 negative group. We also extracted
506 exclusively up-regulated genes in each HER2 group for these targeted GO terms
507 (**Supplementary Table 17**). In the list of exclusive genes from DNA repair GO terms, it is
508 worth noting that *H2AFX* (known as *H2AX*) and *BRCA2* genes, important genes in DNA
509 repair[42,44], are significantly expressed in the HER2 high group of tumors comparing with its
510 corresponding NAT but not in the HER2 low and negative groups (**Figure 4D**, **Supplementary**
511 **Table 17**). Strikingly, *BRCA1* gene is expressed significantly higher in the tumor comparing
512 with NAT in the HER2 high group (Log2(Fold Change) = 0.94, FDR = 0.00013) and low group
513 (Log2(Fold Change) = 0.97, FDR = 0.00014), but not in the HER2 negative group (Log2(Fold
514 Change) = 0.28, FDR = 0.3463), even though the Fold Change is slightly lower than the cutoff.
515 Putting together, we further confirmed that strong DNA repair features are only available when
516 HER2 is expressed in GCA patients. Combining CNA analysis of *BRCA1* and *BRCA2* loci
517 from three HER2 groups (**Figure 3D**, **3E**), our results suggested that the amplification of
518 *BRCA1* and *BRCA2* could potentially contribute positively to the higher expression of these
519 two genes in HER2 positive groups, boost the DNA repair capacities in HER2 expressed group
520 and further contribute to the better prognosis of GCA patients. Subsequently, we also extracted
521 the significantly enriched MHC class I and class II GO term from three groups; it clearly
522 showed MHC class II GO terms are only enriched in the negative group (**Supplementary**
523 **Figure 9D**). The list of exclusive genes from the HER2 negative group in such MHC class II
524 GO terms contains a large number of MHC class II genes and its relevant genes, *TREM2*, *CTSL*,
525 *CTSS*, *PYCARD*, *HLA-DRB1*, *HLA-DMB*, *HLA-DRA*, *HLA-DQA1*, *HLA-DQB1*, *HLA-DQB2*,
526 et al (**Supplementary Table 17**). Such findings further demonstrate the existence of distinct
527 anti-inflammatory responses from the immune system in the HER2 negative group.
528
529 We also examined the top-ranking enriched GO terms for each HER2 group. Notably, our
530 findings reveal a striking pattern (**Figure 4F**): in the HER2 high group, a remarkable all the
531 top 15 GO terms pertain to processes associated with the mitotic cycle and chromosome
532 segregation. This pattern is mirrored in the HER2 low group, where 9 of the top 15 GO terms
533 similarly center around mitotic cycle processes and chromosome segregation. However, the
534 HER2 low group exhibits an additional layer of complexity, with terms being relevant to

535 inflammation, including processes such as leukocyte chemotaxis. In contrast, the top 9 of top
536 15 GO terms in the HER2 negative group predominantly revolve around inflammation-related
537 processes, accounting for a substantial 60% of the terms. Furthermore, a noteworthy
538 observation emerges when comparing the top three GO terms in both the HER2 low and
539 negative groups, as they overlap and pertain to extracellular matrix organization, extracellular
540 structure organization, and external encapsulating structure organization. When taken in
541 conjunction with the GSEA results, this convergence strongly supports the presence of
542 heightened inflammation and cytokine secretion in the HER2 negative groups. To validate our
543 hypothesis, we first examined the differential expression levels of all cytokine genes between
544 tumor and tumor-adjacent tissue within each HER2 group (**Figure 4G**). Our analysis revealed
545 the presence of commonly active cytokine genes across all three HER2 groups (*IL-11*, *CSF2*,
546 *CXCL6*, *CXCL8*, *CXCL9*, et al), as well as shared activation between the high and low groups
547 (*CMTM7*, *CCL7*, *MET,* et al) and the low and negative groups (*OSM*, *CCL13*, *CCR1*, *CCR8,*
548 et al). Notably, the HER2 negative groups exhibited a greater number of active cytokine genes
549 compared to the other two groups. Specifically, 22 cytokine genes were exclusively active in
550 the tumors of the HER2 negative group, including *IL-6* and *IFNG* (**Figure 4G**). *IL-6* is well-
551 known for its function in host defense through the stimulation of acute phase responses and
552 also plays a pathological role in chronic inflammation and autoimmunity[46]. In humans, the
553 IFN-γ protein, encoded by the *IFNG* gene, is the only known type II class of interferons and
554 plays an important role in both innate and adaptive immunity[47]. It was also reported that IFN-
555 γ is able to promote inflammation, antiviral or antibacterial activity, and cell proliferation and
556 differentiation[48]. The higher gene expression of *IL-6* and *IFNG* genes in tumors of the HER2
557 negative group further demonstrates the existence of distinct inflammatory responses from the
558 immune system in the HER2 negative group. While the presence of inflammation features in
559 all tumors is not surprising, given that inflammation is recognized as one of the hallmarks of
560 tumors[49], the enhanced inflammation observed in the HER2 negative and low groups is a novel
561 finding. In our second examination, we assessed the gene expression levels of a reported set of
562 tumor inflammation genes[50] (**Supplementary Figure 10**) (n = 18). Our analysis revealed that
563 50% of these genes were significantly higher expressed in tumors of the HER2 negative group,
564 44.4% in tumors of the HER2 low group, and only 16.6% in tumors of the HER2 high group
565 (**Supplementary Figure 10**). The heightened inflammation features and the activation of MHC
566 molecules in the HER2 negative groups strongly suggest the existence of distinct anti-
567 inflammatory responses and unique tumor microenvironments within these HER2 groups.

568 These findings provide valuable insights into the complex interplay between the immune
569 system and HER2 subtypes of GCA cancer
570
571 **Distinct tumor immune microenvironment and immune checkpoints in different group**
572 **of HER2 patients**
573 In order to gain a deeper understanding of the tumor microenvironment within distinct HER2
574 groups, we employed a versatile computational method, CIBERSORTx[51], to profile tumor-
575 infiltrating immune cells and quantify their fractions using bulk RNA-Seq data derived from
576 both tumors and NAT in the different HER2 groups. Our objective was to compare the
577 composition of immune cells among these three groups. A total of 22 types of immune cells
578 were identified in both tumors and NAT (**Figure 5A**, **Supplementary Figure 11A**), with no
579 significantly different proportion of any immune cell components observed in the NAT tissues
580 (**Supplementary Figure 11B**). In the comparison of tumors among three HER2 groups, the
581 only significant proportion difference is observed in M2 macrophages (**Figure 5A**, **5B**,
582 **Supplementary Figure 11C**). Notably, significant differences emerged only between the
583 HER2 high and HER2 negative groups in terms of M2 macrophages ($p = 0.036$) (**Figure 5B**),
584 with higher numbers of M2 macrophages in the HER2 negative group. At the same time, the
585 HER2 low group also has a bigger proportion of M2 macrophages comparing with the HER2
586 high group, even though statistically it is not significant ($p = 0.21$) (**Figure 5B**). To confirm
587 our computational predication of the availability of M2 macrophages in the tumor, we
588 performed immunofluorescent staining of M2 macrophage specific marker CD163[52] in three
589 different groups (**Figure 5C**, **5D**, **Supplementary Table 18**). The result proved there are more
590 M2 macrophage in HER2 low ($p = 0.016$) and negative group ($p = 0.18$) comparing with the
591 HER2 high group. M2 macrophages are often considered as anti-inflammatory or
592 immunoregulatory cells[53]. They help to limit and resolve the inflammatory response by
593 producing anti-inflammatory cytokines and promoting tissue repair[53-55]. It is not surprising to
594 observe a larger proportion of M2 macrophage in the HER2 negative and low group, since the
595 stronger inflammation is observed in them, and a larger proportion of M2 macrophages may
596 play a role in suppressing excessive inflammation in them. In addition, it was shown that M2
597 macrophages are associated with tumor-promoting activities and contribute to an
598 immunosuppressive environment within the tumor[53-56], making it more difficult for the immune
599 system to mount an effective anti-tumor response. Thus, our result also suggests HER2
600 negative and low groups are with a tumor-suppressive immune microenvironment and could
601 contain different immune response systems comparing with the HER2 high group. These

602 variations in the proportions of M2 macrophages suggest the presence of distinct immune
603 environments within the different HER2 groups, potentially characterized by differing immune
604 inhibitory checkpoints.
605
606 Given the widespread use of immune checkpoint blockade therapies in gastrointestinal
607 tumors[23-25,57], we sought to determine whether there were distinct immune inhibitory
608 checkpoints among three HER2 groups. To achieve this, we compared the RNA expression
609 levels of key immune inhibitory and stimulatory checkpoint genes, along with their paired
610 ligands and receptors[58], between tumor and NAT in each HER2 group (**Figure 5E**).
611 Surprisingly, we did not observe significant differences in the PD-L1 (*CD274*) and PD1
612 (*PDCD1*) gene pairs. Instead, we noted substantially higher PD-L2 (*PDCD1LG2*) gene
613 expression in the HER2 low and negative groups, in contrast to the HER2 high group. While
614 PD1/PD-L1 inhibitors are frequently employed in immune therapy in gastroesophageal cancers,
615 their outcomes vary among patients[23,24]. Our findings suggest that PD-L2 inhibitors may be a
616 more suitable option for immune therapy in HER2 low or negative groups. Furthermore, we
617 identified significantly higher expression of the *SIRPA* gene in tumor tissue compared to NAT
618 in both the HER2 low and negative groups, but not in the HER2 high group. The interaction
619 between macrophage checkpoint CD47-SIRPα has garnered attention as a potential target for
620 cancer therapy[59-61], although it has not been extensively explored in gastrointestinal tumors.
621 Our findings provide compelling evidence that SIRPA or CD47 inhibitors may hold promise
622 for therapeutic use in HER2 low and negative groups. Additionally, we observed higher
623 expression of *FGL1* in the HER2 negative group. *LAG3* is considered one of the most
624 promising immune checkpoints alongside PD-1 and CTLA-4[62]. Elevated expression of LAG3
625 and FGL1 promotes tumor growth by inhibiting the immune microenvironment[63,64]. Therefore,
626 specific LAG3/FGL1 inhibitors may prove to be ideal candidates for the HER2 negative group
627 in the future. Lastly, we identified higher expression of *HHLA2* in both the HER2 high and low
628 groups. Among the common active immune checkpoint genes across all three HER2 groups
629 are *CD86*, *TNFSF18*, *CD86*, *IDO1*, *TNFRSF9*, *TNFRSF4*, and *HAVCR2*. The HER2 low group
630 displayed specific immune checkpoints in *PVR* and *CD276*. In summary, the identification of
631 common and unique immune checkpoints within different HER2 groups in GCA offers
632 valuable insights into potential targets for future clinical trials in immune therapy. These
633 findings hold promise for the development of tailored immune-based therapeutic strategies to
634 improve patient outcomes.
635

636 **HER2 group-specific ligand-receptor signaling between tumors and NAT macro-**
637 **environment**

638 The distinct inflammation features and unique tumor immune microenvironments observed
639 within the various HER2 groups prompted us to investigate ligand-receptor signaling between
640 tumor and NAT from paracrine pathways (**Figure 6**, **Supplementary Figure 12**). Our analysis
641 focused on growth factors, inflammation-related factors, and fibrosis-related ligand-receptor
642 pairs in these tissues. We visualized these interactions by considering their directionality and
643 connectivity strength (**Figure 6A**). We identified different ligand-receptor signaling patterns
644 for each HER2 group (**Figure 6B**). Specifically, ACTIVIN, NODAL, SEMA3, and BMP were
645 unique to the HER2 negative group. It is worth noting that NODAL and BMP, members of the
646 TGF-beta superfamily[65,66], were both specific to the HER2 negative group. However, NODAL
647 was secreted from the NAT to the tumor tissue, while BMP is secreted from the tumor to NAT.
648 In the HER2 low group, we found specific pathways involving AVP and SOMATOSTATIN.
649 The HER2 high group exhibited six unique pathways, including EGF, WNT, EDA, AGT,
650 PMCH, and BRADYKININ. Notably, the common pathways between the HER2 low and
651 negative groups were LIFR, IL10, IFN-I, ENHO, CALCR, which are inflammation-relevant
652 factors[67], underscoring shared inflammation features in these groups. There is no shared
653 pathway among all three HER2 groups (**Figure 6B**). NRG pathway, which belongs to the
654 epidermal growth factor family and interacts with receptors of ERBB family[68], is only observed
655 in HER2 high and negative groups. However, the directionality and connectivity features
656 within the NGR pathway were notably distinct among them (**Figure 6C**). This pathway
657 initiated from the NAT with NRG1 and targeted the tumor tissue through ERBB2 and ERBB3
658 receptors in the HER2 high group. In the HER2 negative group, where ERBB2 was absent, the
659 receptor in the tumor was ITGAV and ITGB3, activated by the signal from NRG1 in the NAT.
660 However, in the HER2 low group, the pathway began with NRG4 in the NAT, targeting NAT
661 through ERBB2 and ERBB4 receptors. Our newly unveiled HER2 group-specific interactions
662 between the tumor microenvironment and macroenvironment further support the distinct tumor
663 features present in the different HER2 groups. Additionally, these findings provide potential
664 molecular targets for future therapeutic applications.
665

666 **Negative HER2 expression is associated with fatty acid metabolic profiles and**
667 **inflammation in blood of GCA patients**

668 Next, we conducted a meticulous metabolic profiling of peripheral blood mononuclear cells
669 (PBMC) utilizing the ultrasensitive liquid chromatography with tandem mass spectrometry

670 (LC-MS-MS) method in our cohort of 128 GCA patients. The objective was to perform a
671 comprehensive comparison among three HER2 groups, aiming to identify potential peripheral
672 metabolic features or biomarkers. From this analysis, we identified a total of 784 components
673 from PBMC (**Supplementary Figure 13**, **Supplementary Table 19-21**).
674
675 We proceeded with paired comparisons, including HER2 high group vs. HER2 low group,
676 HER2 high group vs. HER2 negative group, and HER2 low group vs. HER2 negative group.
677 When comparing HER2 high vs. HER2 low groups, only a few significantly different
678 components were identified (Fold Change > 1.3, $p < 0.05$) (**Figure 7A**). Specifically, three
679 components (2-Phenylacetamide, Benzoic Acid, and Norambreinolide) were unique to the
680 HER2 high group, while eight components (1-Aminopropan-2-ol, Trimethylamine-N-Oxide,
681 Carnitine-C20-2, Arachidyl glycine et al) were specific to the HER2 low group (**Figure 7B**).
682 This observation indicated a high degree of similarity between the metabolic profiles of PBMC
683 in the HER2 high and low groups. Notably, the three specific components found in the HER2
684 high group were natural products in the blood with unclear biological functions.
685 Trimethylamine-N-Oxide, previously reported to be highly relevant to inflammation in the
686 intestine[69], likely reflects inflammation features in the HER2 low group. Carnitine-C20-2 is
687 associated with fatty acid metabolism[70], suggesting different fatty acid metabolic mechanisms
688 between the HER2 high and low groups. In the comparison between HER2 low and negative
689 groups (**Figure 7A**, **7B**), 16 specific components were identified for the HER2 low group, and
690 9 specific components were found for the HER2 negative group (Fold Change > 1.3, $p < 0.05$).
691 Notably, components related to chronic inflammation, such as prostaglandin F2 alpha (PGF2
692 alpha) and thromboxane B2 (TXB2), were enriched in the HER2 negative group, corroborating
693 the presence of inflammation features in this group. Among the 9 specific components in the
694 negative group, Glycocholic Acid, Glycine deoxycholic acid, and 3-Methylcrotonyl glycine
695 were products of fatty acid metabolism. In contrast, products of carbohydrate metabolism,
696 including Kojibiose, D-positive Turanose, and D-Glucose, were only enriched in the HER2
697 low group. This divergence indicated an association between HER2 expression and distinct
698 metabolic mechanisms in PBMC. This association was further observed in the comparison
699 between HER2 high and negative groups (**Figure 7A**, **7B**), where 12 specific components were
700 identified for the HER2 high group, and 34 specific components were found for the HER2
701 negative group (Fold Change > 1.3, $p < 0.05$). Within the HER2 negative-specific components,
702 11 out of 34 components, such as Carnitine ph C14, glycine deoxycholic acid, and glycocholic
703 acid, were related to fatty acid metabolism[71]. Conversely, fatty acid metabolism-related

704 products were not significantly enriched in the HER2 high group, while carbohydrate
705 metabolic-relevant products, such as D-glucose, D-positive Turanose, Kojibiose, and D
706 Glucoronic Acid, were specific to the HER2 high group. Additionally, components relevant to
707 inflammation, PGF2 and TXB2[72], were also observed in the HER2 negative-specific list.
708 Remarkably, lysophosphatidylcholine (LPC) family products, including LysoPC-15, -17, and
709 -20, were significantly enriched in the HER2 negative group. LPC is reported to play a
710 significant role in atherosclerosis and inflammatory diseases[73].
711
712 To confirm this intriguing finding, we cross-checked metabolic components by comparing
713 PBMC metabolic lists between HER2-positive GCA patients (IHC HER2 3+, n = 6) and HER2-
714 negative GCA patients (IHC HER2 0+, n = 69) from another GCA cohort (**Figure 7C**,
715 **Supplementary Table 22**). We identified 10 HER2 3+ specific metabolic products and 46
716 HER2 0+ specific metabolic products. The results clearly demonstrated that LPC family
717 products, such as LysoPC-18, were specifically significantly enriched in HER2 0+ GCA
718 patients. Therefore, the higher enrichment of LPCs in HER2-negative groups and HER2 0+
719 GCA patients strongly indicates the association between inflammation features and the absence
720 of HER2 expression. Furthermore, our metabolic analysis in PBMC strongly indicates an
721 association between HER2 expression, metabolic types, and inflammation in patients' blood.
722 Blood tests are common procedures in clinical diagnosis, and our findings could be valuable
723 for revealing potential prognostic biomarkers in PBMC to identify HER2-relevant groups of
724 GCA patients. In the future, conducting studies with a larger sample size of GCA patients could
725 further elucidate valuable HER2-relevant prognostic markers during the early blood tests for
726 GCA patients.
727
728 **Discussion**
729 In this study, we employed a highly sensitive molecular counting method utilizing mass
730 spectrometry to assess HER2 expression in GCA patients. The assessment categorized patients
731 into HER2-high, -low, and -negative groups, leading to the acquisition of novel insights into
732 GCA and the identification of new therapeutic targets, particularly within the HER2-negative
733 subgroup. Our analysis revealed HER2 as a significant prognostic marker for esophagogastric
734 junction adenocarcinoma, GCA, and EAC. The HER2-high group exhibited a better prognosis
735 independent of therapeutic strategies, contrary to the typically worse prognosis associated with
736 high HER2 expression in other tumors, such as breast cancer[43]. This intriguing observation
737 suggests a distinctive role of HER2 in GCA compared to other cancer types. While anti-HER2

738 therapy combined with immune therapy shows promise for HER2-positive patients with IHC
739 scoring[23,24,31], the limited positive rate of HER2 IHC staining necessitates alternative
740 therapeutic approaches, such as chemotherapy and immune therapy[26-28], for HER2-negative
741 groups. Our multiple omics molecule profiling and HER2 grouping method uncovered new
742 therapeutic targets for HER2-low and -negative groups. Despite observing no significant
743 difference in mutation burdens among the three HER2 groups, we found heightened genome
744 instability in the HER2-high group. Notably, there was a significant enrichment of DNA repair
745 pathways in the HER2-high GCA group, possibly contributed by the amplification and
746 overexpression of TSGs, *BRCA1*, and *BRCA2* genes, potentially explaining the improved
747 prognosis in this subgroup. Strong proliferation features in the HER2-high group could serve
748 as targets for therapeutic designs. Conversely, HER2-low, particularly HER2-negative groups,
749 displayed significantly stronger inflammation features. Thus, it is reasonable to consider anti-
750 inflammatory drugs as part of the treatment regimen for HER2-low and -negative group
751 patients, in conjunction with other therapeutic methods.
752
753 Furthermore, our result also suggested HER2-negative and low groups have a tumor
754 suppressive immune microenvironment compared with the HER2-high group. Our work delves
755 into the response variability of GCA patients to specific immune inhibitory checkpoint
756 treatments, such as anti-PD-1 and PD-L1[23,24]. Identifying distinct tumor microenvironments
757 and variations in immune inhibitory checkpoints across HER2 expression groups, we propose
758 PD-L2 and the CD47/SIRPA pair as potential targets for HER2-negative and low groups. These
759 newly identified immune inhibitory checkpoints offer prospective therapeutic avenues for
760 individualized treatment in GCA patients. We also unveiled HER2 group-specific interactions
761 between the tumor microenvironment and macroenvironment and provide potential molecular
762 targets for future therapeutic applications. Lastly, our work indicated negative HER2
763 expression is associated with fatty acid metabolic profiles and inflammation in the blood of
764 GCA patients, and a larger sample size of GCA patients could further elucidate valuable HER2-
765 relevant prognostic markers during the early blood tests for GCA patients. In summary, our
766 study not only validates HER2 as a prognostic marker for GCA but also identifies molecular
767 targets tailored to specific GCA subsets. These insights hold the potential to guide future
768 clinical trials and advance targeted therapy approaches in gastroesophageal cancers.

Acknowledgments

This work is supported by the National Key R&D Program of China (2012AA02A503, 2016YFC0901403 to L.D.W.), the National Natural Science Foundation of China (81872032, U1804262, 30025016 to L.D.W.; 81972571, 81472234 to S.G.G.), the State Key Laboratory of Esophageal Cancer Prevention & Treatment Key R&D Program of Henan province (202305425 to L.D.W.), Henan Medical Science and Technology Research Project (LHGJ20190001 to X.K.Z. and L.D.W.), Henan Province Key R&D and Promotion Special (Science and Technology) Project (232102311032 to X.S. and L.D.W.), the Wallenberg Academy Fellow in Medicine from Knut and Alice Wallenberg foundation (2023.0046 to X. C.), the Swedish Research Council (2022-00658 to X.C.), the Swedish Cancer Foundation (21 1449Pj, 22 0491 JIA to X.C.), and Åke Wibergs stiftelse (to X.C.). The funders played no role in the study design, data acquisition and interpretation, or decision to publish.

Author contributions

L.D.W. and X.C conceived and designed the study. P.X analyzed all omics data. X.K.Z and X.S analyzed the correlation of omics and clinic-pathological data and follow-up data. X.K.Z and L.L.L analyzed the immunohistochemistry. All the other authors collected clinical samples and related clinical information, performed experiments, and interpreted data. P.X and M.X.W wrote the materials and methods. X.C wrote the manuscript by collecting information from all authors. L.D.W. made critical comments and suggestions to finalize the manuscript. All authors read the manuscript.

Declaration of interests

There is no conflict of interest from all authors.

794 **Materials and Methods**

795 **Study population, tissue and blood collection**

796 All the 128 patients clinically diagnosed with GCA from January 2019 to February 2020 were
797 enrolled in this study, including 102 males with an mean age ± SD of 64.6 ± 7.5, and 26 females
798 with an mean age of 64.7 ± 6.3. All the patients were from Henan, Hebei, and Shanxi provinces,
799 northern China, the highest incidence areas for both GCA and esophageal cancer. None of these
800 patients had undergone preoperative radiation therapy or chemotherapy, and they had no
801 history of other malignant tumors. All the patients were performed radical cardiectomy of GCA.
802 The tumor tissues and normal tissue adjacent to the tumor (NAT) from GCA patients were all
803 collected in the operating room, and all the samples were processed within half an hour after
804 removal, and each sample of tumor tissue and NATs was certified through pathological
805 examination by two well-trained pathologists separately. The clinical characteristics and
806 survival data were summarized in the analysis (**Supplementary Table 1**). Staging of GCA was
807 determined by two pathologists based on the eighth edition of the AJCC (American Joint
808 Committee on Cancer's Staging System). This study was approved by the Ethics Committee of
809 Zhengzhou University (Approval No: 2021-0019). The last follow-up was at the end of March
810 2023.
811
812 Fasting blood samples were meticulously obtained from GCA patients before surgical
813 interventions during their hospitalizations. Each patient contributed two whole blood samples,
814 with distinct processing purposes. One sample was drawn into a non-anticoagulant tube to
815 facilitate metabolomic analysis following serum separation. The second sample was drawn into
816 an anticoagulant tube containing ethylenediaminetetraacetic acid (EDTA) for Whole Exome
817 Sequencing (WES). This study implemented an integrative approach, encompassing whole
818 exome sequencing, RNA sequencing, proteomics, and metabolomics analyses. The
819 investigation utilized formalin-fixed paraffin-embedded (FFPE) tumor tissue blocks for
820 immunohistochemistry and immunofluorescence staining.
821

822 **DNA extraction, library preparation, and whole exome sequencing**

823 Whole exome sequencing (WES) was performed on 113 pairs of fresh-frozen tissues and blood
824 (n = 112) or NAT (n = 1) from GCA. Genomic DNA from tumor tissue and blood was isolated
825 using the DNeasy Blood & Tissue Kit (69504, Qiagen, Netherlands), following the
826 manufacturer's instructions. Subsequently, precise quantification of DNA concentration was

827 carried out using the Qubit 2.0. DNA samples with a concentration of ≥20 ng/μL and a total
828 amount of at least 0.6 μg were used for library construction by Novogene (Novogene
829 Bioinformatics Technology Co. Ltd, Beijing, China). Whole exome library construction was
830 generated using the NEB Next® Ultra RNA Library Prep Kit for Illumina (E7530L, NEB, USA)
831 after DNA shearing, end repair, adenylate 3' ends, adapter ligation, size selection, and PCR
832 amplification, similar to the previous study12. High-fidelity polymerase was then used to
833 amplify the original library to ensure a sufficient total exome library. After library construction
834 was completed, Qubit 3.0 (Invitrogen, USA) and NGS3K/Caliper were used for quantification.
835 Following cluster generation, the DNA libraries were sequenced on the Illumina NovaSeq 6000
836 platform, and 150 bp paired-end reads were generated.
837
838 **RNA isolation, library preparation, and sequencing**
839 RNA sequencing involved 54 pairs of fresh-frozen tissues and corresponding normal adjacent
840 tissues (NAT) from GCA patients. Total RNA extraction from each sample employed the RNA
841 Easy Fast Cell Total RNA Extraction Kit (DP451, Tiangen, Beijing), following the
842 manufacturer's protocol. RNA integrity and total amount were assessed using the Agilent 2100
843 Bioanalyzer (G2939A, Agilent, USA). For mRNA library construction, the NEB Next® Ultra
844 RNA Library Prep Kit for Illumina (E7530L, NEB, USA) was used. Polyadenylated mRNA
845 was enriched from total RNA using oligo(dT) magnetic beads, followed by random
846 fragmentation. The first cDNA strand was synthesized using random oligonucleotides as
847 primers in the M-MuLV reverse transcriptase system. Subsequently, RNaseH degraded the
848 RNA strand, and the second cDNA strand was synthesized using dNTPs in the DNA
849 polymerase I system. The double-stranded cDNA underwent end-repair, A-tailing, and ligation
850 to sequencing adapters. AMPure XP beads were employed to select cDNA fragments of
851 approximately 370~420 bp, followed by PCR amplification and purification to obtain the final
852 library. Following library construction, initial quantification used the Qubit 2.0 Fluorometer,
853 with subsequent library dilution to 1.5 ng/μl. The Agilent 2100 Bioanalyzer was then utilized
854 to confirm the insert size of the library. Upon meeting the specified criteria, qRT-PCR
855 quantified the effective library concentration (ensuring it exceeded 2nM) for quality
856 verification. The final library underwent sequencing on the Illumina NovaSeq6000, generating
857 150 bp paired-end reads.
858
859 **Protein extraction and proteomics**

860 Qualitative and quantitative assessment of proteins were conducted on 128 pairs of fresh-frozen
861 tissues and corresponding NAT from GCA. Initial processing involved the cryogenic grinding
862 of GCA tissues into cell powder using liquid nitrogen, followed by centrifugation.
863 Subsequently, the cell powder underwent sonication on ice, employing a high-intensity
864 ultrasonic processor (Scientz), and the resultant lysate was treated with lysis buffer (8 M urea,
865 1% Protease Inhibitor Cocktail). Centrifugation was employed to eliminate residual debris, and
866 the supernatant, containing proteins, was collected. Protein concentration was determined
867 using a BCA kit following the manufacturer's protocol. The subsequent steps encompassed
868 trypsin digestion, TMT/iTraq labeling, high-performance liquid chromatography (HPLC)
869 fractionation utilizing a Thermo Betasil C18 column (5 μm particles, 10 mm ID, 250 mm
870 length), and liquid chromatography-tandem mass spectrometry (LC-MS/MS) analysis. The
871 acquired data were processed using the MaxQuant search engine (v.1.5.2.8) against the
872 Homo_sapiens_9606 database.
873
874 **Metabolites extraction and metabolomics**
875 Qualitative and quantitative profiling of metabolites were conducted on 115 serum samples
876 obtained from patients diagnosed with GCA. Initial processing involved the separation of
877 serum from whole blood samples, followed by metabolite extraction utilizing a pure methanol
878 internal standard extraction solution. Subsequently, the extracted metabolites underwent
879 analysis using Ultra Performance Liquid Chromatography Tandem Mass Spectrometry (UPLC-
880 MS/MS) employing an UPLC system (ExionLC AD, https://sciex.com.cn/) and MS/MS
881 QTRAP® (https://sciex.com/). The acquired data from UPLC-MS/MS were subjected to
882 analysis using Analyst 1.6.3 software.
883
884 **Immunohistochemistry (IHC) of HER2 protein and HER2 Immunohistochemical**
885 **Scoring Criteria**:
886 IHC of HER2 protein was according to the same method as our previous study[13]. In brief, 5 μm
887 thick formalin fixed paraffin-embedded GCA tissue sections were first deparaffined with
888 xylene 15 min for three times, then were dehydrated through 100% alcohol, 85% alcohol and
889 75% alcohol for 5 min each, followed by distilled water rinsing for 5 min. The epitope retrieval
890 is performed in the microware by putting the tissue into citrate buffer (pH 6.0). After the epitope
891 retrieval, the tissue section is rinsed in Phosphate-Buffered Saline buffer (PBS, pH 7.4). After
892 blocked with 3% bovine serum albumin (BSA) 30 min at room temperature, the tissues were
893 incubated with ERBB2 antibody (1:100 dilution, K00125, Roche) overnight at 4 °C. In the next

894 day, the washing is performed with PBS buffer for three times, 15 min each. The secondary
895 antibody (1:1000 dilution, Horseradish Peroxidase, HRP marked, PV-9000, ZSGB-BIO) was
896 incubated for 50 min at room temperature. After the secondary antibody incubation, the
897 washing is performed with PBS buffer three times on shaker, 15 min each. The tissue is stained
898 with the Harris Hematoxylin for 3 min. At last, the tissue section was mounted and imaged.
899 The HER2 scoring criteria were established and validated by two senior pathologists. Tumor
900 specimens were evaluated for membranous HER2 staining intensity using the following criteria:
901 HER2 0+: No reaction or less than 10% of tumor cells exhibited membranous HER2 staining.
902 HER2 1+: Faint or faintly visible membranous HER2 staining in at least 10% of tumor cells,
903 with only partial cell membrane HER2 staining observed.
904 HER2 2+: Weak to moderate basolateral, lateral, or complete membranous HER2 staining
905 observed in at least 10% of tumor cells. HER2 3+: Basolateral, lateral, or complete
906 membranous HER2 staining present in at least 10% of tumor cells.
907 Note: The HER2 scoring criteria were meticulously applied to assess membranous HER2
908 staining intensity in tumor cells, ensuring consistency through validation by two senior
909 pathologists.
910
911 **Immunofluorescence staining of CD163**
912 The immunofluorescence assay was conducted on paraffin-embedded (FFPE) sections
913 obtained from GCA specimens. Initially, FFPE slices of GCA paraffin-embedded sections
914 underwent baking in an oven for paraffin fixation. Immediate dewaxing of the paraffin slices
915 followed, involving sequential treatments with an eco-friendly dewaxing solution, anhydrous
916 ethanol, 90% alcohol, 70% alcohol, and distilled water. Dewaxed slices were then subjected to
917 low-temperature fixation. The fixing solution was meticulously prepared in a dedicated fixing
918 box and heated in a microwave until boiling, ensuring the absence of air bubbles. Following
919 fixation, rapid cooling of the slices was achieved using ice cubes. Subsequent steps included
920 the removal of the fixing solution with TBST, application of an appropriate sealing solution,
921 removal of excess sealing solution, and sequential addition of primary and secondary
922 antibodies targeting CD163 (ab182422, Abcam, UK). Incubation at room temperature allowed
923 for antibody binding. Afterwards, residual primary and secondary antibody solutions were
924 washed off using TBST. The cleaned slides were treated with corresponding fluorescent dyes,
925 followed by incubation at room temperature. Subsequent TBST washes removed any excess
926 dye. DAPI working solution was applied for nuclear staining, with thorough cleaning to

927 eliminate residual DAPI, dewaxing solution, xylene, or debris. The slides were then sealed for
928 further analysis.
929
930 The image acquisition was performed using the FUISON model full-spectrum scanner from
931 the American company Akoya, capturing all image information of the entire tissue on the slides.
932 Image analysis was conducted using VISIOPHARM software, initially focusing on tissue
933 contour recognition. Experienced pathology experts further delineated tumor tissue regions by
934 overlaying the mIHC-stained images onto the corresponding HE images. During this process,
935 the software calculated the areas of the entire tissue and tumor regions. The VISIOPHARM
936 software employed its inherent deep learning algorithms for cell segmentation, facilitating the
937 determination of total cell counts within the tissue.
938 The Phenplex Guided Workflow functionality in VISIOPHARM software was utilized for cell
939 phenotype identification, enabling the quantification of individual positive cells for each
940 channel and the determination of co-positive cells between channels. Subsequently, statistical
941 calculations leveraging the obtained data on the entire tissue and tumor area, total cell count,
942 positive cell counts for each channel, and co-positive cell counts between channels were
943 conducted. These calculations included the determination of positivity rates, area density, as
944 well as mean, standard deviation, and inter-batch P-values among samples.
945
946 **TCGA data processing**
947 Transcriptome profiling data from The Cancer Genome Atlas Program (TCGA) were
948 downloaded from the GDC Data Portal with the project IDs ESCA (Esophageal Carcinoma)
949 and STAD (Stomach Adenocarcinoma). The expression data, represented by TPM (Transcripts
950 Per Million) normalized values, were extracted from each sample. Subsequently, all samples
951 were merged into a unified TPM matrix. The samples were stratified into two groups based on
952 the median value of ERBB2 RNA levels, distinguishing between ERBB2 high and low
953 expression groups. The categorization was determined by the median values of ERBB2 across
954 the samples.
955
956 **Proteomics data processing and statistical analysis**
957 The raw LC-MS datasets were initially searched against a database and converted into matrices
958 containing the reporter intensity of peptides across samples. Subsequently, the relative
959 quantitative value for each modified peptide was determined through the following procedures:
960 First, the intensities of modified peptides (I) were centralized and transformed into relative

961 quantitative values (U) for each modified peptide in each sample: Uij = Iij / Mean(Ij), where i
962 represents the sample, and j denotes the modified peptide. Second, the relative quantitative
963 values (Q) of modified peptides were corrected by the median value: Qij = Uij / Median(Ui).
964 All patients were categorized into three groups based on HER2 expression level. Those with
965 NA values for HER2 expression were assigned to the HER2-Negative group. The remaining
966 samples were divided into HER2-High and HER2-Low groups based on the median value.
967 Proteins with 50% NA values across all samples were excluded. The protein expression ratio
968 (R) between tumor samples (T) and normal adjacent samples (NAT) was calculated with Rmn
969 = Tmn/NATmn, where m denotes each protein, and n denotes each sample.
970 Principal component analysis (PCA) was conducted on T and NAT matrices using the R
971 packages "FactoMineR" [74] and "factoextra" [75]. Differential analysis among the three groups
972 with the "One v.s. Rest" strategy was conducted on the Rmn matrix using the wilcox.test
973 function in R. Additionally, differential analysis between tumors and NATs was performed
974 based on T and NAT using the wilcox.test function in R. Proteins were considered differentially
975 expressed if their |FoldChange| was greater than or equal to 1.5, and the p-value was less than
976 or equal to 0.05.
977
978 **Metabolomics data analysis**
979 The categorization of groups in the metabolomics data aligned with the HER2-High, HER2-
980 Low, and HER2-Negative groups identified in proteomics. Differential analysis among the
981 three groups was conducted using the "t.test" function in R. Metabolites were considered
982 differentially expressed if their |FoldChange| was greater than or equal to 1.5, and the p-value
983 was less than or equal to 0.05.
984
985 **Whole exome sequencing data processing**
986 The pair-end sequencing data generated from Illumina NovaSeq 6000 were trimmed using fastp
987 v0.23[76]. Subsequently, the trimmed data were mapped to the hg38 reference genome using bwa
988 mem v0.7.17[77]. The SAM files were converted into BAM format and sorted by samtools
989 v1.16.1[78]. Duplicate reads were marked using "GATK4.3 MarkDuplicates." Base quality scores
990 were recalibrated using "GATK4.3 BaseRecalibrator" and "GATK4.3 ApplyBQSR[79]."
991 employing known variants from the dbSNP database (build 146) [8] and the 1000 Genomes
992 project[80].
993
994 **Somatic short variant calling**

995 The somatic short variants, including SNVs and InDels, were called using GATK Mutect2[81],
996 leveraging matched normal samples as reference background and utilizing the "af-only-
997 gnomad" file from the Gnomad datasets as germline resources. Subsequently, "GATK
998 GetPileupSummaries" and "GATK CalculateContamination" were employed to compute cross-
999 sample contamination. Finally, "GATK FilterMutectCalls" was used to filter short variants with
1000 the contamination table, retaining mutations with a "PASS" filter flag for subsequent analysis.
1001 Copy number alterations (CNAs) were identified using both CNVkit/0.9.8[82] and FREEC-11.6[83],
1002 utilizing tumor-matched normal samples as the reference background. Copy numbers equal to
1003 or less than 1 were categorized as CNA loss, while copy numbers equal to or greater than 3
1004 were considered as CNA gain. CNAs identified by both software tools were retained for
1005 subsequent analysis.
1006
1007 **SNVs and InDels analysis**
1008 All SNVs and InDels identified by GATK were annotated using snpEff v5.1[84]. Subsequently,
1009 the annotated SNVs and InDels were transformed into Mutation Annotation Format (MAF)
1010 using a custom script which is deposited in https://github.com/pengweixing/GCA_multi-omics,
1011 following the guidelines provided in
1012 https://docs.gdc.cancer.gov/Encyclopedia/pages/Mutation_Annotation_Format_TCGAv2/.
1013 For each sample, variant types including "Missense_Mutation", "Nonsense_Mutation",
1014 "Splice_Site", "Frame_Shift_Del", "Frame_Shift_Ins", "In_Frame_Del", and "In_Frame_Ins"
1015 were selectively extracted. The identified SNVs and InDels from all samples were subsequently
1016 aggregated. The distribution of mutated genes within three groups was visualized using the R
1017 package "ComplexHeatmap"[85] through a waterfall plot. Only mutated genes that align with
1018 entries in the Cancer Gene Database (COSMIC) were retained for further analysis. The tumor
1019 mutation burden (TMB) was quantified as the number of SNVs per million nucleotides in the
1020 coding region. Synonymous alterations were also counted separately for the purpose of
1021 reducing sampling noise[86].
1022
1023 **CNA analysis**
1024 Copy number alterations (CNAs) across the entire genome for each group were depicted using
1025 the R package Circlize[87]. Additionally, CNAs in specific regions for each group were visualized
1026 utilizing the R package karyoploteR[88]. The genome was divided into bins with a 1Mb window,
1027 and the CNAs were counted in each bin for three groups, with a subsequent application of the

1028 Chi-square test. CIN was estimated through genome integrity index (GII), the proportion of
1029 altered genome segments[89].
1030
1031 **RNA-seq data processing and differential analysis**
1032 The paired-end sequencing data were processed through the nf-core/rnaseq 3.10.1[90] pipeline.
1033 Briefly, fastq files were subjected to trimming using Trim Galore v0.6.10[91], followed by
1034 alignment to the hg38 genome using STAR v2.7.0[92]. Sorting and indexing of the resulting BAM
1035 file were performed using samtools v1.16.1[78] as. Subsequently, Salmon was employed to
1036 quantify the expression levels of individual genes. The gene expression levels were further
1037 normalized using transcripts per million (TPM).
1038 The categorization of groups in RNA-seq data aligned with the HER2-High, HER2-Low, and
1039 HER2-Negative groups identified in proteomics. Differential analysis was conducted within
1040 tumor samples, comparing HER2-High versus Rest, HER2-Low versus Rest, and HER2-
1041 Negative versus Rest. A cutoff of |FoldChange| greater than or equal to 1.5 and a p-value less
1042 than or equal to 0.05 was applied to identify differentially expressed genes. Additionally,
1043 differential analysis was performed between HER2-High versus NATs, HER2-Low versus
1044 NATs, and HER2-Negative versus NATs, with a cutoff of |log2(FoldChange)| >= 1 and FDR
1045 <= 0.05 to filter differentially expressed genes.
1046
1047 **Cellular composition analysis**
1048 CIBERSORTx[51] analysis was conducted in accordance with previously established procedures.
1049 The docker-based tool of CIBERSORTx was utilized to estimate the relative fractions of 22
1050 immune cell sub-populations, employing the LM22 reference gene expression signatures.
1051 Comparisons were conducted among three groups for each cell type. Statistical differences
1052 were calculated with "t-test" function in R.
1053
1054 **Gene Ontology (GO) enrichment and Gene set enrichment analysis (GSEA)**
1055 Differentially expressed genes and proteins identified in transcriptomics and proteomics
1056 datasets were chosen for Gene Ontology (GO) enrichment analysis. The enrichGO function
1057 within the R package clusterProfiler v4.0[93] was employed for conducting gene ontology
1058 analysis, with FDR of 0.05 applied to filter significant GO terms.
1059 For Gene Set Enrichment Analysis (GSEA), 50 hallmark gene sets from the Human MSigDB[94]
1060 collections were adopted. The genes for input were ranked based on their weights which
1061 calculated with "$Gene_{weight} = sign(foldchange) * -\log10(FDR)$". "GSEA" function in

clusterProfiler package was adopted for GSEA analysis. A significance threshold of FDR = 0.05 was applied to filter GSEA hallmarks.

Cell-cell communication inference

Cell-cell communication was estimated using bulk RNA-seq data, treating each sample as an individual cell. The tumor group and NAT group were designated as distinct cell types. The R package CellChat v2[95] was employed to identify ligand-receptor signaling pathways. Visualization of signaling roles was achieved using the "netAnalysis_signalingRole_heatmap" function. Additionally, circle plots illustrating tumor–NAT interactions for each organ were generated using the "netVisual_chord_gene" function.

Survival time analysis

Survival analysis was conducted using the R package survival v.3.5-7[96] and survminer v.0.4.9[97]. The Kaplan-Meier method was employed to estimate overall survival time, and statistical differences were assessed with log-rank test.

Data processing and visualization

In addition to the previously mentioned R packages, the data processing and visualization also incorporated other tools, including dplyr v1.1.4[98], stringr v1.5.1[99], pheatmap v1.0.12[100], ggplot2 v3.4.4[101], ggpubr v0.6.0[102], and ggvenn v0.1.10[103].

Code availability

The code to perform all analyses and regenerate all the figures in this study is provided at https://github.com/pengweixing/GCA_multi-omics.

Data availability

All raw data is deposited in the China National Center for Bioinformation with access number of HRA006640.

TCGA data that used in this study were downloaded from https://portal.gdc.cancer.gov/projects/TCGA-ESCA and https://portal.gdc.cancer.gov/projects/TCGA-STAD.

References

1 Li, K. Mortality and incidence trends from esophagus cancer in selected geographic areas of china circa 1970-90. *Int J Cancer* **102**, 271-274 (2002). https://doi.org:10.1002/jhc.10706

2 Wang, L. D., Zhou, Q. & Yang, C. S. Esophageal and gastric cardia epithelial cell proliferation in northern Chinese subjects living in a high-incidence area. *J Cell Biochem Suppl* **28-29**, 159-165 (1997).

3 Wang, L. D. *et al.* Genome-wide association study of esophageal squamous cell carcinoma in Chinese subjects identifies susceptibility loci at PLCE1 and C20orf54. *Nat Genet* **42**, 759-U746 (2010). https://doi.org:10.1038/ng.648

4 Hu, N. *et al.* Genomic Landscape of Somatic Alterations in Esophageal Squamous Cell Carcinoma and Gastric Cancer. *Cancer Res* **76**, 1714-1723 (2016). https://doi.org:10.1158/0008-5472.Can-15-0338

5 James D. Brierley, M. K. G., Christian Wittekind. *TNM Classification of Malignant Tumours, 8th Edition*. (Wiley-Blackwell, 2016).

6 Li, Y., Li, J. & Li, J. Two updates on oesophagogastric junction adenocarcinoma from the fifth WHO classification: Alteration of definition and emphasis on HER2 test. *Histol Histopathol* **36**, 339-346 (2021). https://doi.org:10.14670/HH-18-296

7 Maric, R. & Cheng, K. K. Classification of adenocarcinoma of the oesophagogastric junction. *Br J Surg* **86**, 1098-1099 (1999). https://doi.org:10.1046/j.1365-2168.1999.01197-15.x

8 Moureau-Zabotto, L. *et al.* Impact of the Siewert Classification on the Outcome of Patients Treated by Preoperative Chemoradiotherapy for a Nonmetastatic Adenocarcinoma of the Oesophagogastric Junction. *Gastroenterol Res Pract* **2015**, 404203 (2015). https://doi.org:10.1155/2015/404203

9 Siewert, J. R. & Stein, H. J. Classification of adenocarcinoma of the oesophagogastric junction. *Br J Surg* **85**, 1457-1459 (1998). https://doi.org:10.1046/j.1365-2168.1998.00940.x

10 Wang, L. D., Zheng, S., Zheng, Z. Y. & Casson, A. G. Primary adenocarcinomas of lower esophagus, esophagogastric junction and gastric cardia: in special reference to China. *World J Gastroenterol* **9**, 1156-1164 (2003). https://doi.org:10.3748/wjg.v9.i6.1156

11 Y. Guanrei, a. Q. S. Incidence Rate of Adenocarcinoma of the Gastric Cardia, and Endoscopic Classification of Early Cardial Carcinoma in Henan Province, the People's Republic of China. *Endoscopy* **19**, 7-10 (1987).

12 Li, S. *et al.* Integrative proteomic characterization of adenocarcinoma of esophagogastric junction. *Nat Commun* **14**, 778 (2023). https://doi.org:10.1038/s41467-023-36462-8

13 Zhao, X. K. *et al.* Focal amplifications are associated with chromothripsis events and diverse prognoses in gastric cardia adenocarcinoma. *Nat Commun* **12**, 6489 (2021). https://doi.org:10.1038/s41467-021-26745-3

14 Osumi, H. *et al.* Clinicopathological features of Siewert type II adenocarcinoma: comparison of gastric cardia adenocarcinoma and Barrett's esophageal adenocarcinoma following endoscopic submucosal dissection. *Gastric Cancer* **20**, 663-670 (2017). https://doi.org:10.1007/s10120-016-0653-x

15 Wang, Z. *et al.* NNMT enriches for AQP5(+) cancer stem cells to drive malignant progression in early gastric cardia adenocarcinoma. *Gut* **73**, 63-77 (2023). https://doi.org:10.1136/gutjnl-2022-328408

16 Hu, N. *et al.* Genome-wide association study of gastric adenocarcinoma in Asia: a comparison of associations between cardia and non-cardia tumours. *Gut* **65**, 1611-1618 (2016). https://doi.org:10.1136/gutjnl-2015-309340

17 Moasser, M. M. The oncogene HER2: its signaling and transforming functions and its role in human cancer pathogenesis. *Oncogene* **26**, 6469-6487 (2007). https://doi.org:10.1038/sj.onc.1210477

18 Goutsouliak, K. *et al.* Towards personalized treatment for early stage HER2-positive breast cancer. *Nat Rev Clin Oncol* **17**, 233-250 (2020). https://doi.org:10.1038/s41571-019-0299-9

19 Tarantino, P. *et al.* Comprehensive genomic characterization of HER2-low and HER2-0 breast cancer. *Nat Commun* **14**, 7496 (2023). https://doi.org:10.1038/s41467-023-43324-w

20 Rha, S. Y. *et al.* The phase III, randomized, double-blind, placebo-controlled KEYNOTE-811 study of pembrolizumab plus trastuzumab and chemotherapy for HER2+metastatic gastric or gastroesophageal junction (mG/GEJ) adenocarcinoma. *Ann Oncol* **34**, S1521-S1522 (2023). https://doi.org:10.1016/j.annonc.2023.10.266

21 Slamon, D. J. *et al.* Use of chemotherapy plus a monoclonal antibody against HER2 for metastatic breast cancer that overexpresses HER2. *New Engl J Med* **344**, 783-792 (2001). https://doi.org:Doi 10.1056/Nejm200103153441101

22 Bang, Y. J. *et al.* Trastuzumab in combination with chemotherapy versus chemotherapy alone for treatment of HER2-positive advanced gastric or gastro-oesophageal junction cancer (ToGA): a phase 3, open-label, randomised controlled trial. *Lancet* **376**, 687-697 (2010). https://doi.org:10.1016/S0140-6736(10)61121-X

23 Janjigian, Y. Y. *et al.* The KEYNOTE-811 trial of dual PD-1 and HER2 blockade in HER2-positive gastric cancer. *Nature* **600**, 727-730 (2021). https://doi.org:10.1038/s41586-021-04161-3

24 Janjigian, Y. Y. *et al.* Pembrolizumab plus trastuzumab and chemotherapy for HER2-positive gastric or gastro-oesophageal junction adenocarcinoma: interim analyses from the phase 3 KEYNOTE-811 randomised placebo-controlled trial. *Lancet* **402**, 2197-2208 (2023). https://doi.org:10.1016/S0140-6736(23)02033-0

25 Lv, H. F. *et al.* Expression of Human Epidermal Growth Factor Receptor-2 Status and Programmed Cell Death Protein-1 Ligand Is Associated With Prognosis in Gastric Cancer (vol 10, 580045, 2021). *Front Oncol* **11** (2021). https://doi.org:ARTN 672599
10.3389/fonc.2021.672599

26 Zhang, H. *et al.* Intratumoral and intertumoral heterogeneity of HER2 immunohistochemical expression in gastric cancer. *Pathol Res Pract* **216** (2020). https://doi.org:ARTN 153229
10.1016/j.prp.2020.153229

27 Van Cutsem, E. *et al.* HER2 screening data from ToGA: targeting HER2 in gastric and gastroesophageal junction cancer. *Gastric Cancer* **18**, 476-484 (2015). https://doi.org:10.1007/s10120-014-0402-y

28 Kim, W. H. *et al.* HER2 Status in Gastric and Gastroesophageal Junction Cancer: Results of the Large, Multinational HER-EAGLE Study. *Appl Immunohistochem Mol Morphol* **26**, 239-245 (2018). https://doi.org:10.1097/PAI.0000000000000423

29 Slamon, D. J. *et al.* Human breast cancer: correlation of relapse and survival with amplification of the HER-2/neu oncogene. *Science* **235**, 177-182 (1987). https://doi.org:10.1126/science.3798106

30 Plum, P. S. *et al.* HER2/neu (ERBB2) expression and gene amplification correlates with better survival in esophageal adenocarcinoma. *BMC Cancer* **19**, 38 (2019). https://doi.org:10.1186/s12885-018-5242-4

31 Boku, N. HER2-positive gastric cancer. *Gastric Cancer* **17**, 1-12 (2014). https://doi.org:10.1007/s10120-013-0252-z

32 Bailey, M. H. *et al.* Comprehensive Characterization of Cancer Driver Genes and Mutations. *Cell* **173**, 371-385 e318 (2018). https://doi.org:10.1016/j.cell.2018.02.060

33 Sophocleous, R. A., Ooi, L. & Sluyter, R. The P2X4 Receptor: Cellular and Molecular Characteristics of a Promising Neuroinflammatory Target. *Int J Mol Sci* **23** (2022). https://doi.org:10.3390/ijms23105739

34 Hedl, M., Sun, R., Huang, C. & Abraham, C. STAT3 and STAT5 Signaling Thresholds Determine Distinct Regulation for Innate Receptor-Induced Inflammatory Cytokines, and
/
Disease Variants Modulate These Outcomes. *J Immunol* **203**, 3325-3338 (2019). https://doi.org:10.4049/jimmunol.1900031

35 Forsburg, S. L. Eukaryotic MCM proteins: beyond replication initiation. *Microbiol Mol Biol Rev* **68**, 109-131 (2004). https://doi.org:10.1128/MMBR.68.1.109-131.2004

36 Xu, J., Lamouille, S. & Derynck, R. TGF-beta-induced epithelial to mesenchymal transition. *Cell Res* **19**, 156-172 (2009). https://doi.org:10.1038/cr.2009.5

37 Tye, B. K. MCM proteins in DNA replication. *Annu Rev Biochem* **68**, 649-686 (1999). https://doi.org:10.1146/annurev.biochem.68.1.649

38 Bailis, J. M. & Forsburg, S. L. MCM proteins: DNA damage, mutagenesis and repair. *Curr Opin Genet Dev* **14**, 17-21 (2004). https://doi.org:10.1016/j.gde.2003.11.002

39 Diamond, M. S. & Farzan, M. The broad-spectrum antiviral functions of IFIT and IFITM proteins. *Nat Rev Immunol* **13**, 46-57 (2013). https://doi.org:10.1038/nri3344

40 Hiam-Galvez, K. J., Allen, B. M. & Spitzer, M. H. Systemic immunity in cancer. *Nat Rev Cancer* **21**, 345-359 (2021). https://doi.org:10.1038/s41568-021-00347-z

41 Roy, R., Chun, J. & Powell, S. N. BRCA1 and BRCA2: different roles in a common pathway of genome protection. *Nat Rev Cancer* **12**, 68-78 (2011). https://doi.org:10.1038/nrc3181

42 Huang, R. & Zhou, P. K. DNA damage repair: historical perspectives, mechanistic pathways and clinical translation for targeted cancer therapy. *Signal Transduct Target Ther* **6**, 254 (2021). https://doi.org:10.1038/s41392-021-00648-7

43 Dawood, S., Broglio, K., Buzdar, A. U., Hortobagyi, G. N. & Giordano, S. H. Prognosis of women with metastatic breast cancer by HER2 status and trastuzumab treatment: an institutional-based review. *J Clin Oncol* **28**, 92-98 (2010). https://doi.org:10.1200/JCO.2008.19.9844

44 Mah, L. J., El-Osta, A. & Karagiannis, T. C. gammaH2AX: a sensitive molecular marker of DNA damage and repair. *Leukemia* **24**, 679-686 (2010). https://doi.org:10.1038/leu.2010.6

45 Ochando, J., Mulder, W. J. M., Madsen, J. C., Netea, M. G. & Duivenvoorden, R. Trained immunity - basic concepts and contributions to immunopathology. *Nat Rev Nephrol* **19**, 23-37 (2023). https://doi.org:10.1038/s41581-022-00633-5

46 Rose-John, S., Jenkins, B. J., Garbers, C., Moll, J. M. & Scheller, J. Targeting IL-6 trans-signalling: past, present and future prospects. *Nat Rev Immunol* **23**, 666-681 (2023). https://doi.org:10.1038/s41577-023-00856-y

47 Katze, M. G., He, Y. & Gale, M., Jr. Viruses and interferon: a fight for supremacy. *Nat Rev Immunol* **2**, 675-687 (2002). https://doi.org:10.1038/nri888

48 MacMicking, J. D. Interferon-inducible effector mechanisms in cell-autonomous immunity. *Nat Rev Immunol* **12**, 367-382 (2012). https://doi.org:10.1038/nri3210

49 Hanahan, D. Hallmarks of Cancer: New Dimensions. *Cancer Discov* **12**, 31-46 (2022). https://doi.org:10.1158/2159-8290.CD-21-1059

50 Braun, D. A. *et al.* Interplay of somatic alterations and immune infiltration modulates response to PD-1 blockade in advanced clear cell renal cell carcinoma. *Nat Med* **26**, 909-918 (2020). https://doi.org:10.1038/s41591-020-0839-y

51 Newman, A. M. *et al.* Determining cell type abundance and expression from bulk tissues with digital cytometry. *Nat Biotechnol* **37**, 773-782 (2019). https://doi.org:10.1038/s41587-019-0114-2

52 Mantovani, A., Allavena, P., Marchesi, F. & Garlanda, C. Macrophages as tools and targets in cancer therapy. *Nat Rev Drug Discov* **21**, 799-820 (2022). https://doi.org:10.1038/s41573-022-00520-5

53 Chen, S. *et al.* Macrophages in immunoregulation and therapeutics. *Signal Transduct Target Ther* **8**, 207 (2023). https://doi.org:10.1038/s41392-023-01452-1

54 Mair, F. *et al.* Extricating human tumour immune alterations from tissue inflammation. *Nature* **605**, 728-735 (2022). https://doi.org:10.1038/s41586-022-04718-w

55 Wynn, T. A. & Vannella, K. M. Macrophages in Tissue Repair, Regeneration, and Fibrosis. *Immunity* **44**, 450-462 (2016). https://doi.org:10.1016/j.immuni.2016.02.015

56 Hao, N. B. *et al.* Macrophages in tumor microenvironments and the progression of tumors. *Clin Dev Immunol* **2012**, 948098 (2012). https://doi.org:10.1155/2012/948098

57 Shitara, K. *et al.* Nivolumab plus chemotherapy or ipilimumab in gastro-oesophageal cancer. *Nature* **603**, 942-948 (2022). https://doi.org:10.1038/s41586-022-04508-4

58 Pardoll, D. M. The blockade of immune checkpoints in cancer immunotherapy. *Nat Rev Cancer* **12**, 252-264 (2012). https://doi.org:10.1038/nrc3239

59 Zhao, X. W. *et al.* CD47-signal regulatory protein-alpha (SIRPalpha) interactions form a barrier for antibody-mediated tumor cell destruction. *Proc Natl Acad Sci U S A* **108**, 18342-18347 (2011). https://doi.org:10.1073/pnas.1106550108

60 Chao, M. P. *et al.* Anti-CD47 antibody synergizes with rituximab to promote phagocytosis and eradicate non-Hodgkin lymphoma. *Cell* **142**, 699-713 (2010). https://doi.org:10.1016/j.cell.2010.07.044

61 Hao, Y., Zhou, X. X., Li, Y. L., Li, B. L. & Cheng, L. The CD47-SIRPα axis is a promising target for cancer immunotherapies. *Int Immunopharmacol* **120** (2023). https://doi.org:ARTN 110255 10.1016/j.intimp.2023.110255

62 Aggarwal, V., Workman, C. J. & Vignali, D. A. A. LAG-3 as the third checkpoint inhibitor. *Nat Immunol* (2023). https://doi.org:10.1038/s41590-023-01569-z

63 Wang, J. *et al.* Fibrinogen-like Protein 1 Is a Major Immune Inhibitory Ligand of LAG-3. *Cell* **176**, 334-+ (2019). https://doi.org:10.1016/j.cell.2018.11.010

64 Chocarro, L. *et al.* Clinical landscape of LAG-3-targeted therapy. *Immunooncol Technol* **14**, 100079 (2022). https://doi.org:10.1016/j.iotech.2022.100079

65 Kumar, A. *et al.* Nodal signaling uses activin and transforming growth factor-beta receptor-regulated Smads. *J Biol Chem* **276**, 656-661 (2001). https://doi.org:10.1074/jbc.M004649200

66 Pickup, M. W., Owens, P. & Moses, H. L. TGF-beta, Bone Morphogenetic Protein, and Activin Signaling and the Tumor Microenvironment. *Cold Spring Harb Perspect Biol* **9** (2017). https://doi.org:10.1101/cshperspect.a022285

67 Ji, L. *et al.* The crucial regulatory role of type I interferon in inflammatory diseases. *Cell Biosci* **13**, 230 (2023). https://doi.org:10.1186/s13578-023-01188-z

68 Crovello, C. S., Lai, C., Cantley, L. C. & Carraway, K. L., 3rd. Differential signaling by the epidermal growth factor-like growth factors neuregulin-1 and neuregulin-2. *J Biol Chem* **273**, 26954-26961 (1998). https://doi.org:10.1074/jbc.273.41.26954

69 Liu, Y. R. & Dai, M. Trimethylamine N-Oxide Generated by the Gut Microbiota Is Associated with Vascular Inflammation: New Insights into Atherosclerosis. *Mediat Inflamm* **2020** (2020). https://doi.org:Artn 4634172 10.1155/2020/4634172

70 van Vlies, N. *et al.* Characterization of carnitine and fatty acid metabolism in the long-chain acyl-CoA dehydrogenase-deficient mouse. *Biochem J* **387**, 185-193 (2005). https://doi.org:10.1042/BJ20041489

71 Jia, X. *et al.* A possible role of chenodeoxycholic acid and glycine-conjugated bile acids in fibrotic steatohepatitis in a dietary rat model. *Dig Dis Sci* **59**, 1490-1501 (2014). https://doi.org:10.1007/s10620-014-3028-3

72 Trang, L. E., Granstrom, E. & Lovgren, O. Levels of prostaglandins F2 alpha and E2 and thromboxane B2 in joint fluid in rheumatoid arthritis. *Scand J Rheumatol* **6**, 151-154 (1977). https://doi.org:10.3109/03009747709095440

73 Matsumoto, T., Kobayashi, T. & Kamata, K. Role of lysophosphatidylcholine (LPC) in atherosclerosis. *Curr Med Chem* **14**, 3209-3220 (2007). https://doi.org:10.2174/092986707782793899

74 Lê, S., Josse, J. & Husson, F. FactoMineR: An R Package for Multivariate Analysis. *Journal of Statistical Software* **25**, 1-18 (2008). https://doi.org:10.18637/jss.v025.i01

75 Kassambara, A. & Mundt, F. (Foundation for Statistical Computing, Vienna, Austria, 2017).

76 Chen, S., Zhou, Y., Chen, Y. & Gu, J. fastp: an ultra-fast all-in-one FASTQ preprocessor. *Bioinformatics (Oxford, England)* **34**, i884-i890 (2018). https://doi.org:10.1093/bioinformatics/bty560

77 Li, H. & Durbin, R. Fast and accurate short read alignment with Burrows-Wheeler transform. *Bioinformatics (Oxford, England)* **25**, 1754-1760 (2009). https://doi.org:10.1093/bioinformatics/btp324

78 Li, H. *et al.* The Sequence Alignment/Map format and SAMtools. *Bioinformatics (Oxford, England)* **25**, 2078-2079 (2009). https://doi.org:10.1093/bioinformatics/btp352

79 DePristo, M. A. *et al.* A framework for variation discovery and genotyping using next-generation DNA sequencing data. *Nature Genetics* **43**, 491-498 (2011). https://doi.org:10.1038/ng.806

80 Consortium, G. P. *et al.* A global reference for human genetic variation. *Nature* **526**, 68-74 (2015). https://doi.org:10.1038/nature15393

81 Benjamin, D. *et al.* Calling Somatic SNVs and Indels with Mutect. (2019).

82 Talevich, E., Shain, A. H., Botton, T. & Bastian, B. C. CNVkit: Genome-Wide Copy Number Detection and Visualization from Targeted DNA Sequencing. *PLOS Computational Biology* **12**, e1004873 (2016). https://doi.org:10.1371/journal.pcbi.1004873

83 Boeva, V. *et al.* Control-FREEC: a tool for assessing copy number and allelic content using next-generation sequencing data. *Bioinformatics* **28**, 423-425 (2012). https://doi.org:10.1093/bioinformatics/btr670

84 Cingolani, P. *et al.* A program for annotating and predicting the effects of single nucleotide polymorphisms, SnpEff. *Fly* **6**, 80-92 (2012). https://doi.org:10.4161/fly.19695

85 Gu, Z. Complex heatmap visualization. *iMeta* **1**, e43 (2022). https://doi.org:10.1002/imt2.43

86 Chalmers, Z. R. *et al.* Analysis of 100,000 human cancer genomes reveals the landscape of tumor mutational burden. *Genome Medicine* **9**, 34 (2017). https://doi.org:10.1186/s13073-017-0424-2

87 Gu, Z., Gu, L., Eils, R., Schlesner, M. & Brors, B. circlize Implements and enhances circular visualization in R. *Bioinformatics (Oxford, England)* **30**, 2811-2812 (2014). https://doi.org:10.1093/bioinformatics/btu393

88 Gel, B. & Serra, E. karyoploteR: an R/Bioconductor package to plot customizable genomes displaying arbitrary data. *Bioinformatics (Oxford, England)* **33**, 3088-3090 (2017). https://doi.org:10.1093/bioinformatics/btx346

89 Chin, S. F. *et al.* High-resolution aCGH and expression profiling identifies a novel genomic subtype of ER negative breast cancer. *Genome Biology* **8**, R215 (2007). https://doi.org:10.1186/gb-2007-8-10-r215

90 Ewels, P. A. *et al.* The nf-core framework for community-curated bioinformatics pipelines. *Nature Biotechnology* **38**, 276-278 (2020). https://doi.org:10.1038/s41587-020-0439-x

91 Krueger, F. (2015).

92 Dobin, A. & Gingeras, T. R. Mapping RNA-seq Reads with STAR. *Current protocols in bioinformatics / editoral board, Andreas D. Baxevanis ... [et al.]* **51**, 11.14.11-11.14.19 (2015). https://doi.org:10.1002/0471250953.bi1114s51

93 Yu, G., Wang, L.-G., Han, Y. & He, Q.-Y. clusterProfiler: an R package for comparing biological themes among gene clusters. *Omics: a journal of integrative biology* **16**, 284-287 (2012).

94 Liberzon, A. *et al.* Molecular signatures database (MSigDB) 3.0. *Bioinformatics* **27**, 1739-1740 (2011). https://doi.org:10.1093/bioinformatics/btr260

95 Jin, S., Plikus, M. & Nie, Q. CellChat for systematic analysis of cell-cell communication from single-cell and spatially resolved transcriptomic. (2023).

96 Therneau, T. M. & Lumley, T. Package 'survival'. *R Top Doc* **128**, 28–33 (2015).

97 Kassambara, A., Kosinski, M., Biecek, P. & Fabian, S. Package 'survminer'. *Drawing Survival Curves using 'ggplot2'(R package version 03 1)* **3** (2017).

98 Wickham, H., François, R., Henry, L., Müller, K. & Wickham, M. H. Package 'dplyr'. *A Grammar of Data Manipulation. R package version* **8** (2019).

99 Wickham, H. & Wickham, M. H. Package 'stringr'. (2019).

100 Kolde, R. & Kolde, M. R. Package 'pheatmap'. *R package* **1**, 790 (2015).

101 Wickham, H. ggplot2. *Wiley interdisciplinary reviews: computational statistics* **3**, 180-185 (2011).
102 Kassambara, A. & Kassambara, M. A. Package 'ggpubr'. *R package version 0.1* **6** (2020).
103 Yan, L. & Yan, M. L. Package 'ggvenn'. (2021).

1337 **Figure legends**

1338 **Figure 1**: **The expression of *ERBB2*/HER2 could be a favorable prognosis marker for**
1339 **esophageal adenocarcinoma (EAC) and gastric cardia adenocarcinoma (GCA)**.

1340 **A.** The Pearson correlation of *ERBB2* RNA expression and HER2 protein expression from
1341 GCA cohort. N = HER2 protein level detected with mass spectrometry.

1342 **B.** The distribution of *ERBB2* RNA expression in GCA cohort, EAC and STAD from
1343 TCGA. ESCC = Esophageal squamous-cell carcinomas; STAD = Stomach
1344 adenocarcinoma; TPM = Transcripts Per Million.

1345 **C.** The survival analysis of different patient groups based on the level *ERBB2* RNA
1346 expression.

1347 **D.** The strategy for dividing the GCA cohort into three groups based on the HER2 protein
1348 expression level.

1349 **E.** Representative immunohistochemistry (IHC) staining of HER2 for score 3+, 2+, 2+, and
1350 0+.

1351 **F.** Relationship between IHC staining HER2 scores and HER2 groups with quantification of
1352 HER2 protein expression using mass spectrometry.

1353 **G.** The survival analysis of GCA patient groups in three HER2 groups.

1354 **H.** Therapeutic treatments in three HER2 groups.

1355 **I.** Surviving analysis of different therapeutic treatments.

1356 **Figure 2**: **Protein expression landscape of different HER2 groups from GCA patients.**

1357 **A.** The illustration of multiple omics data from GCA patients.

1358 **B.** Unique protein profiles of different HER2 GCA patient groups from tumor only.

1359 **C.** Gene set enrichment analysis (GSEA) with protein of different HER2 GCA patient groups
1360 from tumor only.

1361 **D.** GSEA of different HER2 GCA patient groups by comparing tumors with corresponding
1362 normal tissue adjacent to the tumor (NAT).

1363 **E.** Differential protein expression in HER2 high group by comparing tumors with
1364 corresponding NAT.

1365 **F.** Differential protein expression in HER2 low group by comparing tumors with
1366 corresponding NAT.

1367 **G.** Differential protein expression in HER2 negative group by comparing tumors with
1368 corresponding NAT.

1369 **H.** Top 15 enriched Gene oncology (GO) term of differential protein expression comparing
1370 tumor with NAT in different HER2 groups.

1371 **Figure 3**: **Somatic mutation and amplification landscape of different HER2 groups from**
1372 **GCA patients.**
1373 **A.** Top 20 mutation oncogenes and tumor suppressor genes captured in the GCA cohort and
1374 its mutation frequency in different HER2 groups.
1375 **B.** Comparison of chromosome instability (CIN) among three different HER2 groups using
1376 the genome integrity index.
1377 **C.** Comparison of copy number alterations (CNAs) among three different HER2 groups.
1378 **D.** The significant different CNAs regions in three different HER2 groups with bin size of
1379 1Mbp; Oncogenes and tumor suppressor genes were labeled on the side.
1380 **E.** Examples of significant CNAs regions in three different HER2 groups on chromosome
1381 13, 15 and 17.
1382
1383 **Figure 4**: **Gene expression signature of different HER2 groups from GCA patients**
1384 **A.** Gene set enrichment analysis (GSEA) using RNA expression from tumors of different
1385 HER2 GCA patient groups.
1386 **B.** Gene expression signatures from tumors of different HER2 GCA patient groups.
1387 **C.** GSEA with RNA expression of different HER2 GCA patient groups by comparing tumors
1388 with corresponding normal tissue adjacent to the tumor (NAT).
1389 **D.** Left: Differential RNA expression in HER2 high group by comparing tumors with
1390 corresponding NAT.
1391 Middle: Differential RNA expression in HER2 low group by comparing tumors with
1392 corresponding NAT.
1393 Right: Differential RNA expression in HER2 negative group by comparing tumors with
1394 corresponding NAT.
1395 **E.** Differential RNA expression from genes of major histocompatibility complex (MHC) class
1396 I and II in different HER2 groups by comparing tumors with corresponding NAT.
1397 **F.** Top 15 enriched Gene oncology (GO) term of differential RNA expression comparing
1398 tumor with NAT in different HER2 groups.
1399 **G.** Differential RNA expression from genes of cytokines from different HER2 groups by
1400 comparing tumors with corresponding NAT.
1401 FDR = false discovery rate.
1402
1403
1404

1405 **Figure 5**: **Deciphering tumor microenvironment of different HER2 groups from GCA**
1406 **patients**
1407 **A.** Cell component comparison from tumor bulk RNA-seq prediction from different HER2
1408 groups.
1409 **B.** Quantitative comparison of M2 macrophages in tumor only from different HER2 groups.
1410 **C.** Representative images from immunohistochemistry (IHC) staining of CD163 from tumor
1411 in different HER2 groups.
1412 **D.** Quantification of IHC staining of CD163 from tumor in different HER2 groups.
1413 **E.** Comparison of differential gene expression between tumors and corresponding normal
1414 tissue adjacent to the tumor (NAT) for paired immune checkpoints receptors and ligands
1415 in different HER2 groups; FC = Fold Change; white block = False discovery rate (FDR)
1416 is larger than 0.05; Star indicates |log2(Fold Change)| >= 1 and FDR is less than 0.05.
1417
1418 **Figure 6**: **HER2 group-specific ligand-receptor signaling between tumors and normal**
1419 **tissue adjacent to the tumor (NAT) macroenvironment**
1420 **A.** Gene expression level of incoming and outgoing signal from tumor and its corresponding
1421 NAT in different HER2 groups.
1422 **B.** Group-specific and common signal transduction among the three HER2 groups.
1423 **C.** Signal transduction of ERBB family genes and its ligands among three HER2 groups.
1424
1425 **Figure 7**: **Negative HER2 expression is associated with inflammation in blood of GCA**
1426 **patients**
1427 **A.** Volcano plots show differential metabolic comparisons of different HER2 groups; the
1428 number of significant different subtracts determined in each pair comparison is labeled in
1429 each plot.
1430 **B.** Bubble plots show significant differential subtracts among different comparison.
1431 **C.** Metabolic comparison in GCA patients with immunohistochemistry (IHC) staining for
1432 HER2 3+ and HER2 0+.
1433

Figure 1

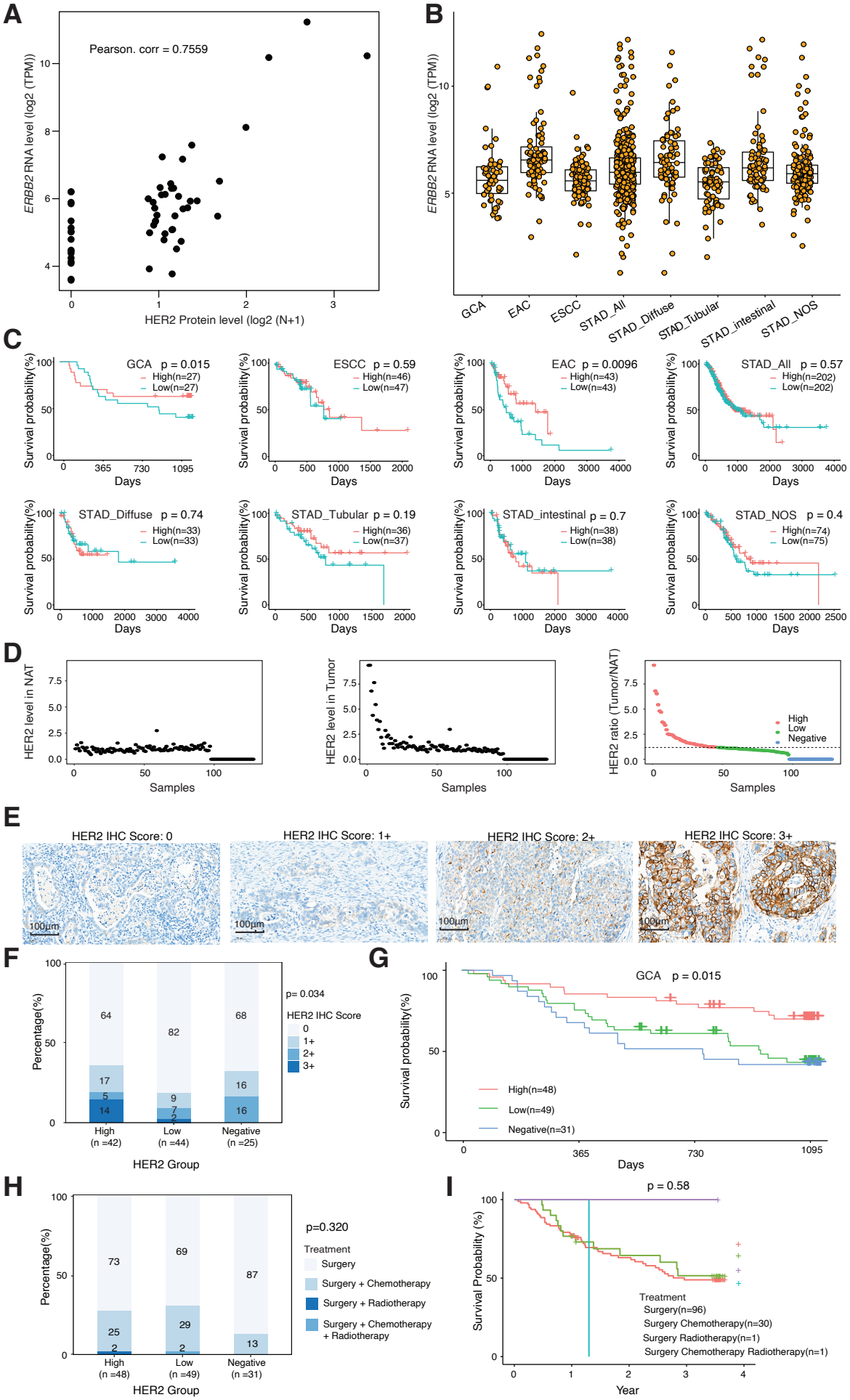
A
Pearson. corr = 0.7559
ERBB2 RNA level (log2 (TPM))
HER2 Protein level (log2 (N+1)
B
ERBB2 RNA level (log2 (TPM))
GCA
EAC
ESCC
STAD_All
STAD_Diffuse
STAD_Tubular
STAD_intestinal
STAD_NOS
C
GCA p = 0.015
High(n=27)
Low(n=27)
ESCC p = 0.59
High(n=46)
Low(n=47)
EAC p = 0.0096
High(n=43)
Low(n=43)
STAD_All p = 0.57
High(n=202)
Low(n=202)
STAD_Diffuse p = 0.74
High(n=33)
Low(n=33)
STAD_Tubular p = 0.19
High(n=36)
Low(n=37)
STAD_intestinal p = 0.7
High(n=38)
Low(n=38)
STAD_NOS p = 0.4
High(n=74)
Low(n=75)
Survival probability(%)
Days
D
HER2 level in NAT
HER2 level in Tumor
HER2 ratio (Tumor/NAT)
High
Low
Negative
Samples
E
HER2 IHC Score: 0
HER2 IHC Score: 1+
HER2 IHC Score: 2+
HER2 IHC Score: 3+
100μm
F
Percentage(%)
p= 0.034
HER2 IHC Score
0
1+
2+
3+
High (n =42)
Low (n =44)
Negative (n =25)
HER2 Group
G
GCA p = 0.015
Survival probability(%)
High(n=48)
Low(n=49)
Negative(n=31)
Days
H
Percentage(%)
p=0.320
Treatment
Surgery
Surgery + Chemotherapy
Surgery + Radiotherapy
Surgery + Chemotherapy + Radiotherapy
High (n =48)
Low (n =49)
Negative (n =31)
HER2 Group
I
p = 0.58
Survival Probability (%)
Treatment
Surgery(n=96)
Surgery Chemotherapy(n=30)
Surgery Radiotherapy(n=1)
Surgery Chemotherapy Radiotherapy(n=1)
Year

Figure 2

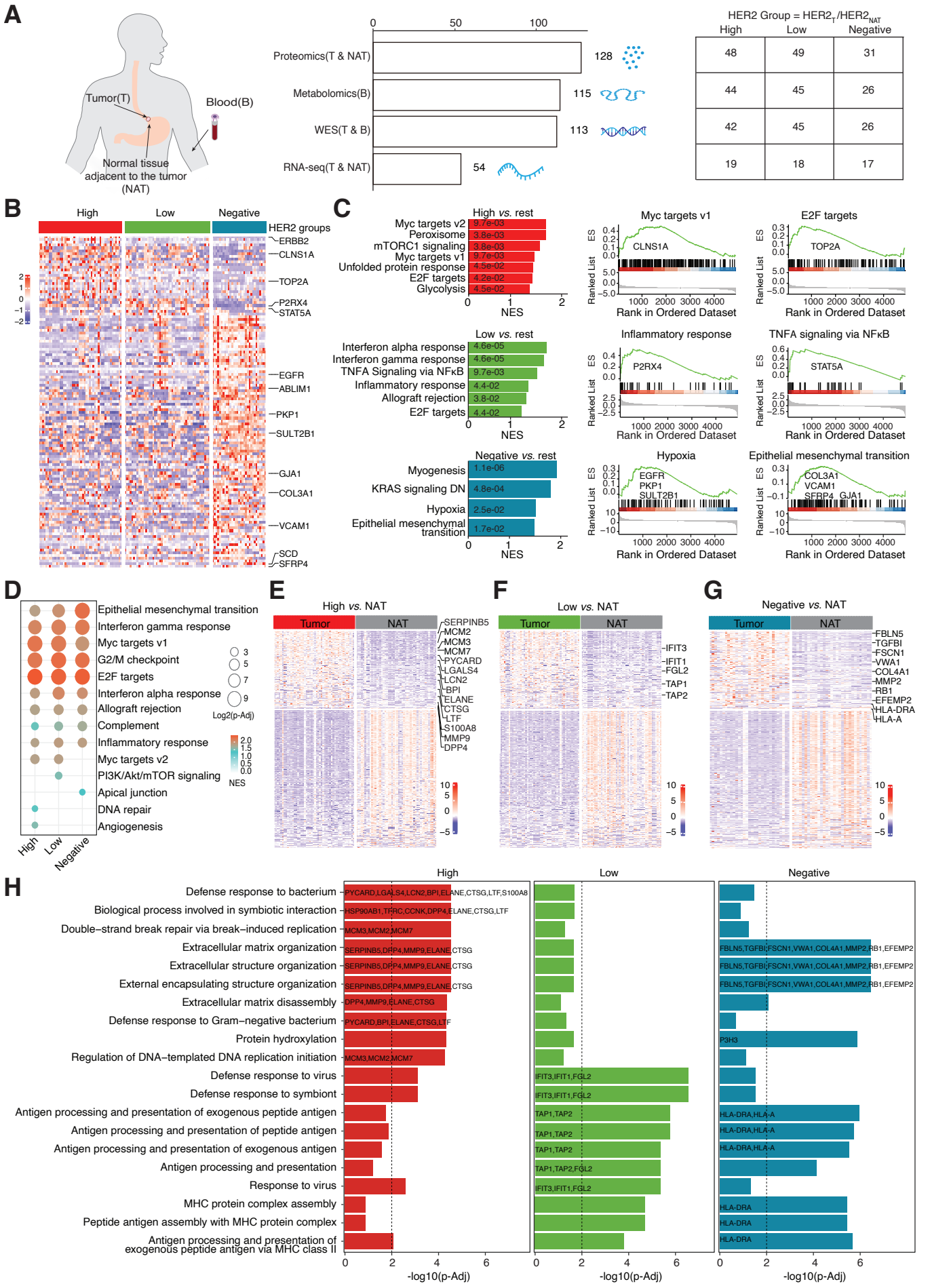
A
Tumor(T)
Blood(B)
Normal tissue adjacent to the tumor (NAT)
Proteomics(T & NAT)
Metabolomics(B)
WES(T & B)
RNA-seq(T & NAT)
128
115
113
54
HER2 Group = HER2T/HER2NAT
High Low Negative
48 49 31
44 45 26
42 45 26
19 18 17
B
High Low Negative
HER2 groups
ERBB2
CLNS1A
TOP2A
P2RX4
STAT5A
EGFR
ABLIM1
PKP1
SULT2B1
GJA1
COL3A1
VCAM1
SCD
SFRP4
C
High vs. rest
Myc targets v2
Peroxisome
mTORC1 signaling
Myc targets v1
Unfolded protein response
E2F targets
Glycolysis
Low vs. rest
Interferon alpha response
Interferon gamma response
TNFA Signaling via NFκB
Inflammatory response
Allograft rejection
E2F targets
Negative vs. rest
Myogenesis
KRAS signaling DN
Hypoxia
Epithelial mesenchymal transition
NES
Myc targets v1
E2F targets
Inflammatory response
TNFA signaling via NFκB
Hypoxia
Epithelial mesenchymal transition
Ranked List
Rank in Ordered Dataset
D
Epithelial mesenchymal transition
Interferon gamma response
Myc targets v1
G2/M checkpoint
E2F targets
Interferon alpha response
Allograft rejection
Complement
Inflammatory response
Myc targets v2
PI3K/Akt/mTOR signaling
Apical junction
DNA repair
Angiogenesis
Log2(p-Adj)
NES
High Low Negative
E
High vs. NAT
Tumor NAT
SERPINB5
MCM2
MCM3
MCM7
PYCARD
LGALS4
LCN2
BPI
ELANE
CTSG
LTF
S100A8
MMP9
DPP4
F
Low vs. NAT
Tumor NAT
IFIT3
IFIT1
FGL2
TAP1
TAP2
G
Negative vs. NAT
Tumor NAT
FBLN5
TGFBI
FSCN1
VWA1
COL4A1
MMP2
RB1
EFEMP2
HLA-DRA
HLA-A
H
High Low Negative
Defense response to bacterium
Biological process involved in symbiotic interaction
Double-strand break repair via break-induced replication
Extracellular matrix organization
Extracellular structure organization
External encapsulating structure organization
Extracellular matrix disassembly
Defense response to Gram-negative bacterium
Protein hydroxylation
Regulation of DNA-templated DNA replication initiation
Defense response to virus
Defense response to symbiont
Antigen processing and presentation of exogenous peptide antigen
Antigen processing and presentation of peptide antigen
Antigen processing and presentation of exogenous antigen
Antigen processing and presentation
Response to virus
MHC protein complex assembly
Peptide antigen assembly with MHC protein complex
Antigen processing and presentation of exogenous peptide antigen via MHC class II
-log10(p-Adj)

Figure 3

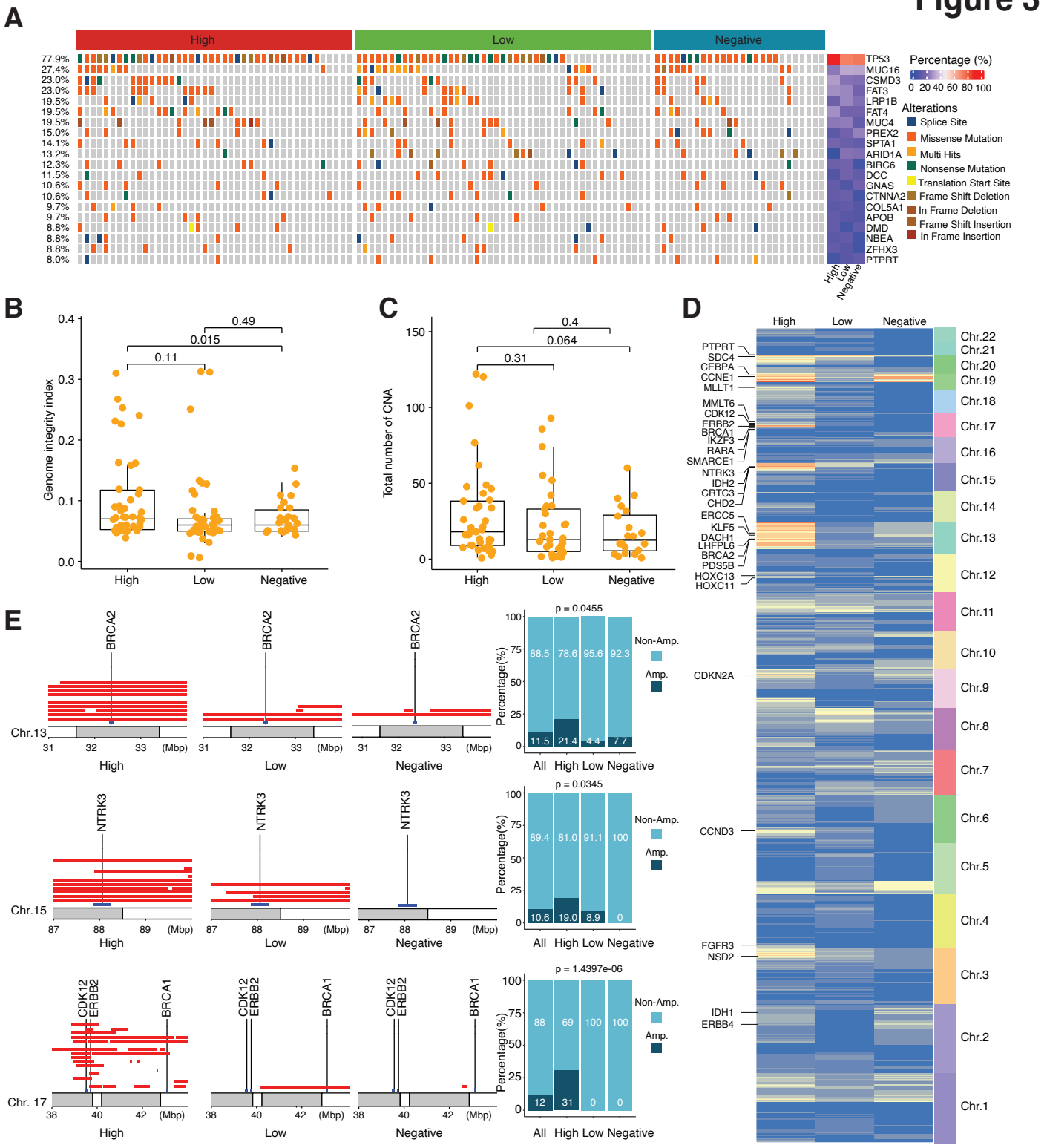
A
High
Low
Negative
77.9%
27.4%
23.0%
23.0%
19.5%
19.5%
19.5%
15.0%
14.1%
13.2%
12.3%
11.5%
10.6%
10.6%
9.7%
9.7%
8.8%
8.8%
8.8%
8.0%
TP53
MUC16
CSMD3
FAT3
LRP1B
FAT4
MUC4
PREX2
SPTA1
ARID1A
BIRC6
DCC
GNAS
CTNNA2
COL5A1
APOB
DMD
NBEA
ZFHX3
PTPRT
Percentage (%)
0 20 40 60 80 100
Alterations
Splice Site
Missense Mutation
Multi Hits
Nonsense Mutation
Translation Start Site
Frame Shift Deletion
In Frame Deletion
Frame Shift Insertion
In Frame Insertion
B
Genome integrity index
0.4
0.3
0.2
0.1
0.0
0.49
0.015
0.11
High
Low
Negative
C
Total number of CNA
150
100
50
0
0.4
0.064
0.31
High
Low
Negative
D
High
Low
Negative
PTPRT
SDC4
CEBPA
CCNE1
MLLT1
MMLT6
CDK12
ERBB2
BRCA1
IKZF3
RARA
SMARCE1
NTRK3
IDH2
CRTC3
CHD2
ERCC5
KLF5
DACH1
LHFPL6
BRCA2
PDS5B
HOXC13
HOXC11
CDKN2A
CCND3
FGFR3
NSD2
IDH1
ERBB4
Chr.22
Chr.21
Chr.20
Chr.19
Chr.18
Chr.17
Chr.16
Chr.15
Chr.14
Chr.13
Chr.12
Chr.11
Chr.10
Chr.9
Chr.8
Chr.7
Chr.6
Chr.5
Chr.4
Chr.3
Chr.2
Chr.1
E
BRCA2
Chr.13
31
32
33
(Mbp)
High
Low
Negative
p = 0.0455
Percentage(%)
88.5
78.6
95.6
92.3
11.5
21.4
4.4
7.7
Non-Amp.
Amp.
All
High
Low
Negative
NTRK3
Chr.15
87
88
89
(Mbp)
p = 0.0345
89.4
81.0
91.1
100
10.6
19.0
8.9
0
CDK12
ERBB2
BRCA1
Chr. 17
38
40
42
(Mbp)
p = 1.4397e-06
88
69
100
100
12
31
0
0

Figure 4

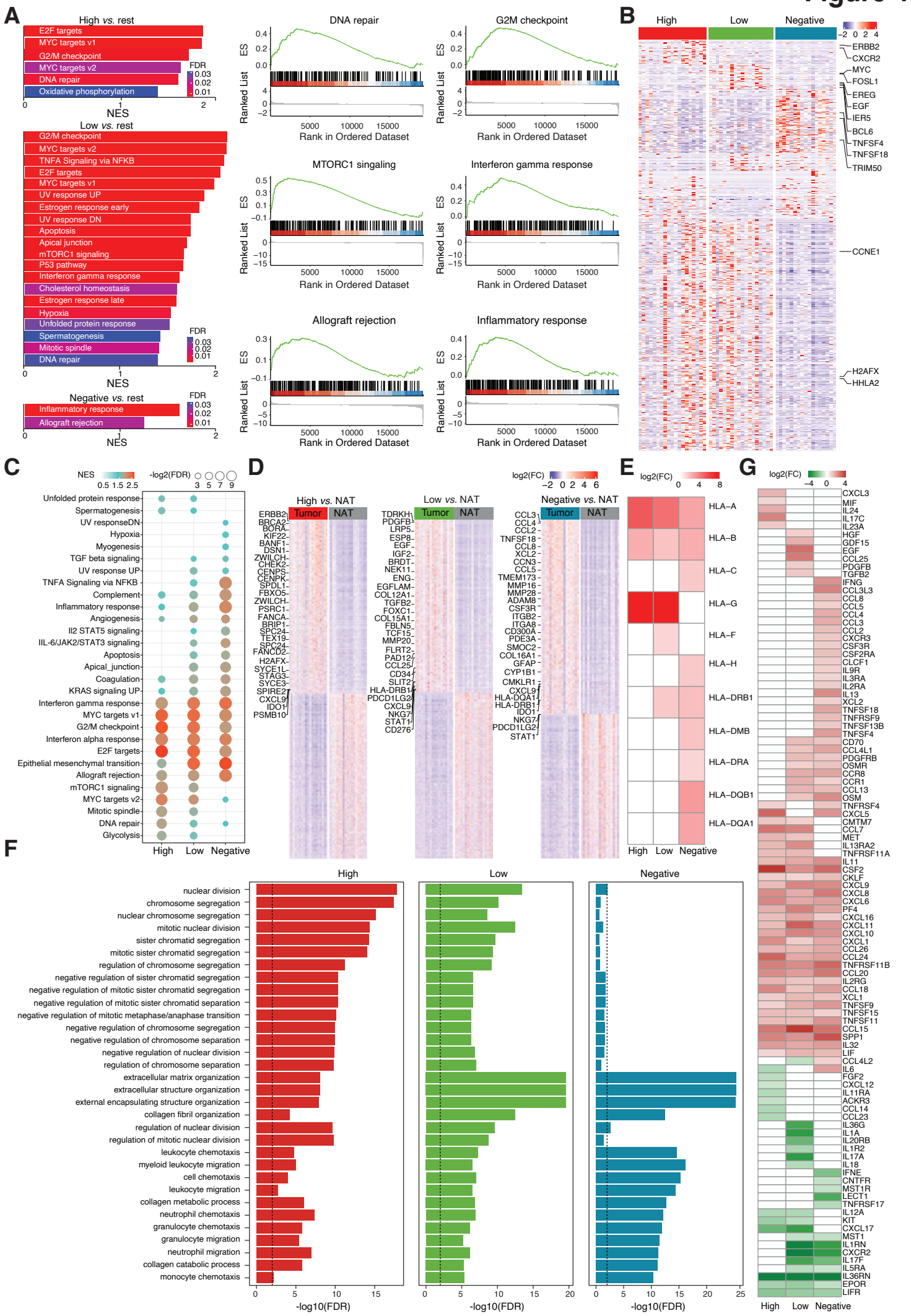
A
High vs. rest
E2F targets
MYC targets v1
G2/M checkpoint
MYC targets v2
DNA repair
Oxidative phosphorylation
FDR
0.03
0.02
0.01
NES
Low vs. rest
G2/M checkpoint
MYC targets v2
TNFA Signaling via NFKB
E2F targets
MYC targets v1
UV response UP
Estrogen response early
UV response DN
Apoptosis
Apical junction
mTORC1 signaling
P53 pathway
Interferon gamma response
Cholesterol homeostasis
Estrogen response late
Hypoxia
Unfolded protein response
Spermatogenesis
Mitotic spindle
DNA repair
Negative vs. rest
Inflammatory response
Allograft rejection
DNA repair
G2M checkpoint
MTORC1 singaling
Interferon gamma response
Allograft rejection
Inflammatory response
ES
Ranked List
Rank in Ordered Dataset
B
High
Low
Negative
ERBB2
CXCR2
MYC
FOSL1
EREG
EGF
IER5
BCL6
TNFSF4
TNFSF18
TRIM50
CCNE1
H2AFX
HHLA2
C
NES
-log2(FDR)
Unfolded protein response
Spermatogenesis
UV responseDN
Hypoxia
Myogenesis
TGF beta signaling
UV response UP
TNFA Signaling via NFKB
Complement
Inflammatory response
Angiogenesis
Il2 STAT5 signaling
IIL-6/JAK2/STAT3 signaling
Apoptosis
Apical_junction
Coagulation
KRAS signaling UP
Interferon gamma response
MYC targets v1
G2/M checkpoint
Interferon alpha response
E2F targets
Epithelial mesenchymal transition
Allograft rejection
mTORC1 signaling
MYC targets v2
Mitotic spindle
DNA repair
Glycolysis
High
Low
Negative
D
log2(FC)
High vs. NAT
Low vs. NAT
Negative vs. NAT
Tumor
NAT
ERBB2
BRCA2
BORA
KIF22
BANF1
DSN1
ZWILCH
CHEK2
CENPS
CENPK
SPDL1
FBXO5
ZWILCH
PSRC1
FANCA
BRIP1
SPC24
TEX19
SPC24
FANCD2
H2AFX
SYCE1L
STAG3
SYCE3
SPIRE2
CXCL9
IDO1
PSMB10
TDRKH
PDGFB
LRP5
ESP8
EGF
IGF2
BRDT
NEK11
ENG
EGFLAM
COL12A1
TGFB2
FOXC1
COL15A1
FBLN5
TCF15
MMP20
FLRT2
PAD12
CCL25
CD34
SLIT2
HLA-DRB1
PDCD1LG2
CXCL9
NKG7
STAT1
CD276
CCL3
CCL4
CCL2
TNFSF18
CCL8
XCL2
CCN3
CCL5
TMEM173
MMP16
MMP28
ADAM8
CSF3R
ITGB2
ITGA8
CD300A
PDE3A
SMOC2
COL16A1
GFAP
CYP1B1
CMKLR1
CXCL9
HLA-DQA1
HLA-DRB1
IDO1
NKG7
PDCD1LG2
STAT1
E
log2(FC)
HLA–A
HLA–B
HLA–C
HLA–G
HLA–F
HLA–H
HLA–DRB1
HLA–DMB
HLA–DRA
HLA–DQB1
HLA–DQA1
High
Low
Negative
G
log2(FC)
CXCL3
MIF
IL24
IL17C
IL23A
HGF
GDF15
EGF
CCL25
PDGFB
TGFB2
IFNG
CCL3L3
CCL8
CCL5
CCL4
CCL3
CCL2
CXCR3
CSF3R
CSF2RA
CLCF1
IL9R
IL3RA
IL2RA
IL13
XCL2
TNFSF18
TNFRSF9
TNFSF13B
TNFSF4
CD70
CCL4L1
PDGFRB
OSMR
CCR8
CCR1
CCL13
OSM
TNFRSF4
CXCL5
CMTM7
CCL7
MET
IL13RA2
TNFRSF11A
IL11
CSF2
CKLF
CXCL9
CXCL8
CXCL6
PF4
CXCL16
CXCL11
CXCL10
CXCL1
CCL26
CCL24
TNFRSF11B
CCL20
IL2RG
CCL18
XCL1
TNFSF9
TNFSF15
TNFSF11
CCL15
SPP1
IL32
LIF
CCL4L2
IL6
FGF2
CXCL12
IL11RA
ACKR3
CCL14
CCL23
IL36G
IL1A
IL20RB
IL1R2
IL17A
IL18
IFNE
CNTFR
MST1R
LECT1
TNFRSF17
IL12A
KIT
CXCL17
MST1
IL1RN
CXCR2
IL17F
IL5RA
IL36RN
EPOR
LIFR
High
Low
Negative
F
High
Low
Negative
nuclear division
chromosome segregation
nuclear chromosome segregation
mitotic nuclear division
sister chromatid segregation
mitotic sister chromatid segregation
regulation of chromosome segregation
negative regulation of sister chromatid segregation
negative regulation of mitotic sister chromatid segregation
negative regulation of mitotic sister chromatid separation
negative regulation of mitotic metaphase/anaphase transition
negative regulation of chromosome segregation
negative regulation of chromosome separation
negative regulation of nuclear division
regulation of chromosome separation
extracellular matrix organization
extracellular structure organization
external encapsulating structure organization
collagen fibril organization
regulation of nuclear division
regulation of mitotic nuclear division
leukocyte chemotaxis
myeloid leukocyte migration
cell chemotaxis
leukocyte migration
collagen metabolic process
neutrophil chemotaxis
granulocyte chemotaxis
granulocyte migration
neutrophil migration
collagen catabolic process
monocyte chemotaxis
-log10(FDR)

Figure 5

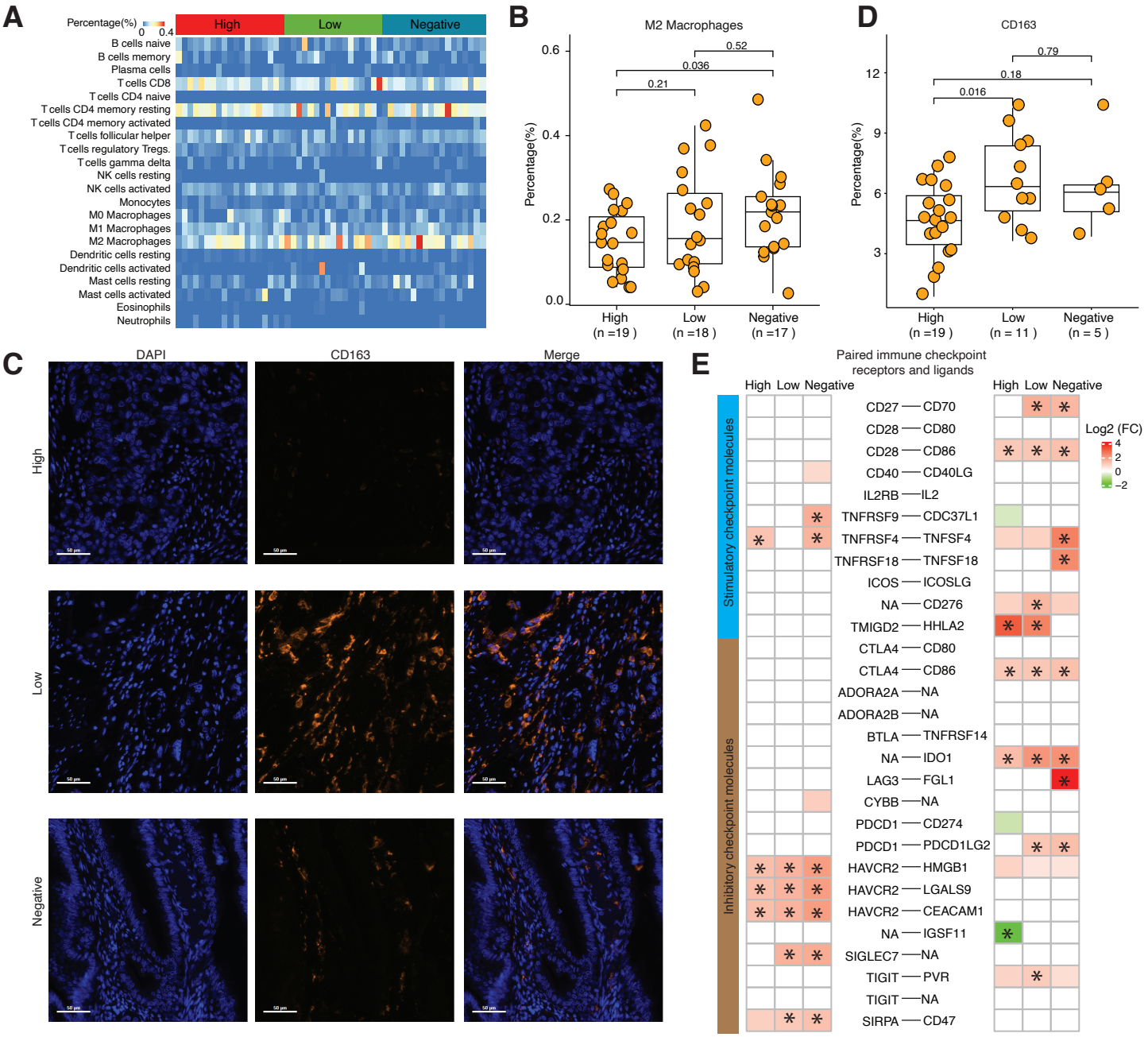
A
Percentage(%)
0
0.4
High
Low
Negative
B cells naive
B cells memory
Plasma cells
T cells CD8
T cells CD4 naive
T cells CD4 memory resting
T cells CD4 memory activated
T cells follicular helper
T cells regulatory Tregs.
T cells gamma delta
NK cells resting
NK cells activated
Monocytes
M0 Macrophages
M1 Macrophages
M2 Macrophages
Dendritic cells resting
Dendritic cells activated
Mast cells resting
Mast cells activated
Eosinophils
Neutrophils
B
M2 Macrophages
Percentage(%)
0.6
0.4
0.2
0.0
0.52
0.036
0.21
High (n =19)
Low (n =18)
Negative (n =17)
D
CD163
Percentage(%)
12
9
6
3
0.79
0.18
0.016
High (n =19)
Low (n = 11)
Negative (n = 5)
C
DAPI
CD163
Merge
High
Low
Negative
E
Paired immune checkpoint receptors and ligands
High Low Negative
High Low Negative
Stimulatory checkpoint molecules
Inhibitory checkpoint molecules
CD27 — CD70
CD28 — CD80
CD28 — CD86
CD40 — CD40LG
IL2RB — IL2
TNFRSF9 — CDC37L1
TNFRSF4 — TNFSF4
TNFRSF18 — TNFSF18
ICOS — ICOSLG
NA — CD276
TMIGD2 — HHLA2
CTLA4 — CD80
CTLA4 — CD86
ADORA2A — NA
ADORA2B — NA
BTLA — TNFRSF14
NA — IDO1
LAG3 — FGL1
CYBB — NA
PDCD1 — CD274
PDCD1 — PDCD1LG2
HAVCR2 — HMGB1
HAVCR2 — LGALS9
HAVCR2 — CEACAM1
NA — IGSF11
SIGLEC7 — NA
TIGIT — PVR
TIGIT — NA
SIRPA — CD47
Log2 (FC)
4
2
0
−2

Figure 6

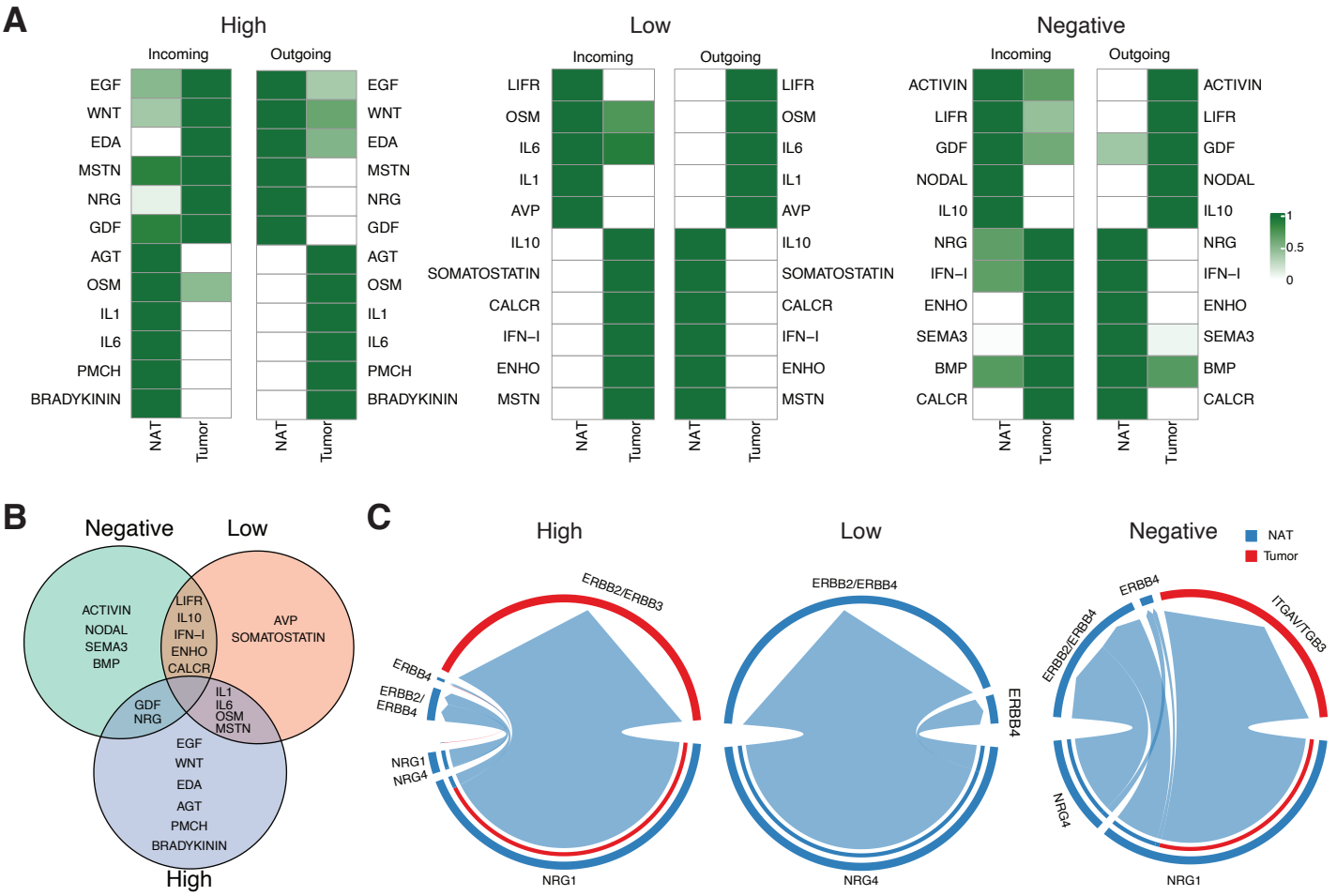
A
High
Low
Negative
Incoming
Outgoing
EGF
WNT
EDA
MSTN
NRG
GDF
AGT
OSM
IL1
IL6
PMCH
BRADYKININ
LIFR
OSM
IL6
IL1
AVP
IL10
SOMATOSTATIN
CALCR
IFN–I
ENHO
MSTN
ACTIVIN
LIFR
GDF
NODAL
IL10
NRG
IFN–I
ENHO
SEMA3
BMP
CALCR
NAT
Tumor
1
0.5
0
B
Negative
Low
High
ACTIVIN
NODAL
SEMA3
BMP
LIFR
IL10
IFN–I
ENHO
CALCR
AVP
SOMATOSTATIN
GDF
NRG
IL1
IL6
OSM
MSTN
EGF
WNT
EDA
AGT
PMCH
BRADYKININ
C
High
Low
Negative
NAT
Tumor
ERBB2/ERBB3
ERBB4
ERBB2/
ERBB4
NRG1
NRG4
ERBB2/ERBB4
ERBB4
NRG1
NRG4
ERBB4
ITGAV/ITGB3
ERBB2/ERBB4
NRG4
NRG1

Figure 7

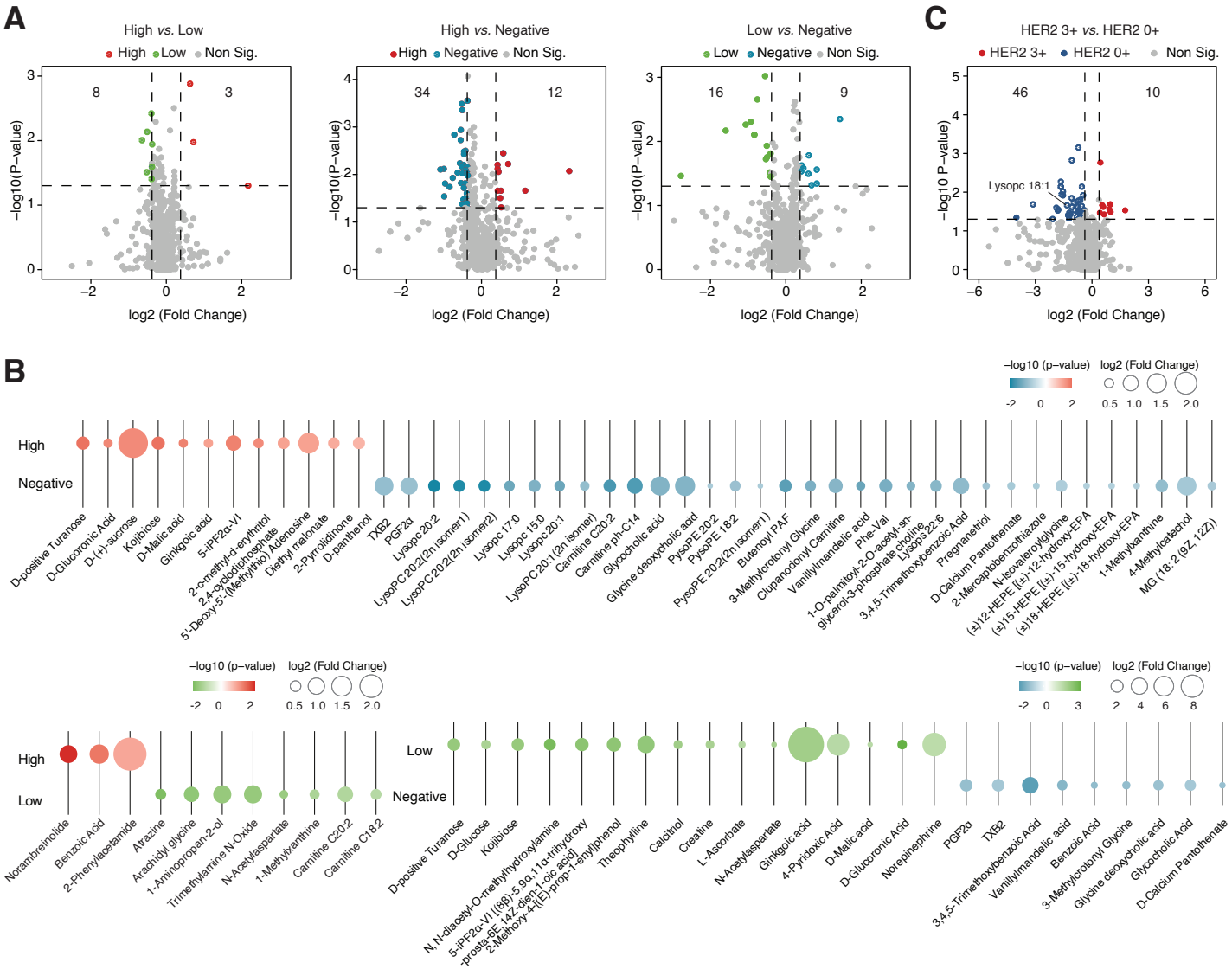
A
High vs. Low
High Low Non Sig.
8
3
High vs. Negative
High Negative Non Sig.
34
12
Low vs. Negative
Low Negative Non Sig.
16
9
C
HER2 3+ vs. HER2 0+
HER2 3+ HER2 0+ Non Sig.
46
10
Lysopc 18:1
−log10(P−value)
log2 (Fold Change)
B
−log10 (p−value)
log2 (Fold Change)
High
Negative
D-positive Turanose
D-Glucoronic Acid
D-(+)-sucrose
Kojibiose
D-Malic acid
Ginkgoic acid
5-iPF2α-VI
2-c-methyl-d-erythritol 2,4-cyclodiphosphate
5'-Deoxy-5'-(Methylthio) Adenosine
Diethyl malonate
2-Pyrrolidinone
D-panthenol
TXB2
PGF2α
Lysopc 20:2
LysoPC 20:2 (2n isomer1)
LysoPC 20:2 (2n isomer2)
Lysopc 17:0
Lysopc 15:0
Lysopc 20:1
LysoPC 20:1 (2n isomer)
Carnitine C20:2
Carnitine ph-C14
Glycocholic acid
Glycine deoxycholic acid
PysoPE 20:2
PysoPE 18:2
PysoPE 20:2 (2n isomer1)
Butenoyl PAF
3-Methylcrotonyl Glycine
Clupanodonyl Carnitine
Vanillylmandelic acid
Phe-Val
1-O-palmitoyl-2-O-acetyl-sn-glycerol-3-phosphate choline
3,4,5-Trimethoxybenzoic Acid
LysoPS 22:6
Pregnanetriol
D-Calcium Pantothenate
2-Mercaptobenzothiazole
N-Isovaleroylglycine
(±)12-HEPE [(±)-12-hydroxy-EPA
(±)15-HEPE [(±)-15-hydroxy-EPA
(±)18-HEPE [(±)-18-hydroxy-EPA
1-Methylxanthine
4-Methylcatechol
MG (18:2 (9Z,12Z))
High
Low
Norambreinolide
Benzoic Acid
2-Phenylacetamide
Atrazine
Arachidyl glycine
1-Aminopropan-2-ol
Trimethylamine N-Oxide
N-Acetylaspartate
1-Methylxanthine
Carnitine C20:2
Carnitine C18:2
Low
Negative
D-positive Turanose
D-Glucose
Kojibiose
N,N-diacetyl-O-methylhydroxylamine
5-iPF2α-VI I (8β),-5,9α,11α-trihydroxy -prosta-6E,14Z-dien-1-oic acid]
2-Methoxy-4-[(E)-prop-1-enyl]phenol
Theophylline
Calcitriol
Creatine
L-Ascorbate
N-Acetylaspartate
Ginkgoic acid
4-Pyridoxic Acid
D-Malic acid
D-Glucoronic Acid
Norepinephrine
PGF2α
TXB2
3,4,5-Trimethoxybenzoic Acid
Vanillylmandelic acid
Benzoic Acid
3-Methylcrotonyl Glycine
Glycine deoxycholic acid
Glycocholic Acid
D-Calcium Pantothenate

Supplementary information:

HER2 Prognostic Significance and Therapeutic Implications in Gastric Cardia Adenocarcinoma: Insights from Multi-Omics Profiling

Li-Dong Wang[1, *], Pengwei Xing[2], Xue-Ke Zhao[1], Xin Song[1], Meng-Xia Wei[1], Ling-Ling Lei[1], Rui-Hua Xu[1], Ran Wang[1], Lei Ma[3], Duo You[1, 4], Pei-Nan Chen[5], Minglu Xie[2], Miao Zhao[2], He Zhang[6], Hui-Fang Lv[4], Ai-Li Li[7], Xian-Zeng Wang[8], Fu-You Zhou[9], She-Gan Gao[10, *], Xingqi Chen[2, *]

[1]State Key Laboratory of Esophageal Cancer Prevention & Treatment and Henan Key Laboratory for Esophageal Cancer Research of the First Affiliated Hospital, Zhengzhou University, Zhengzhou 450052, China.

[2]Department of Immunology, Genetics and Pathology, Uppsala University and Science for Life Laboratory, Uppsala, Sweden

[3]Henan key Laboratory of Tumor Molecular Biology Medicine of First People's Hospital of Nanyang, Nanyang, 473004, China.

[4]Department of Medical Oncology, the Affiliated Cancer Hospital of Zhengzhou University, Zhengzhou, Henan Province, 450008, China

[5]Deaprtment of Thoracic Surgery, the Affiliated Cancer Hospital of Zhengzhou University, Zhengzhou, Henan Province, 450008, China

[6]Deaprtment of Pathology, the Affiliated Cancer Hospital of Zhengzhou University, Zhengzhou, Henan Province, 450008, China

[7]Department of Pathology, Linzhou Tumor Hospital, Linzhou, Henan Province, 456500, China

[8]Department of Thoracic Surgery, Linzhou People's Hospital, Linzhou, Henan Province, 456500, China

[9]Department of Thoracic Surgery, Anyang Tumor Hospital; Henan Key Medical Laboratory of Precise Prevention and Treatment of Esophageal Cancer; Henan Province Engineering Research Center of Cellular Immunotherapy for Esophageal Cancer, Anyang, Henan Province, 455000, China

[10]Henan Key Laboratory of Microbiome and Esophageal Cancer Prevention and Treatment; Henan Key Laboratory of Cancer Epigenetics; Cancer Hospital, The First Affiliated Hospital, College of Clinical Medicine of Henan University of Science and Technology, Luoyang, 471003, China

*Correspondence: ldwang2007@126.com, gsg112258@163.com, or xingqi.chen@igp.uu.se

Supplementary Figures 1-13

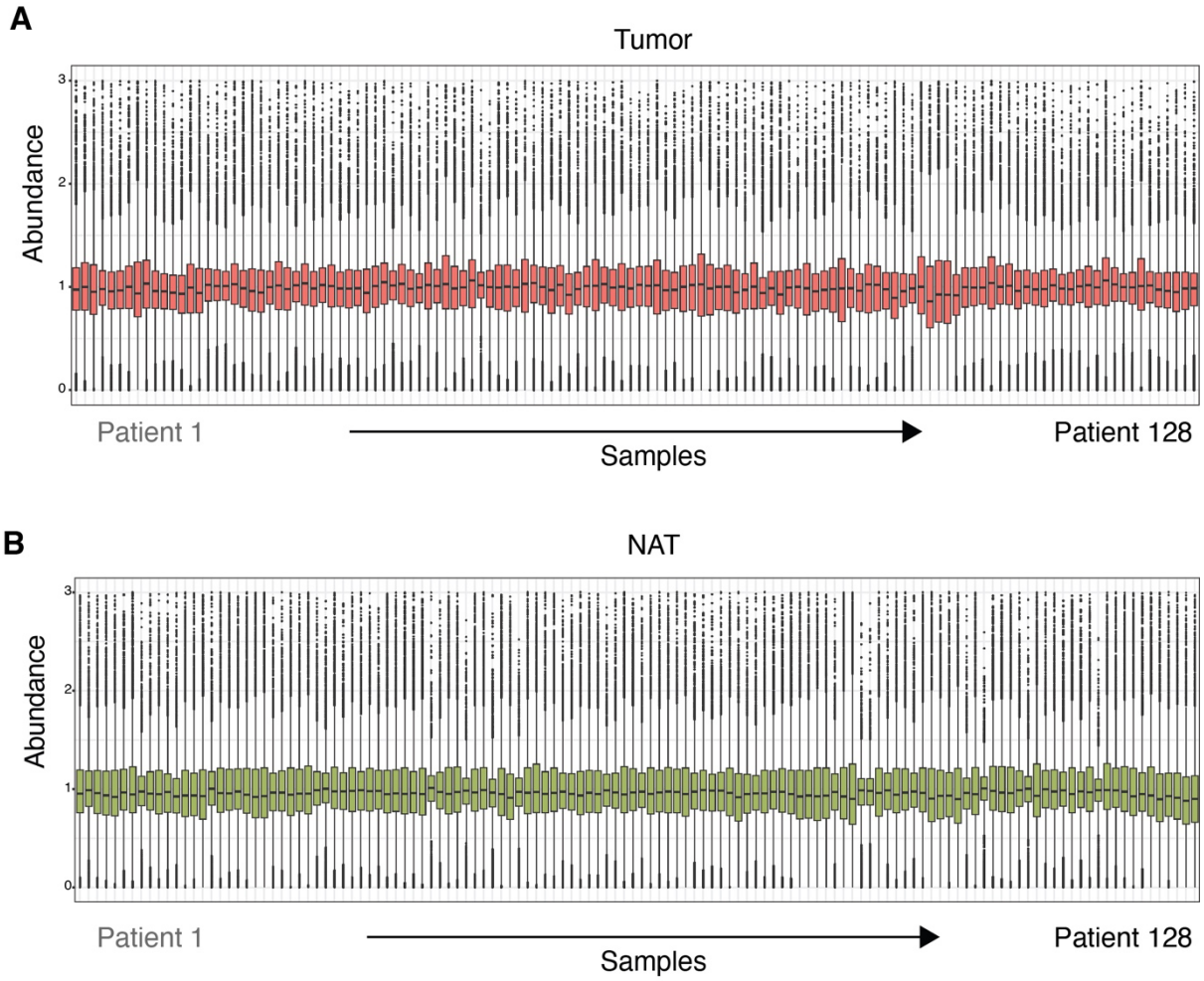

Supplementary Figure 1: Normalized protein levels in tumor (A) and normal tissue adjacent to the tumor (NAT) (B).

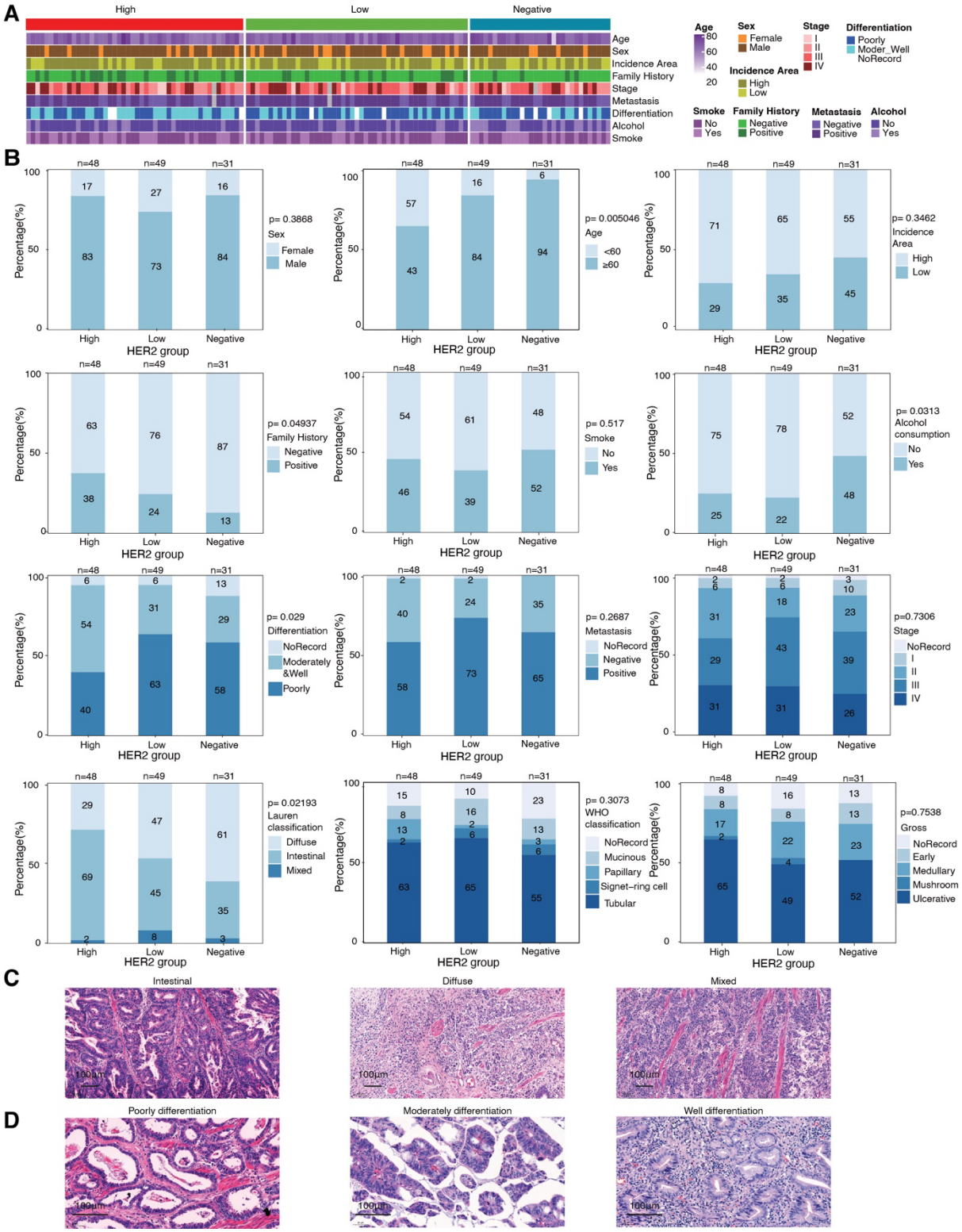

Supplementary Figure 2: Clinical pathological correlation with HER2 grouping from GCA cohort.

A. Distribution of clinical pathological features in GCA cohort.

B. Relationship of HER2 grouping and clinical pathological features in GCA cohort.

C. Representative Haematoxylin & Eosin (H&E) staining of different Lauren classification from the GCA cohort.

D. Representative H&E staining of different tumor differentiation from GCA cohort.

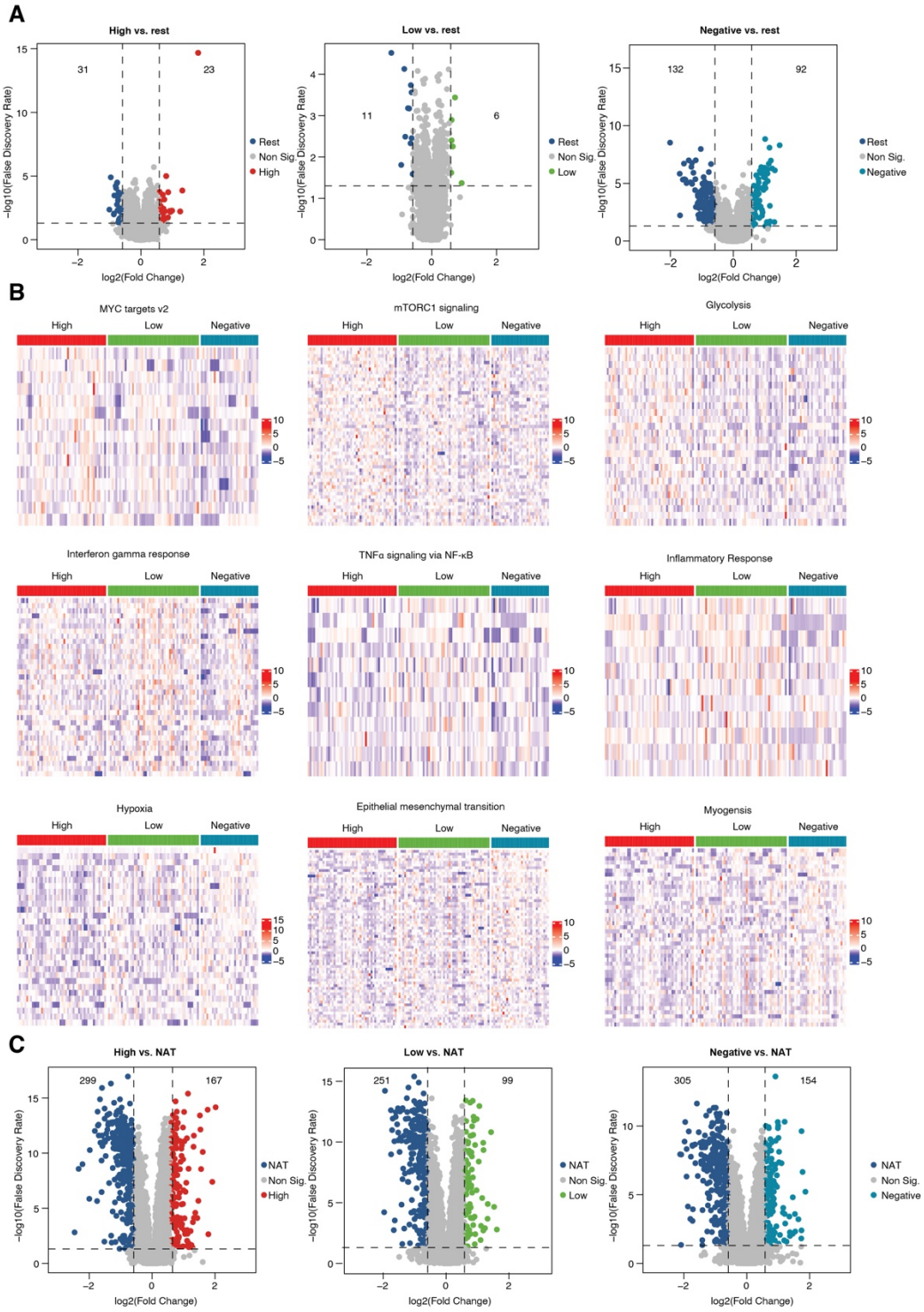

Supplementary Figure 3: Identification of differential protein expression in three HER2 groups of GCA.

A. Volcano plots represent identified differential proteins expressions in each HER2 group from tumor only; number of proteins is indicated.

B. Heatmaps show the enrichment of hallmark genes for each HER2 group.

C. Identification of differential protein expression by comparing tumors with normal tissue adjacent to the tumor (NAT) in each HER2 group.

A

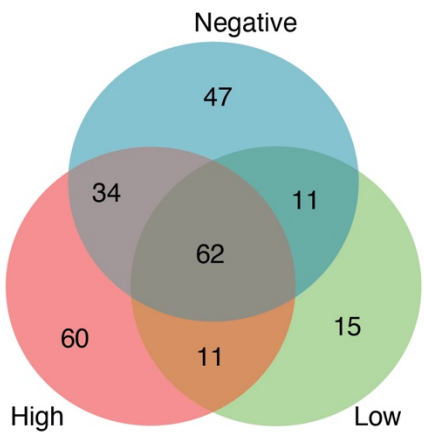

B

High		Low	Negative		High & Low	High & Negative	Low & Negative	High & Low & Negative	
HSP90AB1	LAMC2	IFIT3	ARPC1B	ARHGDIB	DDX21	RCC2	FEN1	IKBIP	MCM4
SSB	SMPDL3B	IFIT1	CNN2	MFGE8	XPO5	FKBP9	ITGB2	AGMAT	VCAN
GGCT	HSP90AB2P	TAP1	FBLN5	FILIP1L	FAP	PLOD3	SERPINB9	IGFBP7	P3H1
PON2	KPNA2	TAP2	PLBD2	FBN1	CDK1	PLOD1	LXN	NNMT	ISG15
MCM3	ACSL5	FGL2	TGFBI	CBFB	MX1	CRTAP	LIPA	STAT1	PLBD1
CAPRIN1	CEACAM6	FCGR2A	LDHA	MMP2	NXT1	NCL	NPL	EFEMP1	IGF2BP3
NOP2	SERPINB8	H1-5	IL4I1	POLD2	TMEM164	STMN1	TAPBP	LTBP2	FTL
RALY	DPP4	DCK	FSCN1	SAAL1	RETN	CTSB	LCP1	FHL3	FN1
PPA1	RRM2	SQSTM1	ITGAM	HAT1	MPO	SET	TNC	FKBP10	THBS2
MCM2	NEU1	NIP7	CNN3	CORO1A	AZU1	CPNE1	DOK2	CTHRC1	CDH17
ERBB2	ISLR	USP11	GUSB	EMILIN2	MMP8	LPCAT1	HLA-DPB1	SERPINH1	COL12A1
HSPH1	LCN2	PRTN3	KIF3B	C1QC		CTSA		GBP1	CEACAM5
DDX27	MMP9	SLCO1B7	CTSC	NOP14		SLC16A3		ITGAX	PLSCR1
PYCARD	PIGR	LPXN	VWA1	C20orf27		MXRA5		TPM4	PLOD2
LACTB2	BPI	FAM117A	MFAP2	HTRA1		DCTPP1		EPCAM	SLC2A3
CBX3	ELANE		SUMO1	EVL		MMP14		TYMP	TOP2A
GAR1	CTSG		AIF1	FASTKD5		CTSS		VIL1	HLA-DMB
HSD17B11	MUC5B		HLA-DRA	RB1		GDA		MUC13	FCER1G
TFRC	PDAP1		NASP	EFEMP2		HK3		PCNA	SASH1
S100A11	LTF		HLA-A	P3H3		PPIC		LTBP1	GPRC5A
RSL1D1	SDCBP2		CACYBP	WDR3		ASS1		CYBB	CAMP
S100A6	PLPP2		COL4A1	SERPINE2		GRN		CTSZ	THBS3
ANXA4	NCAPH		APOE	MAP1LC3B		PUS7		CPVL	OLFM4
SMC2	S100A8		DPYSL3			L1RE1		SPARC	THBS4
LGALS3BP	FUT6					GPNMB		ANP32E	STMN2
SERPINB5	MIEN1					BRIX1		CD55	SFRP4
LGALS4	SPARCL1					MISP		GGH	DMBT1
CCNK	GRB7					AOC1		MNDA	DEFA3
EPS8L3	ANXA13					TMSB10		TIMP1	S100A12
MAGED2	NEURL4					ITPRID2		CYBA	SPINT2
						FABP1		MCM6	CPS1
						ANPEP			
						GCNT3			
						HLA-DRB3			

Supplementary Figure 4: Number (A) and names (B) of proteins specific to HER2 groups and those common among them.

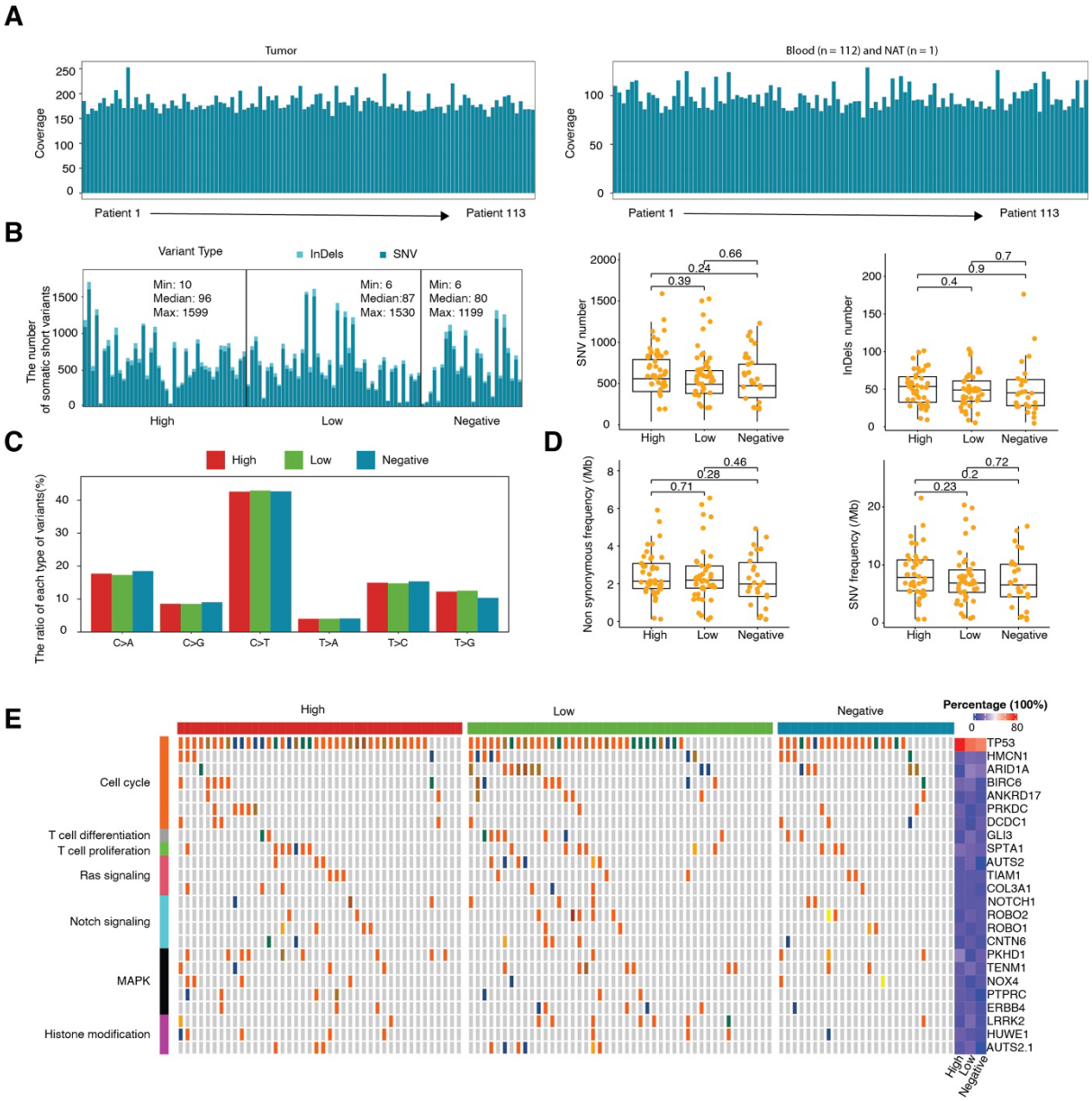

Supplementary Figure 5: comparison of somatic mutations in different HER2 groups.

A. Quantification and comparison of sequencing coverage of whole exon sequencing from GCA cohort.

B. Comparison of somatic short variant types (single-nucleotide variant (SNV) and insertions and deletions (InDels)) in three HER2 groups.

C. Comparison of mutation types in three HER2 groups.

D. Frequency comparison of non-synonymous and SNV in three HER2 group.

E. Ranking plots of the top mutated oncogenes and tumor suppressor genes involved in key signal pathways.

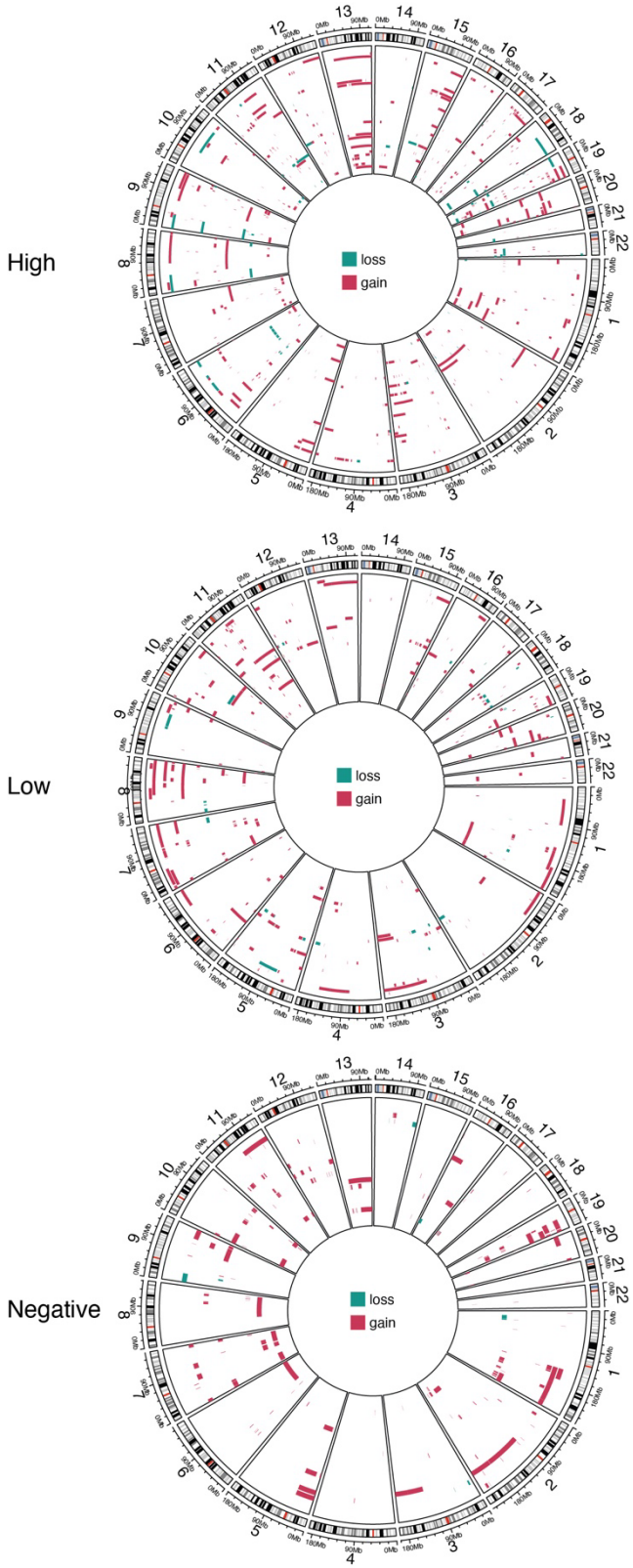

Supplementary Figure 6: Copy number alterations in different HER2 groups.

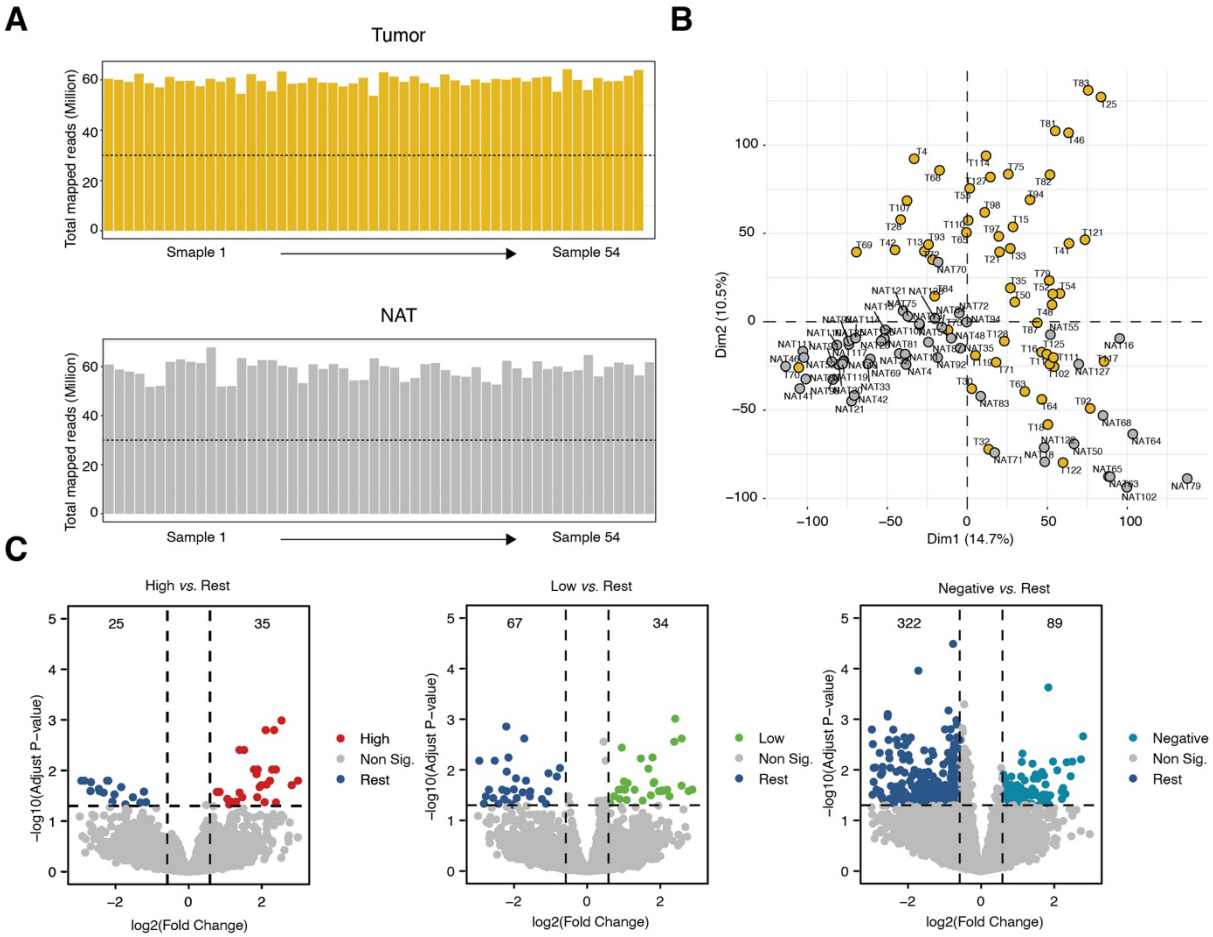

Supplementary Figure 7: RNA expression signature in each HER2 groups.

A. Quantification of mapped sequencing reads from tumor and NAT.

B. Principal component analysis (PCA) of RNA expression in tumors and NAT.

C. Volcano plots show the identification of differential RNA expression by comparing of each HER2 group with rest of groups.

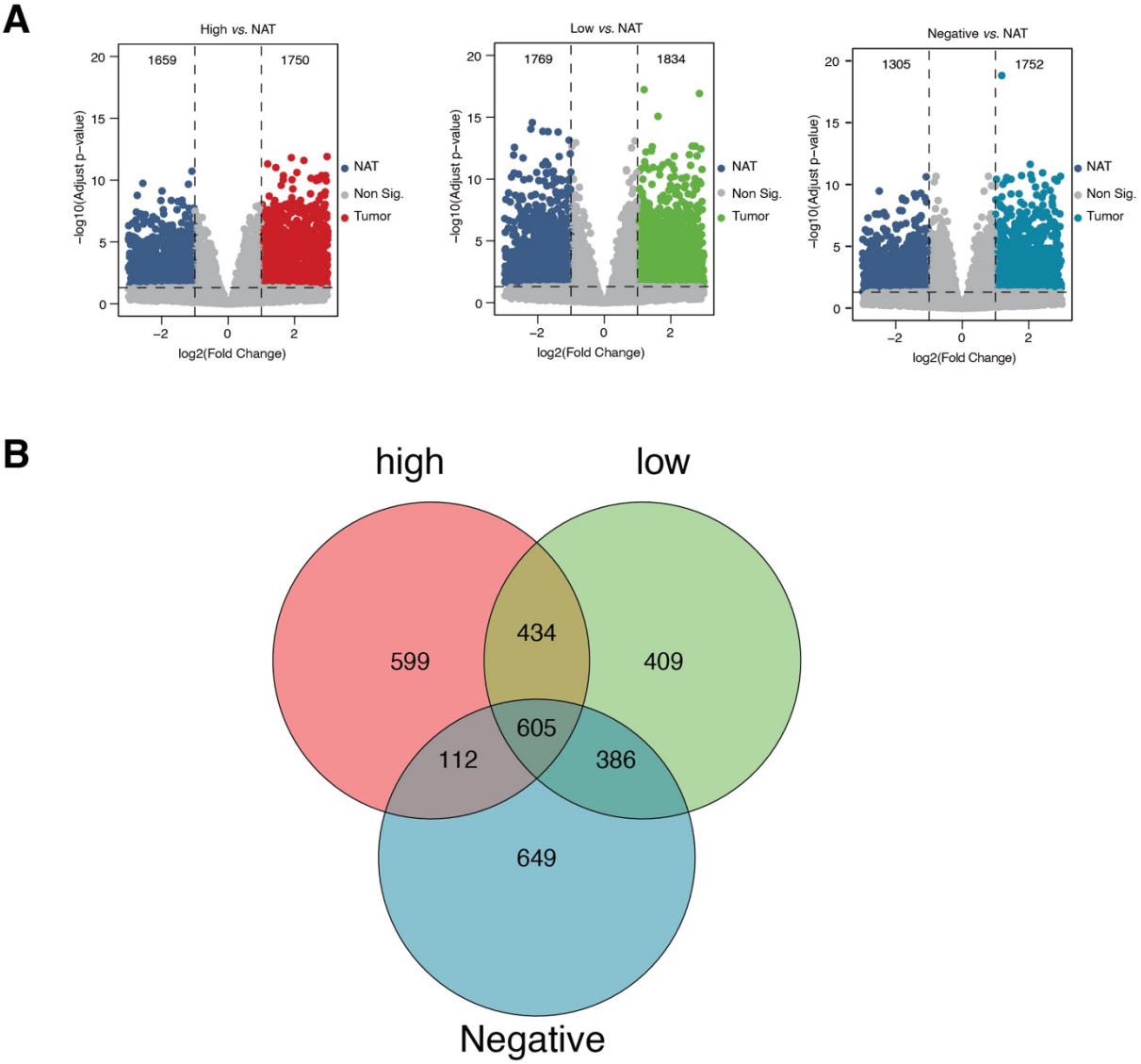

Supplementary Figure 8: Identification of differential RNA expression by comparing tumor with its corresponding NAT in each HER2 group.

A. Volcano plots show the identification of differential RNA expression by comparing of tumor with its corresponding NAT.

B. Venn diagram shows the unique and common differential RNA expression in each HER2 group.

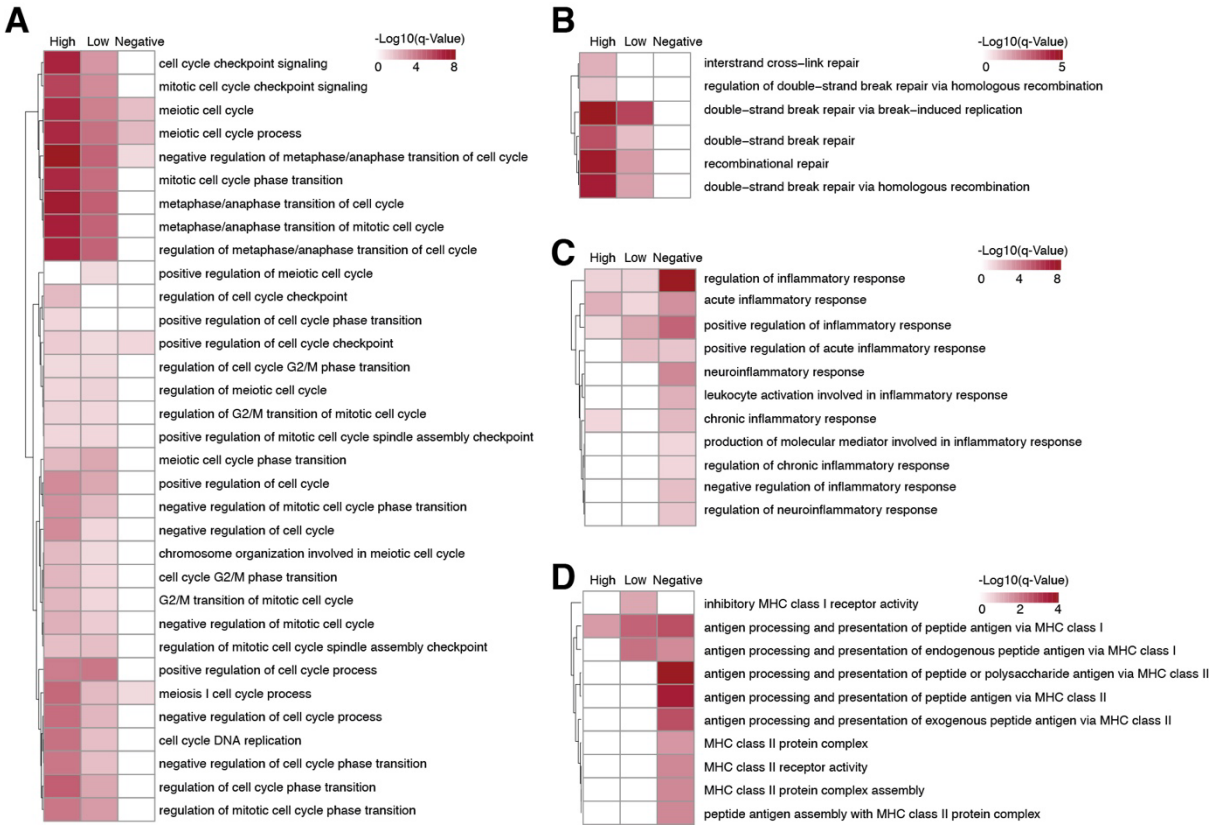

Supplementary Figure 9: Enrichment gene ontology (GO) term comparison in different HER2 groups.

A. GO terms from cell cycle relevant terms.

B. GO terms from DNA repair relevant terms.

C. GO terms from inflammation relevant terms.

D. GO terms from major histocompatibility complex (MHC) relevant terms.

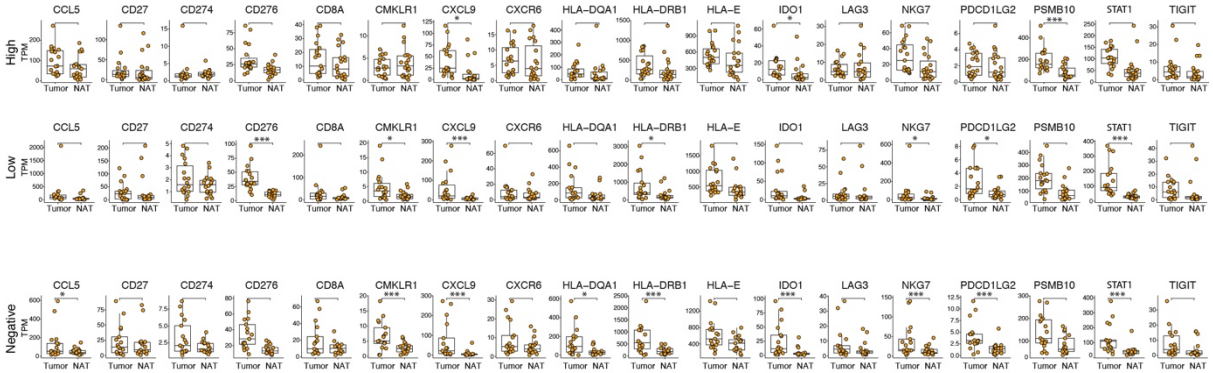

Supplementary Figure 10: Comparison of RNA expression from 18 immune genes between tumors and NAT in different HER2 groups.

* = False discovery rate (FDR) < 0.05; ** = FDR < 0.01; *** = FDR < 0.001; TPM = Transcripts Per Million.

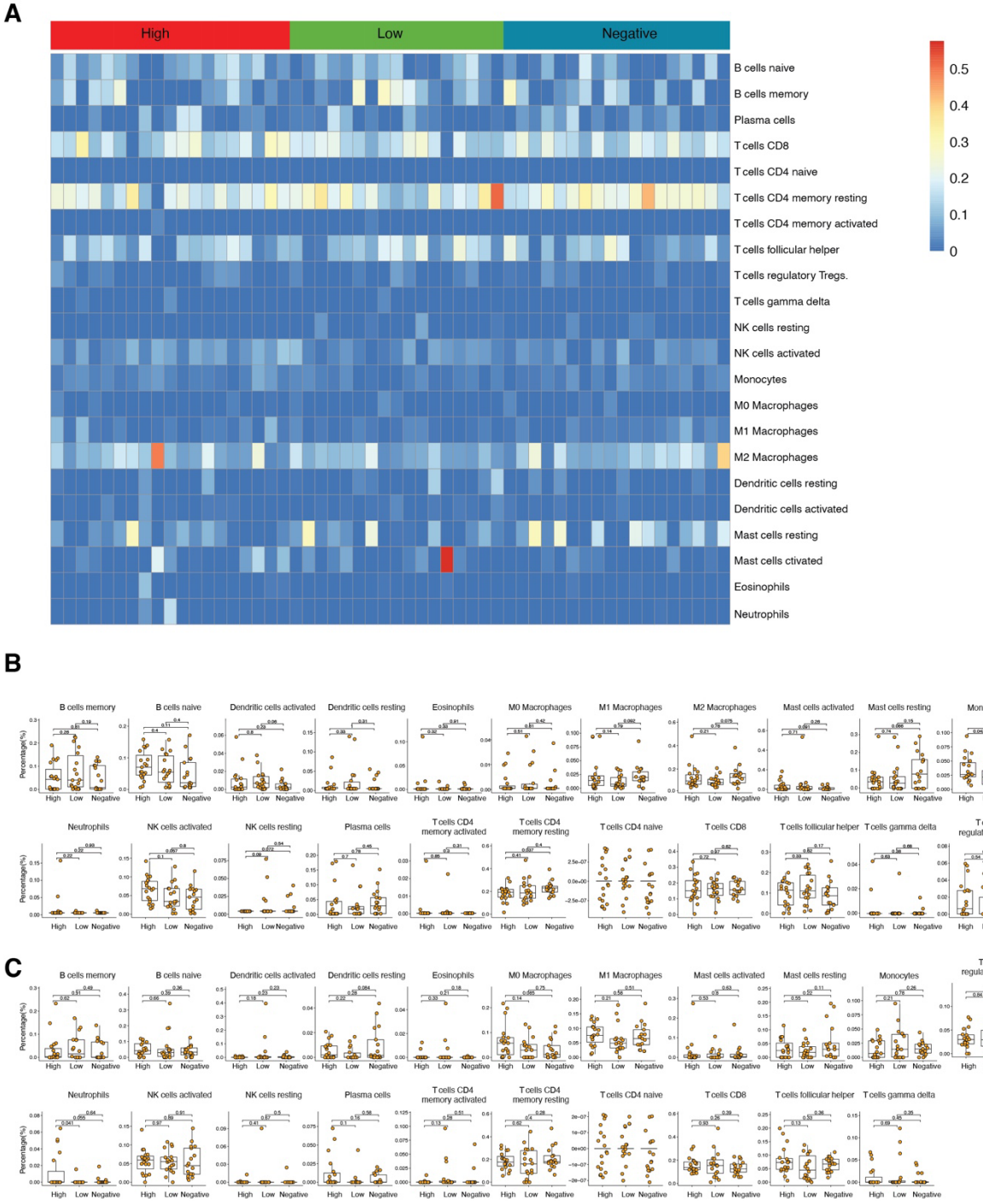

Supplementary Figure 11: Deciphering tumor microenvironment in different HER2 group.

A. Quantitative comparison of different cell types in tumors only from different HER2 groups.

B. Cell component comparison from bulk RNA-seq predictions of NAT in different HER2 groups.

C. Quantitative comparison of different cell types in NAT from different HER2 groups.

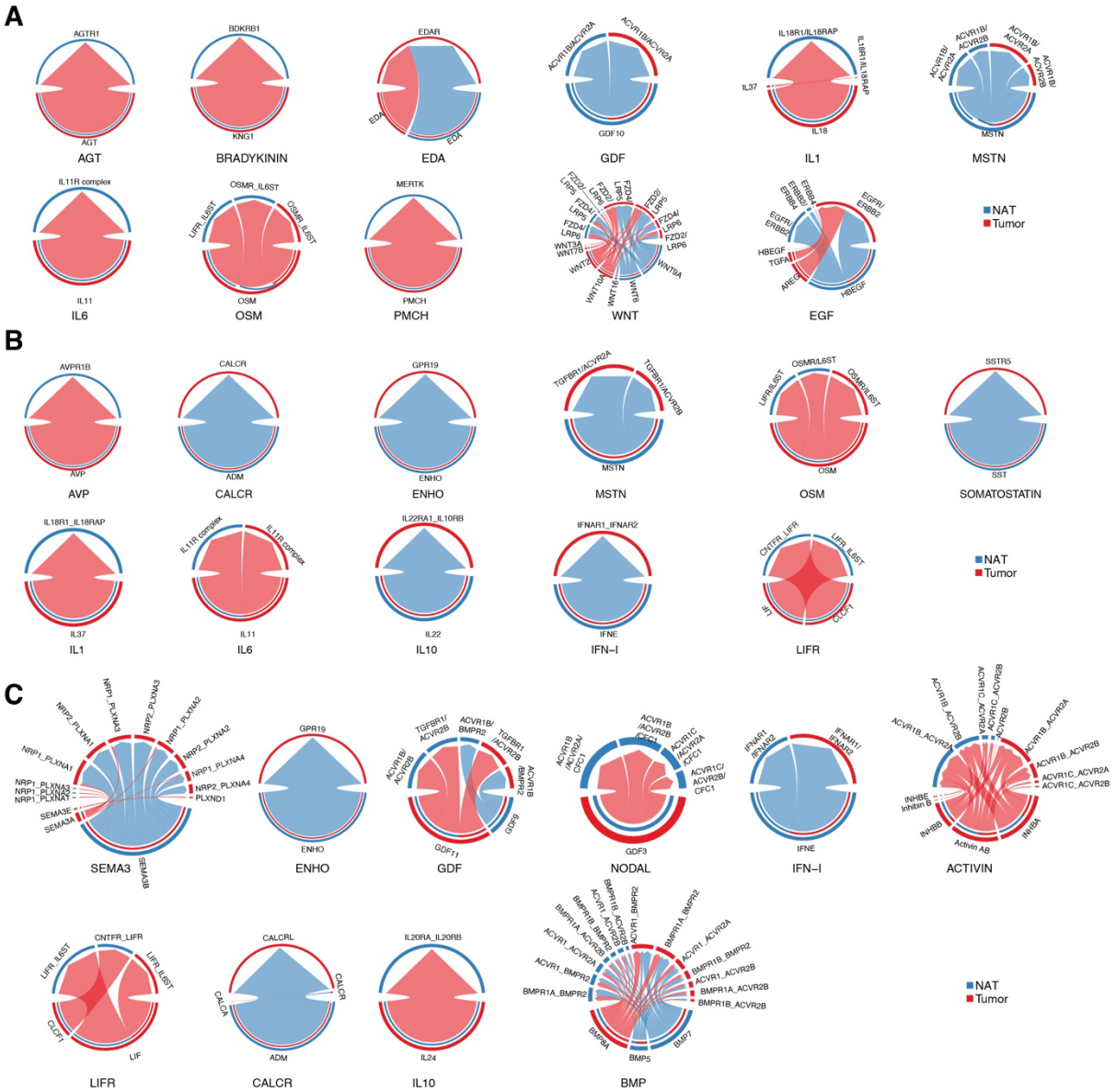

Supplementary Figure 12: Ligand-receptor signaling between tumors and tumor-adjacent tissue macro-environment in different HER2 group.
HER2 high group (**A**), HER2 low group (**B**), and HER2 negative group (**C**).

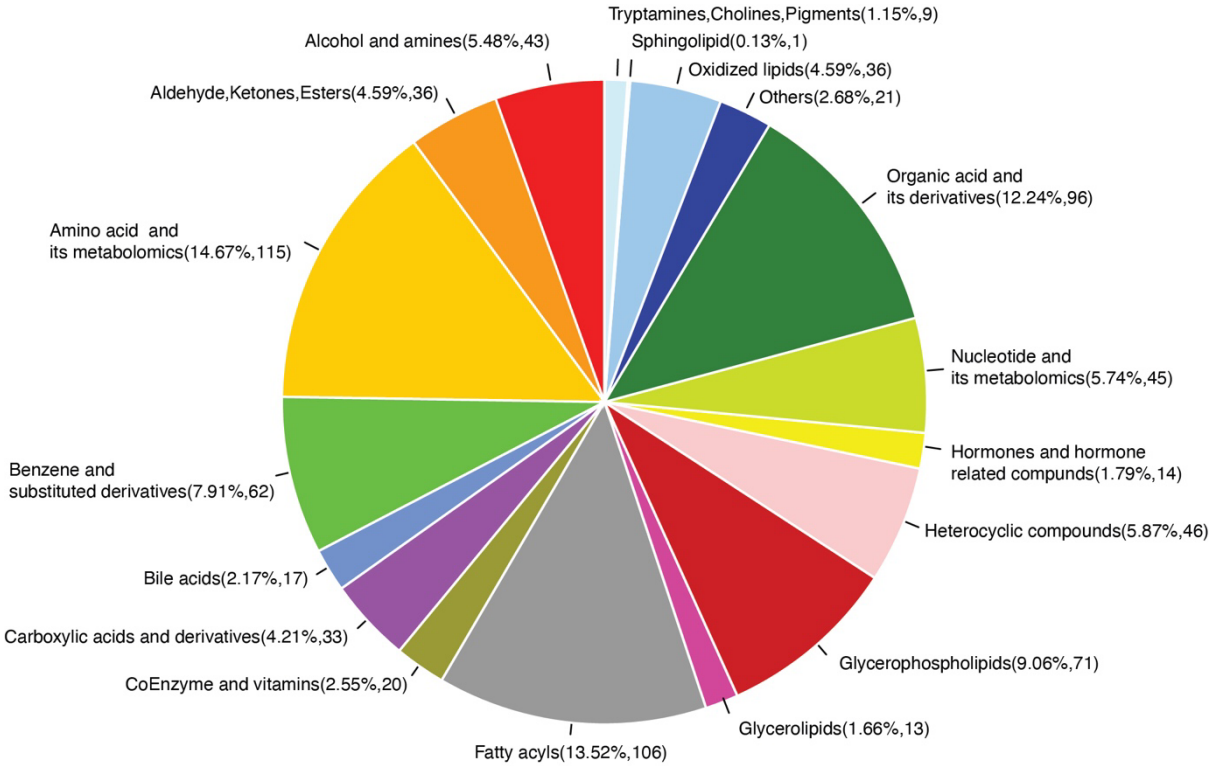

Supplementary Figure 13: Distribution of metabolic substrates detected from periphery blood of GCA patients.

Tables 1-22

Table 1: List of GCA cohort with 128 patients.

Table 2: Protein expression matrix of the GCA cohort.

Table 3: Uniquely identified proteins for each HER2 group.

Table 4: Gene set enrichment analysis of proteins by comparing each HER2 group with the other two groups.

Table 5: Hallmark gene sets analysis of protein expression for each HER2 group in GCA patients.

Table 6: Differential protein expression in each HER2 group by comparing tumors and their corresponding normal tissue adjacent to the tumor (NAT).

Table 7: Gene ontology (GO) terms enrichments from differential protein expression in each HER2 group by comparing tumors and their corresponding normal tissue adjacent to the tumor (NAT).

Table 8: Mapping summary of whole exome sequencing (WES) from tumors and their corresponding peripheral blood.

Table 9: Mutation frequency detected in genes in different HER2 groups.

Table 10: Copy number alteration (CNA) of whole genome with 1Mbp bin size from whole exome sequencing (WES).

Table 11: Hallmark gene sets analysis of RNA expression for each HER2 group in GCA patients from tumors only.

Table 12: Signature gene list for each HER2 group from the expression of tumors only.

Table 13: Hallmark gene sets analysis of RNA expression for each HER2 group by comparing tumors with their corresponding normal tissue adjacent to the tumor (NAT).

Table 14: List of differential genes for each group by comparing tumors with their corresponding normal tissue adjacent to the tumor (NAT).

Table 15: Group specific and common differentially expressed genes from the comparison of tumors and their corresponding normal tissue adjacent to the tumor (NAT) among the three HER2 groups.

Table 16: Gene ontology (GO) terms enrichments from differential RNA expression in each HER2 group by comparing tumors and their corresponding normal tissue adjacent to the tumor (NAT).

Table 17: list of exclusive genes in each HER2 group from GO terms of cell cycle, DNA repair, inflammation and major histocompatibility complex (MHC).

Table 19: Quantification of CD163 immunofluorescent staining in each HER2 group.

Table 19: Metabolic comparison between HER2 high group and HER2 low group from peripheral blood.

Table 20: Metabolic comparison between HER2 high group and HER2 negative group from peripheral blood.

Table 21: Metabolic comparison between HER2 low group and HER2 negative group from peripheral blood.

Table 22: Metabolic comparison between HER2 3+ group and HER2 0+ group from peripheral blood.